Chapter 2
Electron Distributions and Physicochemical Properties

Abstract Electron distributions in the main compounds of rare-earths and actinides are described in relation with the valence of these elements. Their changes as a function of the physical conditions, temperature, pressure and some potential applications of these materials are discussed. Cerium compounds are particularly considered.

Keywords Chemical binding · Valence fluctuation · Rare-earth compounds · Actinide compounds

2.1 Rare-Earth Compounds

Densities of valence states are strongly modified in the compounds with respect to those in the elements and all the electronic levels are shifted. The shifts are a consequence of the chemical binding. Valence electrons of the metal and the ligand are present in bond orbitals, forming the valence band. The bonds are often described as a "charge transfer" from metal to ligand orbitals. This terminology can suggest the transfer of one or eventually more electrons and the existence of ionic bonding. However, the compounds having an ionic bonding are rare and concern mostly alkaline metal compounds. The chemical bondings result from the overlap of the relevant wave functions and their strength depends on the inter-atomic spacing of elements in the solid. Thus, in the oxides, the reduction of the number of valence electrons in the atomic sphere around each metal ion is small for the elements having s and p valence electrons like magnesium and this reduction concerns essentially the s valence electrons [1]. These results can be generalized to the transition elements, which have a fractional number of s, d electrons contributing to the cohesion and to the chemical bonding. All the same, in lanthanides and actinides, the s, d electrons contribute to bonds, which are due to *electron redistribution* rather than a transfer. This feature of the charge redistribution has been discussed by Slater [2]. This redistribution increases with the covalent character of the bond.

C. Bonnelle and N. Spector, *Rare-Earths and Actinides in High Energy Spectroscopy*, Progress in Theoretical Chemistry and Physics 28, DOI 10.1007/978-90-481-2879-2_2

Despite frequent coincidence of the 4f energy levels with the broad s, p, d bands, the interaction of the 4f electrons with the valence electrons of the ligand is negligible and the 4f electrons remain localized as in the metal. In some cases, one of the localized 4f electrons of the metal delocalizes and becomes similar to a valence electron. This is the case of tetravalent cerium compounds.

For an element in a solid state, the valence is defined as the number of electrons per atom contributing to the valence band formation. As previously mentioned, the rare-earth metals are trivalent and have the configuration $4f^n(5d6s)^3$ under SPT conditions, except for europium and ytterbium, which are divalent and have the configuration $4f^n(5d6s)^2$. In a chemical compound, the valence of an element is equal to the number of its bonds with the neighbouring atoms. It was initially suggested that the rare-earth valence was equal to the number of their 6s–5d electrons in the compound and the 4f electrons were not taken into account in the bonding. In the case of oxidation, for example, all the rare-earth elements oxidize readily [3] and, including the two divalent europium and ytterbium, form sesquioxides RE_2O_3 [4]. The rare-earths are trivalent in these compounds. Each rare-earth atom donates three 5d–6s electrons to the bonds with oxygen and has the configuration RE^{3+}; its *oxidation state* is equal to three. The oxidation state characterizes the number of electrons, which participate in the bonding, but not the ionic or covalent character of the bonding. As is well known, the bond is partially covalent in the oxides, it is often defined as having an *intermediate* character.

Lanthanum, gadolinium and lutetium, having a configuration $4f^n5d^16s^2$ in the free atom with $n = 0$, 7 and 14, are considered as forming very stable trivalent compounds. Thus, gadolinium is designated as the archetypal trivalent rare-earth owing to the stability of the half-full 4f sub shell, which remains the same in the free atom and the metal. Other rare-earths, which precede, or follow, these elements, can be, respectively, divalent or tetravalent. Thus samarium, europium, thulium and ytterbium have the +2 oxidation state in numerous compounds [5]; whereas, cerium, praseodymium and terbium can have the +4 oxidation state. In numerous rare-earth compounds, the valence varies with external parameters like pressure, temperature and alloying and this variation is accompanied by changes in the physical properties such as resistivity, optical reflectivity and scattering phenomena.

In the metals and compounds of trivalent rare-earths, whose free atom configuration is $4f^n6s^2$, the integral number of localized 4f electrons is $(n - 1)$ and the three valence electrons are of the s–d type. The electronic configuration changes are induced by the need to obtain an energetically stable solid. Indeed, the cohesion energy increases with the number of the valence electrons. It varies also with their character and is higher for the 5d than for the 4f electrons. In the light rare-earths, the electron configurations are less stable than in the heavy rare-earths and the number of the valence electrons can change. Thus, the number of the 5d electrons is higher in light rare-earth compounds and that increases the cohesion. Concurrently, the number of the 6s electrons decreases to maintain the trivalence. The valence state of the metallic elements is determined theoretically from the difference of the total energies calculated for the divalent and trivalent configurations [6].

If the rare-earths have the same valence in the metal and in its compounds, so is the number of their 4f electrons. These 4f electrons are localized and of atomic-like character and their interactions with the valence electrons are negligible. However, an increase of the valence or a variation of the temperature–pressure conditions can bring about a change in the character of the 4f electrons owing to the interactions between the strongly correlated 4f electrons and the delocalized valence electrons in the solid. Such a change occurs in the light rare-earths because their 4f electrons are less tightly bound and in terbium because the single 4f electron outside the half-filled shell is also weakly bound. In a valence change from a trivalent to a tetravalent rare-earth, the number of the localized 4f electrons decreases while the number of the valence electrons increases. Because the number of the localized electrons is integral, it is reduced by one unit while the number of 4f electrons that participate in the chemical bonding is unspecified. When a localized electron makes a transition to a delocalized state, this delocalization increases the valence as well as the *cohesive energy*. Thus increase of the cohesive energy following the arrival of a 4f electron into a bonding orbital is supplied by the delocalization process.

Compounds with a non-integral number of 4f electrons were considered as formed from a rare-earth with two different valences and were designated as *mixed,* or *intermediate, valence compounds* [7, 8]. Among the 4f-electron materials with atypical properties, compounds and alloys in which the rare-earth is a mixing of divalent and trivalent ions have been particularly studied [9–11]. In the notion of mixed valence, the number of 4f electrons in each ion is integral and a non-integral number of 4f electrons results from the mixing of ions having n 4f electrons with those having $(n - 1)$ 4f electrons. The presence of ions with only $(n - 1)$ 4f electrons is explained by the transfer of one 4f electron into the 5d6s band. The ions fluctuate between the two pure configurations of very close energies. Such coexistence of two different configurations was considered possible only if the energy difference between their two lowest levels is smaller than energy of the order of Δ, which is the width of the Friedel virtual bound state. Δ is around 10^{-2} eV for rare-earth metals [12]. Systems fluctuating between two configurations of very close energies are also named *valence fluctuation compounds*. Initially limited to a few monochalcogenides, this representation now concerns many compounds of cerium, samarium, europium, thulium and ytterbium, that exhibit non-integral valence at ambient conditions.

Various models have been developed to treat this type of compounds. It was initially suggested that if the 4f levels were sufficiently close to the valence band, transfer of a non-integral number of 4f electrons/ion could take place to this band [13]. In this case, 4f electrons would be present in the chemical bonds and a covalent ligand nl-4f mixing would exist. A strongly correlated band model has then to be used to treat such a system. More generally, some of the 4f electrons arrive into the 5d6s band and fluctuations between the $4f^n$ and $4f^{n-1}$ configurations render the distribution homogeneous. For this transition to take place, the $4f^n$ localized levels are expected to be very close to the Fermi level. The $4f^{n-1}$ levels are localized and only a non-integral number of the 4f electrons, equal to the number of rare-earth ions having the $4f^{n-1}$ configuration, are delocalized. The time of valence

fluctuations is inversely proportional to the energy width of the configurations. Spectroscopic observations of the compound on a time scale shorter than the fluctuation time can analyze each configuration. Generally, a mixing of configurations is observed.

The existence of intermediate valence phases depends on the lattice constant, whose values can vary between those expected for pure divalent and trivalent compounds. It also depends on the cohesive energy and the chemical bonding, which vary according to the rare-earth valence, hence the contribution of the 4f electrons to the valence. Particular properties of the mixed valence phases are the high electronic specific heat and, in some cases, the absence of magnetic ordering. The delocalization of a non-integral number of 4f electrons per ion accompanies a decrease of atomic volume and compressibility. When atomic volume and compressibility change in a continuous way, the electronic transition takes place gradually. When they change discontinuously, an f $\rightarrow$ d discrete transition is expected. Collapse in the atomic volume is thus characteristic of a change in the electronic structure of the rare-earth ions (cf. Sect. 1.4.1).

The ground state of systems exhibiting valence fluctuations was difficult to treat because the interaction energies between electrons in open shells are not known with precision. A theoretical method was developed to obtain the energy differences between the two configurations with an accuracy better than a few tenths of electronvolt [6]. Initially, it was applied to divalent–trivalent systems and tested for the rare-earth metals. In this method, the energy difference between the divalent and trivalent compounds is calculated from energy differences between a solid and an atom having the same valence because many interaction energies cancel between the atom and the solid. Indeed, the interaction energies within the 4f shell are essentially the same in the solid and the atom having the same valence and cancel. The 4f–5d inter-shell interactions can be considered as being the same for the divalent and trivalent configurations in the solid above the magnetic ordering temperature. The coupling between 4f electron and the electrons in the valence band is weak in the solids and can be neglected. No coupling is present in the divalent atom because only the 4f shell is open. In contrast, the 4f–5d inter-shell interaction is to be taken into account in the trivalent atom. Its energy is to be added to terms calculated without interaction. Thus, the energy difference between the divalent and trivalent atoms is only the 4f–5d excitation energy. The energies of the two valence states in the solid have been calculated using the LMTO method with either the SIC-LDA or GGA density functional. This original calculation method was tested by comparison between the theoretical and experimental energy differences. The valence state is correctly predicted for all the trivalent metals and difference of only some percents is obtained between the GGA calculations and the experimental data. This method, suitably tested for the metals, has been used to predict the rare-earth valence in various series of compounds.

In the heavy rare-earths, the 4f electrons are chemically inert and set up localized magnetic moments. The total magnetic moments have both orbital and spin components and spin–orbit interactions are strong for the rare-earth elements and compounds, in comparison with the Pauli paramagnetism of the itinerant electrons.

As one proceeds along the series adding electrons to the localized 4f ones, the 4f electrons become more tightly bound in the ions, reducing the inter-ion overlap of the 4f wave functions, whose spatial extension remains inside the 5s and 5p core sub shells. Then, despite the fact that the ionization energies of the 4f sub shell are comparable to those of the 5d and 6s valence electrons, the 4f electrons retain an atomic character in the solid and do not participate in the chemical bonding. Therefore, as already underlined for the valence band in the metals, those are the 5d and 6s valence electrons, hybridized with the ligand orbitals, that form the valence band in a series of trivalent compounds. They are responsible for the chemical bonding and their densities of states remain practically unchanged along the series. Thus, the trend toward bivalence of the rare-earths, associated with divalent ligands, is due to the localized nature of the 4f electrons and their well-known lanthanide contraction.

In compounds, the charge distribution due to anions surrounding the metal ion induces a static electric field, named ligand-field, or *crystal field*, which produces a splitting of the energy levels occupied by localized electrons. The angular part of the crystal field parameters reflects the influence of the topological arrangement of the anions. The crystal field splitting tends to decrease with increasing size of the coordination polyhedron. The rare-earth 5d electron interacts strongly with the surrounding anions, making the 4f–5d excitation energy depend on the ligands. Owing to the crystal field, the energy difference between d orbitals varies; it increases with oxidation number. Inversely, the energies of the 4f orbitals are barely sensitive to the crystal field and the 4f orbital moments are not quenched by it. In regard to 4f energy levels in rare-earth ions, their crystal field splitting is generally not taken into account because it is much smaller than the splitting due to the spin–orbit interaction, which is strong for many of the rare-earth compounds. Indeed, partly filled 4f orbitals behave like localized magnetic moments. However, in order to estimate the electron distributions with sufficient accuracy, it appears necessary, in some cases, to take into account the interaction of the 4f orbitals with the crystal field.

Owing to the localization of the 4f electrons, the overlap between 4f orbitals centered on adjacent atoms is very small or negligible. Thus, the dipole–dipole and exchange interactions between these 4f orbitals constitute a negligible portion of interactions between rare-earth ions. An exchange mechanism due to interactions between localized electrons via the other valence electrons, called indirect exchange, was developed by Ruderman and Kittel for transition metal alloys. Kasuya has shown the validity of this indirect exchange model as a basis for describing the interactions in gadolinium metal and more generally in the rare-earths. Consequently, the dominant interaction in the rare-earths is a coupling between the localized 4f electrons and the itinerant valence electrons, named *RKKY* (Ruderman–Kittel–Kasuya–Yoshida) *interaction*. This interaction increases with a decrease of the direct interactions between 4f electrons, i.e. when U decreases. Initially developed for metallic materials, it varies with a change in the bonds and the presence of ligands introduces more complicated interaction mechanisms such as *super-exchange interactions* [14, 15]. Thus, in rare-earth compounds, both

super-exchange interaction and indirect RKKY-type interaction coexist and their relative contribution varies with the ligand radius, the super-exchange increasing with it. In contrast, the RKKY interactions increase considerably with the density of the charge carriers. They increase when the lattice constant decreases and the metallic character of the compounds increases. The RKKY interactions are responsible for the existence of *half-metallic ferromagnets* in intermetallic compounds [16]. In this particular class of materials, an energy gap exists between the valence and conduction bands for electrons of one spin polarization, while this gap is absent for electrons of the other spin polarization. A remarkable consequence is that the electrons at the Fermi level are 100 % spin-polarized in these materials. Half-metallic materials are rare because they require a large exchange splitting and a small band gap.

Theoretical models based on one-electron theories have been used to describe the cohesive properties, such as lattice constant, crystal structure, elastic constant enthalpy. Valence configurations as well as electronic configurations of the ground state can be deduced by minimizing the total energy. Strong on-site Coulomb repulsions exist among the 4f electrons and the independent particle approximation is no longer valid. Essentially, three models have been largely used. In first, the valence spd electrons are treated in the LDA using the LMTO method in the atomic sphere approximation and the 4f electrons are considered as core electrons. Another model, the SIC-LSDA, that has the advantage of being parameter free, introduces a self-correction term to take into account the 4f electron localization. An alternative model is LDA + U. It corresponds to a Hartree–Fock treatment of the 4f electron configuration with a screened effective U parameter. The essential feature of this model is that the energy functional is orbital-dependent rather than density-dependent. SIC-LSDA has been used to predict the valence of numerous rare-earth compounds [17]. In contrast, densities of states and spectral analysis of electron transitions involving the localized 4f electrons must be described by theoretical models taking into account the many-body effects due to localization of 4f electrons. An approximation has been used in which the energy bands are treated with LDA and additional atomic multiplets are included to describe the localized $4f^n$ configurations. The use of multiplets to describe the 4f levels underlines their atomic character. Agreement was found between this description and photoemission spectra. Further theoretical developments were needed to explain the entire spectroscopic observations. They are discussed in Chap. 3.

When the 4f electrons are treated as core electrons and the valence electrons by LDA, both electron systems are considered as independent. The 4f electrons do not interact directly with the valence electrons because they are concentrated on the core but they contribute to the ion field with which the valence electrons interact. Consequently, interactions exist between them. A model has been developed in which the 4f shell retains its atomic-like character but is coupled to the surrounding solid. This approach is based on the LDA + DMFT method in the LMTO basis set [18]. Taking into account intra-atomic Coulomb interactions, spin–orbit coupling and crystal field effects, a *many-body self-energy* is computed within the Hubbard approximation and inserted into the function describing the solid. That is equivalent

to treating the quasi-localized 4f electrons as quantum impurities. Physical properties for only a few compounds have been calculated up to now with this model. The agreement with the observations is improved compared to the LDA + U approach, where interactions in the 4f shell are described by a self-consistent, orbital- and spin-dependent, one-electron potential. In a one-electron description, either Coulomb interactions or lattice symmetry are minimized while both requirements are satisfied in a many-body treatment of the electron correlations. A usual treatment of the interaction effects in the 4f shell improves the description of the quasi-free valence electrons and thus of the electronic properties.

As already mentioned, a particularity of the rare-earths is that they form mixed valence, or *intermediate valence*, compounds, in which the rare-earth is considered as having two distinct configurations, $4f^n$ and $4f^{n-1}$. In these compounds, an integral number of 4f electrons are present on each ion while the number of ions containing each configuration appears to be a fractional number and the two electron configurations have nearly the same energy. The valence of a divalent metal rare-earth present in a mixed valence compound is equal to $2 + n_f$ where n_f is the participation number of the trivalent configuration. In a mixed valence compound of a trivalent rare-earth, the valence is $3 + n_f$ where n_f is the participation number of the tetravalent configuration.

Initially, the presence of mixed valence was associated with the relation $RE^{2+} \rightarrow RE^{3+} + e^{-}5d$ [9]. All the same, Yuan and others have considered the cerium valence as fluctuating between 3 and 4, with the cerium configuration varying between $4f^1$ and $4f^0$ + (5d6s) electrons. This model predicts a large energy shift of the 4f levels from well below to above the Fermi level and a shift in the opposite direction for the 5d bands. These changes have not been confirmed. The presence of an integral number of 4f electrons reveals a strong 4f localization and only very weak interactions between the 4f and the valence electrons.

In a general point of view, a valence change does not correspond to an excitation or ionization but to a partial *delocalization* of a bound electron by transfer into the valence band. This delocalized electron thus interacts with the other valence electrons. This description is in agreement with the characteristics exhibited at low temperature by some intermetallic compounds where two different regimes exist, one where the 4f electrons are all localized and another where one 4f electron per atom is delocalized and interacts with the valence electrons. Cerium clearly illustrates the double character of the 4f electrons, which can be localized and treated as core electrons or strongly correlated with the valence electrons. Trivalent Ce^{3+} ions of $4f^1$ configuration associated with three 5d6s valence electrons are present in the metal and in a large number of compounds. However, in numerous other solids, tetravalent Ce^{4+} ions are associated with four valence electrons having a partial 4f character. The 4f electron is then partially mixed with the 5d6s valence electrons of cerium. The 4f electrons are localized or not as a function of their level positions with respect to the 5d–6s valence band. Nevertheless, the cerium 4f electron always remains relatively near the ion, due to the characteristics of its wave function. Its mobility is not equivalent to that of the other valence electrons. The dual character

of the 4f electrons is an important factor, that influences the valence, and thereby the physicochemical properties of the cerium compounds.

Many rare-earth compounds are mixed valence compounds and show numerous anomalous physical properties [10, 19]. In these compounds, two local electron configurations are present with nearly the same energy. Thus, a valence change can occur between the divalent and trivalent states for samarium, europium, thulium and ytterbium. As an example of such compounds, let us mention here SmS, SmB_6 and TmSe. A change from insulating to metallic conduction occurs at a low temperature when $n_f \approx 0.8$. In the divalent phase, the ground state is an insulator. Through a first-order transition, its valence changes to a mixed valence phase, which is still insulating. Under pressure, a valence change from divalent to trivalent metallic ions can be induced in the monochalcogenides, SmS and TmSe. This change takes place gradually and stable non-integral valences are observed for a large range of pressures. Discontinuous jumps from one mixed state to another have also been reported. Metallic conduction appears for $n_f \approx 0.8$ at a volume that is rather larger than the volume calculated for a pure trivalent configuration.

The hexaborure SmB_6 is mixed valence type in STP conditions, of the same type as that of SmS [20, 21]. The electronic properties of samarium with valence $v < 2.8$, are characteristic of a divalent rare-earth insulator compound. For $v \geq 2.8$, the physical properties become characteristic of a trivalent metallic compound. The pressure-induced insulator–conductor transition appears around 4–6 GPa while the changes in the magnetic properties appear at a higher pressure. That is because each samarium ion is surrounded by a cage of boron ions and the Sm–Sm exchange interactions remain weak. Differences between SmS and SmB_6 are due to the difference of their crystalline structures, thereby also of their band structures. In SmB_6 [22], the resistivity increases strongly with decreasing temperature up to 4 K but below it, a residual low temperature conductivity still exists. Recent interest has been raised by the observation of metallic surface states [23] (cf. Sect. 4.3).

Change in the atomic environment, in the bonds, or in the cohesive properties can cause a valence change. Under pressure, transformation from a divalent ion semiconductor to trivalent ion metal is generally possible. It depends on the energy gap between the 4f levels and the conduction band and on the rate at which this gap decreases with the pressure. The ionic radius of the trivalent ion is much smaller than that of the corresponding divalent ion and such a volume decrease can induce the delocalization of a 4f electron into the valence band. The analysis of the pressure–volume relationship gives a direct measure of the 4f delocalization, i.e. of the valence change. The theoretical treatment is that of the transfer of a localized electron into the valence band where important relaxation effects must be suitably treated. Conversely, the 4f electrons are pushed toward localization when the distances between rare-earth ions increase, i.e. when the on-site f–f interactions are the strongest. These electronic changes induce large changes in the electrical, optical and magnetic properties. Because of the varied and complex structures of many of the rare-earth compounds, there is no complete theory concerning the $4f^n$ electrons that gives theoretical good predictions of the valence.

2.1.1 Oxides

Oxides are the most wide-spread rare-earth compounds. They form a contamination layer at the surface of the metals resulting from the reaction with the atmosphere. They have important applications in catalysis and in electronics, where they are associated with silicon and semiconductors. All the rare-earths form a sesquioxide, [4] the most stable oxygen compound except for cerium, praseodymium and terbium (Table 2.1). In these compounds, each rare-earth donates three electrons to the bonds with oxygen and the 4f electrons stay strongly localized at the rare-earth site. Three different structures exist, hexagonal for the light rare-earths, cubic or monoclinic distortion of the cubic for middle rare-earths and cubic of bixbyite-type for heavy rare-earths. In the first case, each rare-earth ion is surrounded by seven oxygen ions, of which four are closer. In the cubic or distorted structures, only six oxygen first neighbours are present. Following the well-known lanthanide contraction, the lattice parameters decrease along the series. The crystal lattices of the oxides have low symmetry, for which ab initio electronic structure calculations are not adequate.

Stable oxides with an oxidation number superior to three exist in the light rare-earths and terbium (Table 2.2) [24]. Thus, for cerium, praseodymium and terbium, the stable oxides are, respectively, CeO_2, Pr_6O_{11} and Tb_4O_7. Metastable NdO_2 is also predicted to exist. The number of the rare-earth valence electrons is larger in these compounds than in the metal and, consequently, the number of the localized 4f electrons smaller.

Cerium oxide has a well-known particular property: a continuously ongoing transformation exists between the two oxides, the oxygen-rich CeO_2, or ceria and the oxygen-poor Ce_2O_3, depending on the external oxygen concentration [25]. Indeed, cerium that oxidized completely to (IV) oxide in the presence of

Table 2.1 All the rare-earths form a sesquioxide, the most stable oxygen compound except for cerium, praseodymium and terbium

Metal	Oxides
Ground configuration	
La $(6s5d)^3$	La_2O_3
Ce $4f^1$ $(6s5d)^3$	Ce_2O_3, CeO_2
Pr $4f^2$ $(6s5d)^3$	Pr_2O_3, Pr_6O_{11}, PrO_2
Nd $4f^3$ $(6s5d)^3$	Nd_2O_3, NdO_2
Sm $4f^5$ $(6s5d)^3$	SmO, Sm_2O_3
Eu $4f^7$ $(6s5d)^2$	EuO, Eu_2O_3
Gd $4f^7$ $(6s5d)^3$	Gd_2O_3
Tb $4f^8$ $(6s5d)^3$	Tb_2O_3, Tb_4O_7, Tb_6O_{11}, TbO_2
Dy $4f^9$ $(6s5d)^3$	Dy_2O_3
Ho $4f^{10}$ $(6s5d)^3$	Ho_2O_3
Er $4f^{11}$ $(6s5d)^3$	Er_2O_3
Tm $4f^{12}$ $(6s5d)^3$	TmO, Tm_2O_3
Yb $4f^{14}$ $(6s5d)^2$	Yb_2O_3

Table 2.2 **a** Sesquioxide data. **b** Dioxide data

a

Compound	$E_{IV} - E_{III}$ (eV)	V_{hexag} (Å^3)		V_{cubic} (Å^3)	
	Hexagonal	Theory	Expt.	Theory	Expt.
Ce_2O_3	0.38	76.4	79.4	88.18	87.0
Pr_2O_3	0.78	75.6	77.5	86.77	86.7
Nd_2O_3	0.94	74.0	76.0	85.28	85.0
Pm_2O_3	0.97	72.9	74.5	83.89	83.0
Sm_2O_3	1.09	72.0		82.50	81.7
Eu_2O_3	1.13	70.5		82.14	80.2
Gd_2O_3	1.29	68.8		80.70	79.0
Tb_2O_3	1.12	67.6		79.49	77.2
Dy_2O_3	1.21	66.3		78.62	75.9
Ho_2O_3	1.36	65.2		77.30	74.7

b

Compound	$E_{IV} - E_{III}$ (eV)	V_{theo} (Å^3)	V_{exp} (Å^3)
CeO_2	−2.40	39.61	39.6
PrO_2	−1.44	39.22	39.4
NdO_2	−0.65	39.37	–
PmO_2	−0.18	39.15	–
SmO_2	0.49	42.19	–
EuO_2	2.31	41.87	–
GdO_2	1.22	41.08	–
TbO_2	−0.27	36.50	35.6
DyO_2	0.05	39.65	–
HoO_2	0.46	39.06	–

Sesquioxide data $E_{IV} - E_{III}$ is the energy difference between tetravalent and trivalent ground configurations in electron volts. $V_{hexagonal}$ is the calculated volume in (Å)^3 for this structure and the corresponding experimental volume in (Å)^3. V_{cubic} is the calculated volume in (Å)^3 for the cubic structure and the corresponding experimental volume in (Å)^3 (from [24])
Dioxide data $E_{IV} - E_{III}$ is the energy difference between tetravalent and trivalent ground configurations in electron volts. V_{theo} is the volume calculated for the cubic fluorite structure and V_{exp} the corresponding experimental volume. A negative energy difference indicates that the tetravalent configuration is the more stable one (from [24])

atmosphere, can release oxygen by forming various reduced oxides up to the (III) oxide. Inversely, the stoichiometric oxide, Ce_2O_3, can take up oxygen and return to the (IV) oxide. This reversibility is used for the storage and the transport of oxygen and makes ceria interesting as a catalytic converter.

Concerning the structural properties, one expects that such a reversible addition or removal of oxygen atoms should involve a minimal rearrangement of the cerium ions during the transition. This suggests the presence of a common unit cell for both oxides. Ce_2O_3 has a hexagonal lattice with a c/a ratio equal to 1.55. Stoichiometric CeO_2 has the cubic fluorite structure characteristic of compounds such as CaF_2.

However, it was possible to construct a unit cell of the type Ce_2O_3 from eight unit cells of CeO_2 by increasing their volume by 3 % and removing 25 % oxygen ions along four (111) diagonals [26]. The reversibility of the reduction or oxidation processes is thus established and the reduction–oxidation transition can be described as an almost isostructural transition with a 10 % volume contraction, by analogy with the γ-α transition in pure metal with a volume reduction of about 16 %.

A proper description of the Ce_2O_3 4f electron characteristic is difficult with standard band methods. A good estimate of the magnetic and electronic ground state properties of Ce_2O_3 was obtained using the full-potential LMTO method in the framework of the DFT and by treating simply the 4f electron as localized on the cerium ion [27]. Cerium is therefore close to the trivalent state in this oxide. Ce_2O_3 is antiferromagnetic insulator with a magnetic moment of $2.17\mu_B$ by unit cell [28].[1] As two cerium ions are present in the unit cell, one expects a magnetic moment of $1\mu_B$ from each 4f electron, the difference resulting from the polarization due to the valence electrons. This value of the magnetic moment confirms the localized character of the 4f electron, which, therefore, does not contribute to the bond in the Ce_2O_3 oxide.

Various opposite points of view have been formulated to treat the 4f orbital of cerium in CeO_2. In a first model, the dioxide at the ground state was described as a mixed valence compound with a 4f occupation of about 0.5. A specific mechanism was introduced to explain the coexistence of this model with the fact that CeO_2 is insulator [29–31]. Another model considered cerium as having four valence electrons and the 4f orbital as unoccupied [32]. Other pictures were introduced depending on the occupation of the 4f orbital. From an electronic structure calculation by the LAPW method, the 4f and 5d orbitals in tetravalent cerium were described as hybridized with the oxygen 2p band [33]. The magnetic and electronic properties of CeO_2 were found correctly described when the 4f electron was treated as a valence electron. By opposition to the localized character of the 4f electron in cerium metal at room temperature, the 4f electron becomes delocalized in cerium tetravalent compounds. This characteristic had been observed from spectroscopy experiments, specially designed to determine the localization of the valence electrons (cf. Chap. 4). Some cerium orbitals of 5d and 4f character are mixed with the 2p band of oxygen and form the valence states (Fig. 2.1) [27]. This shows that cerium 4f levels are partially occupied. A very narrow empty band of a 4f character is present just above the Fermi level.

The CeO_2–Ce_2O_3 transition involves a localization–delocalization process of the cerium 4f electron. The reduction of CeO_2 was described as due to the formation of an oxygen vacancy and the localization of 4f electrons on the neighbouring cerium ions. In CeO_2, every oxygen atom is surrounded by four cerium ions. A vacancy of

[1] Antiferromagnetism is due to coupling between spin moments carried by near ions in the solid and it is present below the Néel temperature, i.e. at low temperatures. This atomic description is well adapted to rare-earth compounds because of the presence of incomplete 4f sub shell localized on each rare-earth ion.

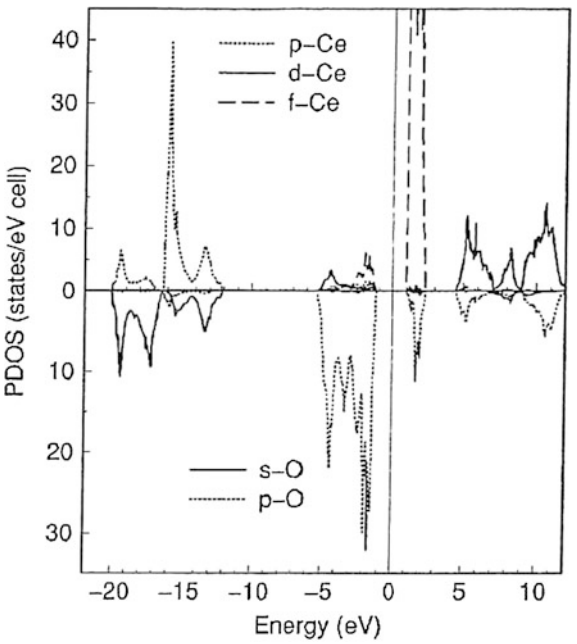

Fig. 2.1 Density of states for CeO_2: *upper part* shows cerium contribution; *lower part* oxygen contribution [27]

oxygen is created when an oxygen atom quits the lattice and leaves other electrons in the vicinity of the vacancy in the lattice. These electrons fill the empty levels of lowest energy, which are the 4f empty ones. Indeed, in CeO_2, narrow empty 4f levels are present in the band gap between the valence and conduction band [34]. Then, electrons are localized on cerium ions in the immediate surrounding of the vacancy and, conversely, a vacancy may be created. The energy for the formation of a vacancy was calculated and it was shown that a minimum energy situation corresponds to two ions Ce^{3+} surrounding an oxygen vacancy [26]. The oxygen vacancy formation depends on the localization–delocalization of the 4f electron in cerium. The localization of the 4f electrons in Ce_2O_3 leads to a volume increase. By analogy with a treatment used for the γ and α phases of the metal, calculations of the electronic, structural and magnetic properties were made for Ce_2O_3 and CeO_2 by considering the 4f electron either as a localized core electron or as being in the valence band [27]. The method used was the full-potential LMTO method in the framework of the LDA–GGA for exchange and correlation. An improved agreement with the experimental data was obtained using the localized model for Ce_2O_3 and the band model for CeO_2. The 4f electron behaves, then, differently according to the different valences of cerium in the compound.

Praseodymium and terbium are also naturally present in several oxidation forms. Praseodymium occurs naturally as Pr_6O_{11}, exhibiting a slightly oxygen-deficient fluorite structure. The stoichiometric fluorite structure PrO_2 exists under oxygen pressure. Terbium behaves as praseodymium: it exhibits an oxygen-deficient fluorite structure Tb_4O_7 and oxidizes, giving the dioxide TbO_2 under oxygen

pressure. Praseodymium and terbium were considered as tetravalent [32, 35] or of mixed valence in these compounds [36, 37]. The REO_2 dioxides have a cubic fluorite structure; each rare-earth has eight first neighbours at a distance a little shorter than the one between first neighbours in the sesquioxides. Consequently, all the rare-earth ions have the same surrounding and their ionic volume is smaller in the dioxides than in the sesquioxides. From this decrease of the ionic volume, one deduces that the number of localized electrons associated with each ion decreases too. It is usual to consider that in all tetravalent rare-earth compounds, the ion RE^{4+} lost one 4f electron with respect to the trivalent ion RE^{3+}. Then, in Pr_6O_{11} and Tb_4O_7, one quasi-delocalized 4f electron is present in the valence band, hybridized with the s–d electrons, while the rest of the 4f electrons of Pr and Tb stay strongly localized at the rare-earth site and their number is integral [24, 38]. In contrast, the number of delocalized electrons is non-integral and these electrons participate in the bonding. The valence band acquires some f character, creating a type of 4f electron that can participate in electron bonding. Theoretically, 4f levels move down into the oxygen 2p band. To conclude, for elements as praseodymium or terbium, which have several 4f electrons, coexistence of localized and partially delocalized f electrons occurs in the dioxide, and more generally, in the tetravalent configuration. This was confirmed by high energy spectroscopy experiments [32, 39].

The two divalent rare-earth metals, europium and ytterbium, maintain their divalent character in some compounds, in particular in the mono-oxides. In YbO, the two Yb valence electrons are transferred into the anion 2p band, which is separated from the conduction band by several electronvolts. The localized 4f orbitals fall in the gap between the valence and conduction bands. YbO is stable under STP conditions. The same is valid for EuO mono-oxide. However, owing to its half-filled 4f shell, EuO is ferromagnetic with a practically complete electron spin polarization. That makes EuO interesting for spin electronic devices [40]. Under pressure, the energy difference between divalent and trivalent ground states of Yb and Eu decreases. Overlap between the 4f and 5d energies induces the formation of a ground state designated as having a mixed valence, obtained from the $4f^n$ and $4f^{n-1}5d$ configurations. High pressures are necessary to induce the 4f–5d energy overlap and transform the divalent rare-earth oxide into a trivalent compound. The transformation takes place gradually and the change is observed through a wide range of pressures. For YbO, the pressure–volume variation shows an anomalous behaviour from about 100 kbar. The volume reaches a lower limit value near 350 kbar for an ytterbium mean valence of the order of 2.6 [41].

Samarium and thulium have also stable divalent oxides. Both metals are trivalent in the bulk because the energy required to displace a localized electron from the 4f level to an extended 5d band state is small. The energy difference between the trivalent and divalent metallic states is only about 6 kcal/mol for samarium. This makes the two valences nearly degenerate and facilitates a valence change for this metal [42]. Thus, at the surface, due to the decrease of the coordination number, samarium has a divalent or partially divalent character. The bonding energy is smaller than in the bulk and the 4f electrons are more strongly bound. Consequently, samarium and thulium frequently appear as divalent in compounds

and SmO and TbO are stable under the SPT conditions. Some other monoxides have been synthesized under high pressure, CeO, PrO and NdO [43].

All the oxides are insulators. This results also from the calculated density of states. They are not ionic compounds and, therefore, the charge density and the valence cannot be directly connected. The densities of states and band structures are similar for all the sesquioxides.

As an example, the densities of states calculated for Nd_2O_3 is presented Fig. 2.2 [24]. The valence band originating from the O-2p and rare-earth 5d–6s electrons is completely filled. An unoccupied 4f level is situated in the band gap above the Fermi level between the valence and conduction band. The latter corresponds essentially to the unoccupied rare-earth d–s levels. The position of the occupied and unoccupied $4f^n$ and $4f^{n+1}$ levels with respect to the band edges is important because they can contribute to the evaluation of the band gap width. If the 4f electrons are more strongly bound than the low-energy valence electrons, the band gap takes place between the valence and conduction bands. However, if unoccupied 4f levels are present in the forbidden band, the band gap is between the valence band and these 4f levels. Finally, if occupied 4f levels are situated above the valence band, the band gap is between these 4f levels and the lower unoccupied levels. According to the position of the 4f levels, the band gap takes place either between the valence and conduction bands or between the valence band and empty 4f levels or between occupied 4f levels and the conduction band. The band gap widths vary with the 4f level positions with respect to the valence and conduction band and, consequently, they vary with the atomic number. For the sesquioxides, the largest band gaps, about 5.5 eV, are associated with the rare-earths having more stable electronic configuration, lanthanum, gadolinium and lutecium. The lowest band gaps, between 2.3 and 4 eV, belong to rare-earths immediately following the two previous ones, namely cerium, praseodymium and terbium. For the rare-earths immediately preceding the more stable, samarium, europium, thullium and ytterbium, the band gaps are slightly bigger than 4 eV while for dysprosium, holmium and erbium, they are of the order of 5 eV. For the rare-earths with a small or medium gap, the 4f levels

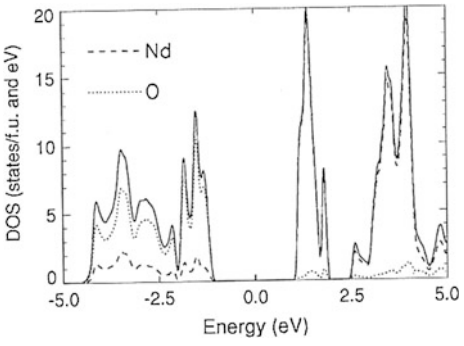

Fig. 2.2 Density of states for Nd_2O_3 in the hexagonal structure: Neodymium is in the trivalent f^3 configuration. The zero of the energies corresponds to the midgap position [24]

are located in the band gap while for a large gap the 4f levels are in the same energy region as the bands. The variation of the band gap value along the series was calculated by considering only the valence and conduction bands and not the 4f levels. Such a calculation is relatively simple, whereas it is complicated to calculate simultaneously the energies of the 4f levels because it necessitates taking into account all the screening and relaxation effects and the use of quasi-atomic model. It should be noticed that the band gap in a thin film is different from the one in the bulk.

Among the applications in microelectronics, there is the possibility to use the dielectric properties of the rare-earth oxides instead of those of SiO_2 in the metal-oxide semiconductor (MOS) electronic devices. In order to increase the performance of these devices, it is necessary to decrease the dielectric thickness of the insulating layer, d/ε, where d is the mechanical thickness and ε the dielectric constant. A high dielectric constant is then a significant condition to be a good candidate for microelectronics, in particular for memory applications [44]. Several rare-earth oxides have a high dielectric constant. Thus, ε is about ten times larger for some sesquioxides, in particular for Sm_2O_3, than for SiO_2. This constant depends on the infrared vibrations, i.e. the crystalline structure [45]. It is higher for structures with the main absorption band at lower energies. Consequently, the light RE oxides of hexagonal structure have higher dielectric constants than the heavy RE oxides crystallized in cubic and monoclinic structures. However, the dielectric constant depends strongly on the conditions of preparation of the sample. Another property, important for an oxide to be usable in MOS electronic devices, is that there should be no interfacial layer between the RE oxide and the semiconductor. As an example, such a well defined interface exists for Pr_2O_3 on Si(111) [46] and Gd_2O_3 on GaAs (100) [47] but generally an interfacial layer cannot be completely avoided.

2.1.2 Chalcogenides

These are, in principle, compounds formed with elements X of the sixth column of the periodic table, X = O, S, Se, Te. However, the term chalcogenide is commonly reserved for the compounds with X = sulphur, selenium and tellurium. Among these, the most studied are the monochalcogenides, of formula RE-X. The electronegativity of the ligand decreases with increasing size, i.e. from oxygen to tellurium. Consequently the ligand p bands move towards lower binding energies. These compounds are semiconductors and have interesting optical, electronic and magnetic properties. In addition to the two divalent rare-earths, europium and ytterbium, two other rare-earths, samarium and thulium, appear in a divalent state in the monochalcogenides. But samarium and europium undergo isostructural transition to intermediate valence state with the pressure. All the rare-earths form mono-sulphides, RE-S and have then a divalent behaviour. The other compounds are expected to be trivalent.

Europium and ytterbium monochalcogenides are stable under STP conditions because divalent rare-earth ions lead to exact charge compensation with divalent

anions. Two valence electrons of the rare-earth, having the s–d character, hybridize with the S 3p electrons and form the valence band. These compounds crystallize in the cubic rock-salt, or NaCl-type, structure. The 4f levels lie in the energy gap between the valence band and the conduction band. The conduction band consists of the rare-earth 5d levels, which are split by the cubic crystal field into lower energy t_{2g} and higher energy e_g levels. From optical absorption, the energy separation between the 4f levels and the conduction band increases in going from the oxide to the telluride.

A NaCl-CsCl-type crystalline transition observed under pressure for the three compounds, EuS, EuSe and EuTe, did not involve a change of the valence, contrary to what is observed for EuO [48]. Valence change is due to the delocalization of one 4f electron per ion into the conduction band and it induces a semiconductor to metal transition. A striking change in the reflectivity has been observed for EuO but not for EuS, EuSe and EuTe. Thus a semiconductor-metal transition occurs only in EuO in the pressure ranges studied. However, from LSDA total energy calculations, europium and samarium chalcogenides showed isostructural transitions into an intermediate valence state with the pressure [49].

YbS, YbSe and YbTe undergo an electronic transition under pressure. Thus, for YbS, near 400 kbar, the mean value of the valence was estimated to be 2.5 [50]. These results are deduced from the experimental pressure-volume data and from optical absorption. The compression curves (Fig. 2.3) [41, 50, 51], show that electronic collapse due to a gradual change in the valence state of ytterbium from two towards three is a continuous function of the pressure in all the ytterbium monochalcogenides. Striking changes in the optical reflectivity are observed above the 200 kbar. YbS, YbSe and YbTe usually of black colour become, respectively, golden yellow, copper-like and purple. These observations confirm the presence of a semiconductor to metal transition at high pressure.

Increase of the valence is easier for divalent samarium and thulium than for europium and ytterbium because the ionization potentials of Sm^{2+} and Tm^{2+} are smaller than those of Eu^{2+} and Yb^{2+} respectively. Thus, all the samarium monochalcogenides can undergo a valence change from divalent semiconductor to trivalent metallic ions. This change is induced by a reduction of the lattice constant under pressure at room temperature [52, 53] or by chemical alloying under SPT conditions [9, 10]. Generally, no change of the crystalline structure accompanies the contraction of the lattice. The valence change observed in the samarium monochalcogenides is associated with a semiconductor to metal transition. This transition is manifested experimentally by the rapid decrease of resistivity with the increase of the pressure. Metallic conductivity is reached under pressure. It is accompanied by a metal-like reflectivity, observed for photons of energy lower than 2 eV [54, 55].

A specially well-known case is the sharp decrease in volume observed in samarium sulphide SmS at 0.65 GPa, due to a first-order phase change. This abrupt change is isostructural and reversible when the pressure decreases below 0.1–0.15 GPa. The crystalline arrangement remains NaCl-type up to very high pressures. At 1 GPa, the volume decrease is about 15 %. Compressibility also decreases with decreasing lattice constant and shows an abrupt reduction at 0.65 GPa. This

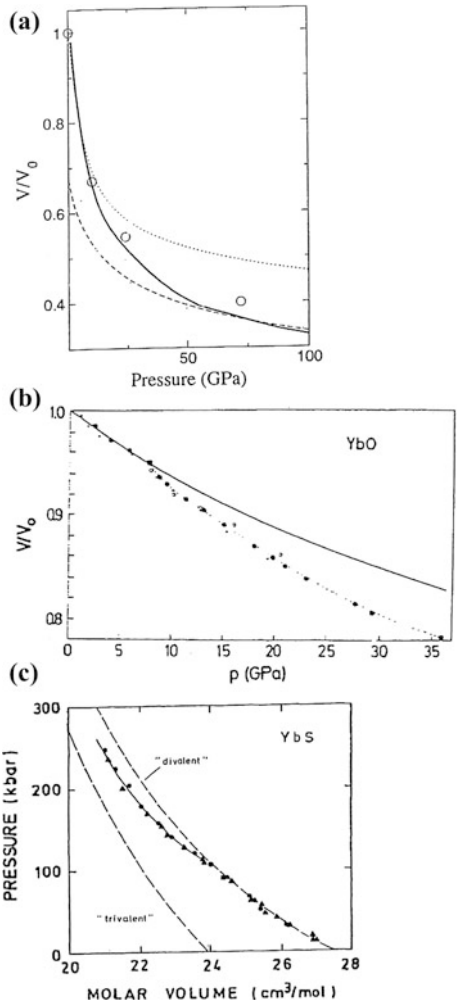

Fig. 2.3 Comparison of the volume-pressure relations: **a** for fcc Yb metal: experiment (*full line*), isothermal equation of states for divalent (*dotted line*) and trivalent (*dashed line*) [51]; **b** for YbO: experiment with or without medium pressure (*point*), calculated (*solid line*) [41]; **c** for YbS: experiment (*closed circles and triangles*), pressure-volume relations (*dashed lines*). Near 400 kbar, the mean value of the valence was estimated to be 2.5 [50]

large volume decrease under pressure triggers a valence change of samarium ions from Sm^{2+} to Sm^{3+}. Under SPT conditions, SmS is a mixed valence-type compound. Abrupt decrease in resistivity by a factor of 5 is observed at 0.65 GPa and transition to the metallic state takes place above 2 GPa. From spectroscopy experiments divalent f^6 ions are present in the ground state and mixed f^5–f^6 ions in the high-pressure metallic phase [56, 57]. The pressure-induced semiconductor to metal transition has been observed from measurement of the optical reflectivity [58]. SmS was found to be opaque to photon radiation of energy higher than 0.37 eV under pressure. Semiconductor to metal transition has also been observed after polishing of the surface of a SmS semiconductor crystal. This treatment is considered as the first phase of a pressure effect. The valence transition is evident from the change of the surface. Black semiconductor at STP conditions, SmS

exhibits after polishing or under pressure a golden yellow metallic coloration [59]. The valence transition takes place at relatively low pressure in this compound because the levels of Sm^{2+} associated with the $4f^6$ ground configuration are located only 0.2 eV below the conduction band [60] whereas this distance is about 1.6 eV for EuS. Valence transitions can also be obtained by alloying with trivalent ions such as Y, La, Ce and Gd.

For SmTe and SmSe, the resistivity decreases by about seven orders of magnitude between 0 and 6 GPa and the $4f^n$–$4f^{n-1}$ transition takes place in a continuous manner over a broad pressure range at room temperature. Strong reduction of the volume is observed. For SmTe, as for SmSe, a crystallographic transition from NaCl-type to a tetragonal structure, equivalent to a distorted CsCl structure was also observed around 11 GPa and for PrTe around 9 GPa. Volume discontinuities accompany these transitions and both phases are present over a large pressure range [61]. There is complete delocalization of one 4f electron and conversion of Sm^{2+} to Sm^{3+}. This behaviour is contrary to that seen for europium because the $4f^6$ sub shell of Sm^{2+} is weakly bound whereas the half-filled $4f^7$ shell of Eu^{2+} is very stable. SmSe and SmTe exhibit under pressure the same changes of coloration as YbSe and YbTe, i.e. a copper-like metallic coloration for SmSe and a deep purple one for SmTe. The energy gap between the 4f levels and the conduction band decreases in going from SmTe to SmSe then to SmS. This variation of the energy gap is in the same direction as the variation observed in the Eu chalcogenides. In contrast, the valence transition of samarium is abrupt in SmS while it is gradual in SmSe and SmTe. This is related to the decrease of the lattice constant with pressure, which is much more pronounced in SmS than in SmSe and SmTe, leading to a discontinuous adjustment and to first-order structural transition. There exists, therefore, a critical inter-atomic distance between the Sm ions which governs the process.

Theoretical studies of the samarium monochalcogenides have been made by using models described in Chap. 1. Conventional band structure calculations cannot be used because they describe the 4f levels as narrow bands. Only models treating the 4f electrons as localized can be considered. Total energy calculations have been made with the help of the SIC-LSD approximation associated with the LMTO method in ASA. The spin–orbit interaction is included in the Hamiltonian [62]. In this scheme the s–d electrons are described as delocalized and either 5 or 6 localized 4f electrons are considered on each samarium ion, corresponding to a trivalent or divalent samarium ion, respectively. From total energies per unit cell volume calculated for the $4f^6$ and $4f^5$ configurations of SmS, it is seen that a configuration of mixed character appears with increasing pressure (Fig. 2.4) [62]. At high pressure, the $4f^5$ configuration is stable. As shown from calculated densities of states, this f^6 to f^5 valence transition is made possible because the $4f^6$ energy levels are energetically very near to the conduction band in the SPT conditions.

In summary, in the samarium chalcogenides, reduction of the lattice constant induces a gradual diminishing of the energy gap until it vanishes, an energy decrease of the 4f level energies and a delocalization of one 4f electron into the

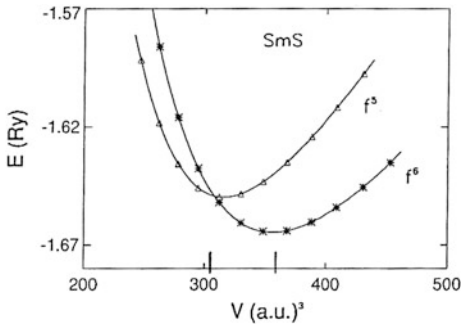

Fig. 2.4 SmS: SIC-LSDA total energy calculated as function of unit cell volume; the position of the minimum of the f^6 *curve* gives an equilibrium lattice constant in STP conditions, 11.25 a.u., in agreement with the experimental value [62]

conduction band, leading to a transition from semiconductor to metal. The probability of the ensuing valence change depends on the matrix elements connecting the localized and extended states. Except for SmS, these transitions are continuous. Stable non-integral valence values are observed over a large pressure range [63]. For SmS, the valence change is abrupt and the reverse metal to semiconductor transition thermally induced is also observed, for example in thin films [64]. In this case, the number of the 4f localized electrons increases. A significant charge transfer is imposed on the system, its energetic cost being balanced by the gain in the localization energy. When SmS becomes metallic, its magnetic properties change from paramagnetic to magnetic. This transformation also is reversible. The above variations are due to the Sm–Sm exchange interactions.

The properties of thulium monochalcogenides vary with the ligand. TmS appears to be a metallic compound at ambient pressure where thulium is trivalent [65]. Its resistivity shows a Kondo-like behaviour [66]. TmSe is a mixed valence compound, with a valence between 2.5 and 2.7. TmTe is a divalent semiconductor [67]. The experimental values of the lattice constants confirm that the valence is 3 for TmS, 2.75 for TmSe and 2 for TmTe, showing a trend towards a greater 4f localization with the increase of the ligand size. Agreement between the lattice constant value calculated in the SIC-LSD approximation and its experimental value was obtained by describing TmS and TmSe with the help of a localized $4f^{12}$ configuration while TmTe is characterized by a localized f^{13} configuration (Fig. 2.5) [68]. The level distribution calculated for the localized $4f^{12}$ configuration consists, in addition to the twelve localized 4f electrons, of a narrow band partly occupied having a 4f character, located just at the Fermi level. This description fits well TmSe, which is known as a mixed valence-type compound. But, this one-electron theoretical model does not give a correct value for the total energy of the f^{13} configuration. Agreement with the valence values has also been obtained from spectroscopic experimental results (cf. Chap. 4). The valence variation reveals an increase of the localization with the increase of the lattice constant, i.e. with the increase of the ligand size. In TmTe under pressure at room temperature, semiconductor to metal transition takes

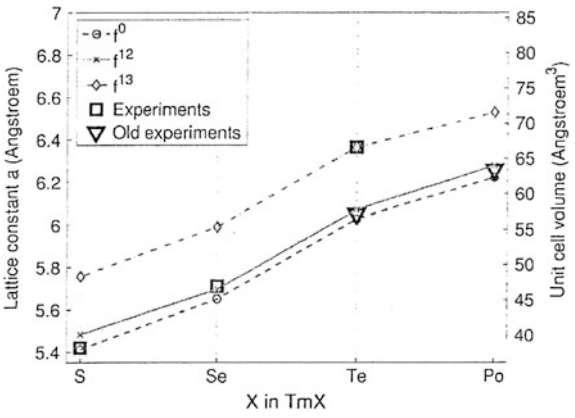

Fig. 2.5 Calculated and experimental lattice constants for Tm chalcogenides [68]

place [69]. This transition is ascribed to the gap decrease and the transfer of 4f electrons into the valence band as this band moves to lower energies and crosses the 4f levels. Finally the gap vanishes above 6GPa and one 4f electron per Tm ion is delocalized into the 5d–6s band. This change of Tm^{2+} to Tm^{3+} results from the decrease of the atomic volume under pressure. In addition, a crystallographic transition from the NaCl-type structure to a tetragonal phase was observed at 8GPa [70].

One of the very first LDA + DMFT calculations was for the mixed valence 4f material TmSe [71]. Energy difference between divalent and trivalent configurations was calculated for the metals [6]. The same method was used to calculate the energy differences between the di- and trivalent samarium and thulium chalcogenides as a function of the pressure [60]. An analogous curve was also obtained for the rare-earth sulphides, showing its universal character (Fig. 2.6) [72].

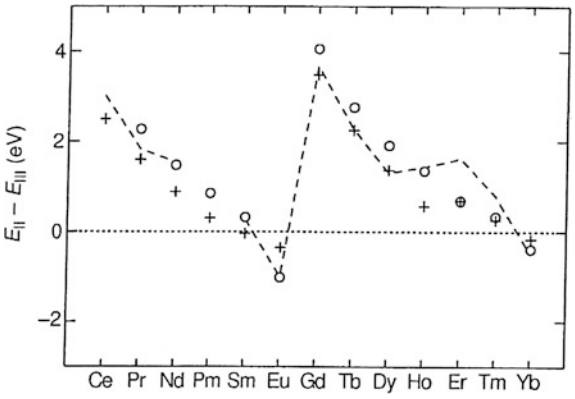

Fig. 2.6 Energy difference in eV between the divalent and trivalent states: experimental values for the rare-earth metals (*dashed line*); calculated values for the metals (*open circles*) and for the sulphides (*crosses*) [72]

From this curve, the divalent to trivalent energy difference is large and positive in the beginning of the series and the trivalent state is predominant. The energy difference drops and becomes negative for Eu and for SmS and EuS. A large jump to positive value occurs at Gd and GdS, which are trivalent. Then the difference gradually falls and becomes negative again for Yb metal and sulphide. Thus a trend to a divalent configuration exists for the heavy chalcogenides under SPT conditions. However, the trivalent ground configuration prevails in a large number of compounds. Calculations of energies as a function of lattice parameters for relevant valence configurations were generalized for numerous materials by using the SIC-LSDA. The calculated values of the lattice parameters in the ground state configuration are within about 1.5 % of the experimental values.

The sulphides constitute a special category of the chalcogenides. Thus, the mono-sulphides RE-S exist for all the rare-earths. They are the monochalcogenides for which the bond between the rare-earth and ligand is strong. Then, the bond strength decreases with the increasing volume of the X element, i.e. down column VI of the periodic table. The valence band is composed of the S 3p electrons hybridized with two valence electrons of the rare-earth. The divalent phase predominates. The rare-earths are divalent and the number of the localized 4f electrons increases. The calculated lattice parameters are compared to their experimental values in Fig. 2.7 [17]. The agreement is good and the calculations reproduce well the sudden increase of the lattice parameter at SmS, EuS and YbS, which accompanies the increasing of the 4f electron localization. It was shown that the

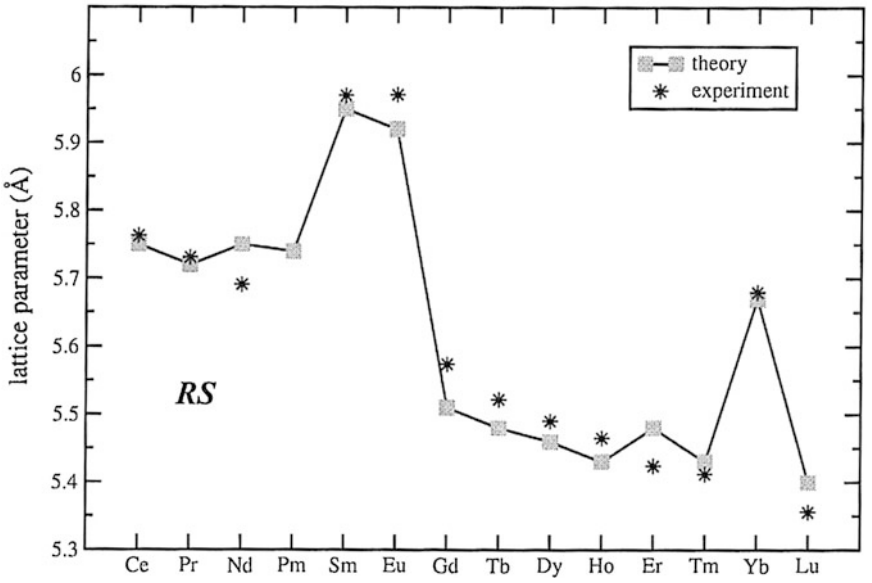

Fig. 2.7 Lattice parameters of the rare-earth sulphides: comparison between values calculated in the ground state configuration and experimental data [17]

energy difference between the valence band and the conduction band is constant throughout the series but that the position of the $4f^n$ energy levels with respect to the conduction band changes along the series. From LaS to NdS and GdS to ErS, the transfer of a 4f electron into the conduction band leads to metallic behaviour, while for EuS and YbS, the $4f^n$ levels are well below the conduction band, resulting in semiconductor-like behaviour. For SmS, the $4f^n$ levels are situated very close to the conduction band and the material can vary between metallic and semiconducting phase under critical perturbation. Thus, under pressure, the bottom of the conduction band overlaps the 4f levels, causing each Sm^{2+} ion to yield one electron to the conduction band and become Sm^{3+}. The material undergoes a discontinuous isostructural transition to a metallic phase. This transition has also been observed in thin films, the pressure effect being replaced by a polishing effect. Reverse metal to semiconductor transition can be induced by relaxing the perturbation. This has been realized by heating, i.e. by thermal lattice expansion of the metallic phase, for films whose thickness varies between 50 and 800 nm [64]. This thermal expansion decreases the crystal field splitting until the bottom of the 5d conduction band rises above the 4f levels.

The rare-earth sulphides, unlike the other chalcogenides, are refractory solids. They are thermally stable with high melting points and are mechanically strong with moderate expansion coefficients. Their electronic properties and infrared transmission characteristics made them good candidates for numerous applications. Changes in the structural and electronic properties induce changes in the electrical conductivity. When the material undergoes a high-pressure structural change, it displays a higher conduction state. This change of the conductivity can be of several orders of magnitude. Thus, the high-pressure phases of SmS exhibit electrical resistivities of about 10^{-4} Ω cm, i.e. smaller by two orders of magnitude than in the SPT conditions. The sulphides can be used as switching circuit devices. If they undergo an irreversible structural change, they can be used as memory switching devices. Owing to their high thermal stability and the existence of compound series of the form $RE_{3-x}S_4$ with optimal thermo-electrical parameters, the rare-earth sulphides can be used as efficient high-temperature materials for thermoelectric energy converters [73]. Among these sulphides, GdS_{1+x} has the highest thermo-electrical efficiency [74].

The optical properties of sulphides originate from the weak RE-S bonds, giving rise to characteristic low vibrational frequencies and resulting in an infrared absorption cut-off. Consequently, the cubic sulphides are transparent in the long wavelength spectral region, in contrast to the oxides. The excellent far-infrared transmission of the rare-earth sulphides together with their glass-forming ability make these materials very good candidate for far-infrared glasses. Mixed with other glass-forming materials, such as gallium, germanium or arsenic sulphides, rare-earth sulphides form systems that are more thermally stable than the other chalcogenides glasses, with transition temperatures higher than 500 °C. Their optimal thermal and mechanical properties, high melting points, high hardness, make them useful in harsh environmental conditions, in particular aerodynamic heating, thermal shock and rain erosion. Associated with their high transmission in

the far-infrared region (3–5 μm), these glass sulphides can play a major role in equipments deployed on aircraft and guided weapons, such as optical windows for heat-seeking missiles, surveillance equipment alerting devices, sensing low temperature objects. Doped with Nd^{3+}, the rare-earth sulphide glasses show fluorescent properties and are good candidates for laser applications. The crystallization of amorphous glasses requires high temperatures and leads to sulphide ceramics that are mechanically and thermally resistant materials with good optical transmission. Chemical processing of the rare-earth sulphides is complex and their extreme affinity for oxygen makes their production difficult. However, because of their useful properties both in the amorphous and crystalline state, rare-earth sulphides emerge as promising optical systems.

2.1.3 Pnictides

These are the compounds formed with the elements of the fifth column of the periodic table, X = N, P, As, Sb, Bi. The X atoms have three unoccupied p-orbitals and can accommodate three electrons from the rare-earth, resulting in a filled hybridized valence band. The rare-earths are in a trivalent state in these compounds, with the exception of cerium, which is tetravalent in CeN. The difference of rare-earth valence between pnictides and chalcogenides is due to the difference in the occupation of the ligand p-orbitals. Pnictides, as chalcogenides, crystallize in the simple rock-salt, or NaCl-type, structure, except EuAs, EuSb and EuBi. The lattice constants of the monopnictides increase from N to Bi and decrease from La to Yb. This variation is explained simply by the increase of anion sizes and the decrease of cation sizes with the increase of atomic number. Pressure can induce structural phase transition of the monopnictides from NaCl structure to a tetragonal structure, which may be considered as a distorted CsCl structure. Change in the lattice parameter can be accompanied by a valence change. Consequently electronic structures and physical properties of these compounds are sensitive to external pressure, strain, impurities. Pnictides, as chalcogenides, have been very widely studied because they offer a wide range of applications and they crystallize in a simple cubic structure, facilitating the theoretical studies [75].

The rare-earth pnictides are semiconductors or semimetallic. The energy gap is between the valence band and the rare-earth unoccupied 5d levels. Overlap between these distributions can give rise to a small density of states. The light rare-earth pnictides tend to have a larger energy gap than the heavy pnictogen compounds because the metallic behaviour increases with decreasing ligand electronegativity. The variation of the energy gap along the rare-earth series is not well defined. However, the energy gap appears to decrease with increasing rare-earth contraction [17]. High values of the dielectric constant are associated with these small values of the gap. These compounds have a large variety of electronic and magnetic properties. The magnetic interactions gradually increase from lanthanum to gadolinium, then decrease from gadolinium to lutecium. Strong exchange interactions exist

between localized 4f electrons and valence electrons and can lead to possible changes of the electronic properties in the presence of an external magnetic field. Most monopnictides are antiferromagnetic in the ground state with some exceptions among the phosphides and especially the nitrides, which are ferromagnetic. A combination of ferromagnetic and antiferromagnetic configuration is also present. Some monopnictides are expected to be half-metallic ferromagnets.

Initially, the 4f electrons were treated as part of the core and the other valence electrons in a band model. Gadolinium monopnictides have been particularly investigated because gadolinium is situated in the middle of the rare-earth group and the Gd 4f orbitals are exactly half-filled. The ground state of Gd^{3+} is $^8S_{7/2}$, where the orbital angular momentum is zero. Under such symmetric conditions the contribution of the spin–orbit interaction and that of the f–p and f–d electrostatic interactions to the Hamiltonian are small, greatly simplifying the problems associated with the electronic structure. The energy distribution of the valence electrons has been calculated by using an APW method with Slater Xα exchange potential [76]. GdN was found to be a semiconductor and the other Gd monopnictides semimetallic. However, it was remarked that by taking into account the exchange interaction, the characteristics of GdN could be different. A model that treats the 4f electrons as core electrons but uses the LMTO method within the LSDA for the valence electrons was applied to cerium, praseodymium and neodymium antimonides [77], then to the gadolinium and erbium pnictides [78, 79]. Concerning these compounds, it was expected that a narrow set of occupied 4f levels would be present several eV below the Fermi level with a narrow set of unoccupied 4f levels several eV above it. Interactions between the 4f multiplets and the bands located in the neighbourhood of the Fermi level were expected to be weak and were neglected. In this model, large overlap exists between valence levels of the rare-earth and pnictogen and the valence band is formed from three pnictogen np orbitals bonding with a rare-earth sd-like band. The conduction band is formed from five bands mainly rare-earth 5d-like, antibonding with pnictogen np orbitals. Gradual increase of the metallic character from N to Bi appears in all the compounds. From the calculated bands, the nitrides have a small gap while the phosphides and arsenides are *semimetals*, i.e. have "holes" in a region of the Fermi surface and electrons in another. This situation is due to fact that the lowest rare-earth 5d band dips below one of the pnictogen np orbital. These calculations concern the non-magnetic case and the perfect solid.

Treatment considering the 4f electrons as core-like electrons was found to be valid for numerous purposes. It provides lattice constants in good agreement with experimental values confirming that the 4f electrons are not significantly involved in the bonding in these compounds (Table 2.3) [79]. It accounts well for the major features of the electronic structure and magnetic properties of this family of materials. In particular, it leads to a semimetallic band structure of the pnictides, accompanied by a possible transition to semiconductors for the nitrides, in agreement with the experiment.

From calculations treating the 4f electrons as localized and not as valence electrons, the praseodymium monopnictides are predicted from LDA + U

Table 2.3 Theoretical and experimental equilibrium lattice constants in (Å) [79]

Compound	a (Å), theor.	a (Å), exp.
GdN	4.977	4.999
GdP	5.704	5.729
GdAs	5.843	5.854
ErN	4.789	4.839
ErP	5.557	5.595
ErAs	5.700	5.732

Table 2.4 Experimental lattice constants in (Å) compared to values calculated in the NaCl-type phase for pentavalent (f^0) and trivalent (f^2) praseodymium (from [81])

Compound	$a(f^0)$ (a.u.)	$a(f^2)$ (a.u.)	a (Expt.) (a.u.)
PrP	10.87	11.13	11.15 [17]
PrAs	11.06	11.43	11.34 [18]
PrSb	11.79	11.99	12.00 [19]
PrBi	11.99	12.14	12.21 [28]
PrS	10.66	10.86	10.83 [28]
PrSe	11.10	11.26	11.23 [28]
PrTe	11.75	11.92	11.93 [28]

calculation to be semimetals with the occupied 4f levels situated about 4 eV below the Fermi level [80], in agreement with spectroscopic results. The effects of pressure on the stability of the NaCl and CsCl phases of praseodymium pnictides and chalcogenides were investigated by using SIC-LSD method and by treating the 4f electrons as localized or itinerant [81]. Under SPT conditions, all the compounds have the NaCl structure. The lattice constants calculated by considering two localized 4f electrons in praseodymium are in good agreement with experimental values (Table 2.4). PrP reveals a crystallographic transition from NaCl-type to distorted CsCl around 26 GPa with a volume collapse of 12.1 % [82]. Similar structural transitions were observed in PrAs, PrSb and PrBi at pressures of 27, 13 and 14 GPa, respectively. These experimental observations are in agreement with the structural transitions expected at 16, 12, 8 and 8 GPa, respectively, for PrP, PrAs, PrSb and PrBi. The pressures predicted to induce the change of the lattice constants are lower than the experimental ones but the experimental and calculated volume reductions are similar. The praseodymium ion remains in the trivalent configuration through the transition and the calculated lattice constants are in agreement with the experimental data.

Calculation for NdSb, and also PrSb, treating also the ions as trivalent and the 4f orbitals as localized, gave good agreement with experiment both for the specific heat and for the photoemission spectrum [77]. Europium and ytterbium, generally divalent, undergo a valence change and are trivalent in the monopnictides. Samarium ion is $4f^5$ in the monopnictides, which are antiferromagnetic with very low Néel temperatures (Table 2.5) [62] while the $4f^6$ ion or mixed valence is present in the chalcogenides, which are non magnetic. The interval $4f^5$–$4f^6$ decreases strongly for the heavier pnictide ligands. From total energies calculated by the

Table 2.5 Experimental lattice constants in (a.u.) compared to values calculated in the NaCl structure with ground state configuration of f^5 for the pnictides and SmO and of f^6 for the other chalcogenides (from [62])

Compound	Lattice constant (a.u.)	
	Calc.	Expt.
SmN	9.46	9.52
SmP	10.99	10.88
SmAs	11.18	11.16
SmSb	11.90	11.84
SmBi	12.14	12.01
SmO	9.41	9.34
SmS	11.25	11.25
SmSe	11.70	11.66
SmTe	12.43	12.46
SmPo	12.64	12.71

SIC-LDA method for the trivalent rare-earth ions, the equilibrium lattice constants have been deduced for all the monopicnides except the cerium compounds and they agree within one percent with experimental values. A comparison between the experimental and calculated lattice parameters is presented in Fig. 2.8 [17] for all the rare-earth monochalcogenides and monopnictides.

The experimental values are plotted along the x-axis and the calculated values from SIC-LSDA along the y-axis. All the data are approximately on the $x = y$ line and that is a measure of the agreement between theory and experiment in the determination of crystalline data. The difference between calculated and experimental values is ≤1.5 % except for CeN and DyTe. Concerning CeN, this anomaly can be explained by the unusual behaviour of the 4f electrons, described below.

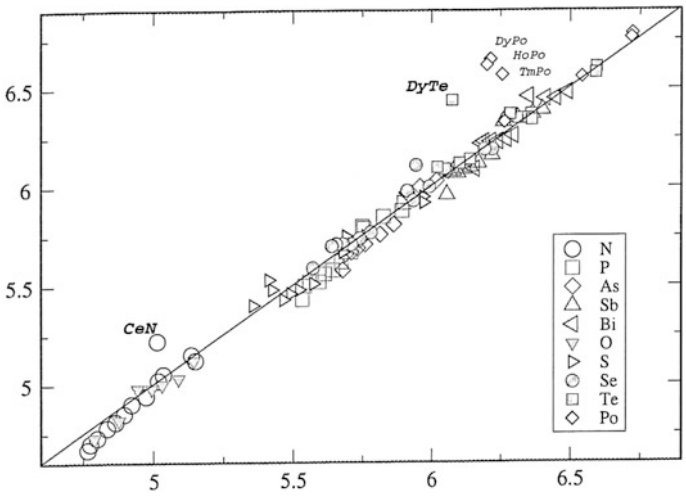

Fig. 2.8 Experimental and calculated lattice parameters (in Å) of the rare-earth monochalcogenides and monopnictides [17]

Therefore, crystallographic data can be predicted with a sufficient precision from the SIC-LSDA model provided the 4f electrons be considered as localized.

Intensive theoretical studies have been made for ErAs because of its technological interest. Calculations based on the LDA and treating the 4f electrons as atomic core electrons correctly obtained a semimetal and the theoretical 4f multiplet structure agreed with photoemission experiments [78, 79]. However, this treatment did not give a sufficiently accurate description of the electronic structure of ErAs near the Fermi level. A new theoretical model has been developed recently. It uses a many-body model to treat the interaction of the 4f electrons with the crystal field and with an external magnetic field [83]. The Slater integrals have been deduced from optical measurements on erbium ions embedded in a rock-salt LaF_3 host. Agreement has been obtained between prediction and experiment for the densities of states near the Fermi level, in particular the repartition of the holes and the electrons. Nevertheless, it must be underlined that possible hybridization between the valence band and 4f orbitals located near the Fermi level is to be expected from the calculations, contrary to the idea that the 4f electrons are thought to be localized.

The peculiar behaviour already found in cerium metal and in some compounds is manifested also in CeN. The observed lattice constant of CeN is 5.007 Å at 4.2 K, 5.019 Å at room temperature, while the calculated value for pure trivalent CeN is 5.24 Å. From an interpolation between the lattice constants of LaN, PrN and NdN, the valence of CeN at room temperature was expected to be 3.46. Three valence electrons of the cerium are present in the valence band mixed with the N 2p electrons. The additional electron of cerium is a localized 4f electron in Ce^{3+}. In Ce^{4+}, this is a delocalized electron [7]. It was, then, suggested that CeN was a mixed valence compound [8] and the additional electron fluctuated between the d and f symmetries. In this model, the 4f levels are considered as located at the vicinity of E_F. However, the energy difference between the f^0 and f^1 configurations is much larger than the hybridization energy. Moreover, the lattice constant calculated by assuming itinerant 4f electrons was 4.91 Å, i.e. relatively close to the experimental value [84]. This result suggested that CeN was not a mixed valence compound. It was, then, considered as a narrow band compound [85, 86]. The cerium 4f levels were treated in a band model. Calculation of the lattice constant was used as a test. From relativistic calculations using LMTO method in the GGA, a value of 5.04 Å was obtained [87]. It is very close to the experimental value. The lattice constant calculated by treating the 4f electron in a band model is thus in better agreement with the anomalously small experimental value than the value obtained by considering localized 4f orbitals. Comparison between experimental and calculated optical reflectivity spectra showed that agreement is good if the 4f electron is treated as itinerant (Fig. 2.9) [87]. These results show that the on-site Coulomb repulsion is strongly screened in this compound resulting in unusual situations of the 4f electrons in CeN under SPT conditions.

In CeN at $T > 1200$ K, cerium becomes trivalent. It is also trivalent in CeP [88], CeAs and CeSb [89] under SPT conditions. These compounds are semimetallic. The 4f electron is localized and the 4f levels are located a few eV below E_F. From

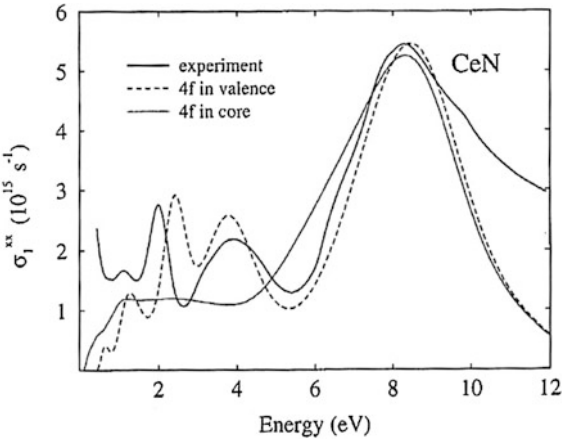

Fig. 2.9 Comparison between calculated real part of the optical conductivity and experimental data for CeN. The calculations are made assuming the 4f electrons as being core electrons or as forming a band [87]

LSDA + U calculation, in CeSb, the Ce 4f levels were found 2 eV below the Fermi level and energetically mixed with the Sb p bands. Anomalous volume contraction was observed in CeP at a pressure of 100 kbar [88]. Valence modification was seen in CeAs and CeSb at low temperatures [89]. More recently, extensive theoretical studies on high-pressure behaviour of cerium pnictides and their electronic structure have been carried out by using the SIC-LSD approximation [90]. Structural phase transition from NaCl to CsCl was shown to occur in parallel with a localized to delocalized transition of the 4f electrons. Consequently, a proper description of the 4f electrons is difficult in the cerium compounds because the on-site electron repulsion, or Hubbard U, is high compared to the bandwidth and these systems are strongly correlated [91, 92]. Nevertheless, the calculated lattice constants are in agreement with the experimental data.

In summary, from calculation methods such as LSDA + U, the positions of the occupied and unoccupied 4f levels have been found several eV below and above the Fermi energy, respectively, in agreement with experiments. The origin of the semimetallic properties in the rare-earth monopnictides was explained by the close proximity of the unoccupied rare-earth 5d states to a point of high symmetry of the Brillouin zone. On the other hand, the metallicity of the rare-earth pnictides was found to increase gradually from N to Bi. Thus, it was showed experimentally from high-quality stoichiometric samples that GdN was ferromagnetic semiconductor and GdP, GdAs and GdSb antiferromagnetic semimetals [93, 94]. However, metal-semiconductor transition observed in some rare-earth pnictide compounds or alloys might be due to impurity doping, temperature or pressure effects, thus explaining the eventual disagreement between predictions and experimental results. Moreover, the uncertainty remained on the electronic structure of GdN because of the spread of the obtained results.

Particular attention must then be given to the rare-earth nitrides, which have been studied specially because of their interesting magnetic properties. Most of them are ferromagnetic with Curie temperature extremely low, of a few degrees

Kelvin. Indeed, the electron exchange splittings of these compounds are significantly larger than those of arsenides and phosphides. This can be explained by a difference in the character of bonds. The latter have a weaker metallic character in the nitrides and the overlap between the orbitals is smaller, predicting these compounds generally to be semiconductors. GdN has been the subject of an intense controversy. Its strong ferromagnetism was explained theoretically [95]. But from resistivity measurements, it was determined to be either semimetallic [96] or insulator [97]. Conductivity was also observed in the presence of nitrogen vacancies. The same equivocal results were obtained theoretically; however, these predictions concerned the non-magnetic case. The smallness of the gap suggested that it would disappear in the magnetic phase. This could be expected for GdN because the exactly half-filled 4f shell makes this material particularly sensitive to magnetic exchange interactions. Spin-polarized ab initio calculations using the LMTO method within LSDA and treating the 4f electrons as localized core-like electrons with various spin orientations were performed [79]. From this model, GdN was found to be semiconductor in the paramagnetic phase and in the minority spin channel of the ferromagnetic phase whereas it was metallic in majority spin channel of the ferromagnetic phase. It appeared thus as being a half-metal. In contrast, with the same theoretical treatment, ErN was found to be a semiconductor in both phases. However, in another theoretical description, GdN was predicted to be a narrow indirect band gap insulator [98], in agreement with the experimental results. The electronic structure of this nitride still remains inscrutable.

Systematic calculations of the thirteen rare-earth nitrides from CeN to YbN were then performed by using the SIC-LSDA methodology [99–101]. From these calculations the rare-earths are trivalent in the mononitride ground state, except for cerium which is tetravalent. These rare-earth nitrides display a wide range of electronic properties, despite their equal structure and similar lattice constants. In the ground state calculations, TbN, DyN and HoN were found to be narrow gap insulators and CeN, ErN, TmN and YbN metallic in both spin channels, while PrN, NdN, SmN, EuN and GdN were found to be half-metallic ferromagnets. From more recent calculations by LSDA + U method [75, 102, 103], GdN has also been predicted to be half-metallic with a gap about 0.5–0.6 eV at the ground state. The occupied 4f levels are expected about 6 eV below the Fermi level and the unoccupied 4f levels about 5 eV above, in agreement with the experimental results. The change of the magnetic order from ferromagnetic in GdN to antiferromagnetic in the other pnictides is a result of the increased ionic radius of the ligand. As the exchange parameters depend strongly on the lattice constant, large changes of the electronic and magnetic properties is expected upon applying stress or by doping impurities. Thus, changes in the conductivity are associated with volume increase and GdN is expected to undergo a phase transition from half-metallic to a semiconductor with lattice expansion. Reduction of the exchange parameters with increasing volume also suggested a decrease of the Curie temperature of GdN with an increase in lattice constant. According to the quasiparticle self-consistent GW method, GdN has also been predicted to be very near a critical point of a metal–insulator transition [104].

Other calculations of electronic structure for all the rare-earth nitrides have been made from the LSDA + U approach in the full-potential LMTO model [105]. Magnetic moments were employed as a validity test. They are given in Table 2.6 [105]. The 4f spin magnetic moments are almost an integral number depending on the number of 4f electrons. The 4f orbital magnetic moments are comparable to the spin moments. Orbital and spin moments are opposite in the first half of the series and parallel in the second half, thus obeying Hund's third rule. The magnetic moments of the d and valence electrons compensate approximately. A quasi-zero total magnetic moment is obtained for SmN. This explains why SmN is not ferromagnetic; it was suggested that it is anti-ferromagnetic at the ground state. Concerning the electronic structure, CeN and EuN are metallic. The other light members of the series, with the exception of NdN, are found to be semimetallic in the majority spin channel only; they are thus half-metals. The heavier members of the series from gadolinium, but also NdN, show semiconducting behaviour. It was suggested that the gap had a tendency to increase through the series. But these suggestions depend on the choice of U_f. The value of U_f used for each rare-earth is equal to the radial Slater-Coulomb integral F^0, obtained from Hartree–Fock calculations. Fitting of the calculated values was made only for GdN using accurate photoemission data obtained for this compound. As the values of U_f increase going from lanthanum to ytterbium, the 4f orbitals are pushed away from the Fermi level, both below and above. The energy interval between occupied and empty 4f levels increases along the series. Except for the cerium compounds, the 4f electrons are

Table 2.6 Experimental and calculated lattice constants a compared

	a (Å)		$m_f^{\sigma}(\mu_B)$	$m_f^{L}(\mu_B)$	$m_d(\mu_B)$	$m_N(\mu_B)$
	Expt.	Theory				
LaN	5.30	5.38	0	0	0	0
CeN	4.87	4.90	0	0	0	0
PrN	5.17	5.29	−1.96	−4.87	0.049	−0.077
NdN	5.15	5.24	2.96	−5.88	0.062	−0.084
PmN[a]		5.19	3.96	−5.88	0.089	−0.140
SmN	5.04	5.10	4.91	−4.85	0.105	−0.136
EuN	5.00	5.14	5.96	−1.61	0.087	−0.129
GdN	4.98	5.08	6.93	0	0.081	−0.083
TbN	4.92	5.05	5.93	2.96	0.066	−0.083
DyN	4.90	5.03	4.95	4.96	0.064	−0.065
HoN	4.87	4.98	3.95	5.94	0.040	−0.026
ErN	4.83	5.00	2.97	5.93	0.032	−0.027
TniN	4.80	4.90	1.98	4.88	0.020	−0.013
YbN	4.78	4.79	0.99	1.54	0.006	0.046
LuN	4.76	4.87	0	0	0	0

4f spin and orbital magnetic moments, 5d spin magnetic moments and N 2p magnetic moments, all in μ_B (from [105])

localized and not hybridized with the rare-earth 5d–6s and pnictogen p bands, contrary to suggestions made in some of the previously cited references.

Experimentally, stoichiometric GdN was found to be semiconductor with an optical gap of about 1.5–2 eV [106] and ferromagnetic with a low Curie temperature. In the presence of nitrogen vacancies, the importance of the charge carrier dynamics for both the transport and magnetism properties of GdN was underlined and the formation of magnetic polarons centred on the vacancies was suggested [107]. Because GdN is on the border between semiconductor and semimetal states, its electronic and transport properties are very sensitive to non-stoichiometry, impurities, defects, external pressure, temperature, magnetic field, etc. High quality of the samples is necessary to obtain semimetals and its absence could explain the difficulty in obtaining the experimental characteristics of GdN. All the same, variance between the various theoretical data could be explained by an ambiguity in the characteristics of this compound, making difficult their exact determination. However, these results also show that theoretical models can be convenient to obtain some properties, as the spatial arrangements, but are incapable of describing the real electronic distributions.

From a technological point of view, the rare-earth monopnictides are materials of great interest due to their remarkable structural, electronic and magnetic properties. Unusual combinations of a semimetallic or semiconducting character associated with the magnetism induced by the 4f localized moments present numerous advantages. Semimetallic ferromagnetic materials at ground state have large potential in electronics. The most promising materials would be the half-metal ferromagnets, which are possible candidate for spin-dependent transport devices [108]. Another interesting materials would be half-metallic antiferromagnets [109] because they would be completely spin-polarized at the Fermi surface but with zero magnetization, that could exist only in mixed compounds. The presence of very small energy gaps in these materials induces large values of the dielectric constant. They are of the order of 22–26 for the gadolinium and erbium pnictides (Table 2.7).

The nitrides have particularly attracted the attention because some of them were predicted to be half-metallic ferromagnets lying on the boundary between metals and insulators. However, experimentally, the electronic structure of the nitrides is not always well determined, partially because it is difficult to obtain pure single crystals.

Table 2.7 Dielectric constants ε of gadolinium and erbium pnictides. Bands gaps E_g (eV) calculated from LSDA, LDA and with self-energy corrections included (from [79])

Compound	ε	$E_g^{P,LSDA}$	$E_g^{P,LDA}$	$E_g^{P,est}$
GdN	26.5	−0.49	−0.18	0.10
GdP	23.9	−1.50	−1.04	−0.77
GdAs	22.8	−1.66	−1.19	−0.91
ErN	22.9	−0.26	−0.15	0.18
ErP	22.9	−1.61	−1.53	−1.24
ErAs	22.1	−1.65	−1.63	−1.41

Among the interesting pnictides for potential spin electronic applications, GdN, GdAs, ErAs, YbN, should be mentioned. They have a semiconductor-like character, the same as conventional semiconductors like AlAs and GaAs, associated with exceptional electronic and magnetic properties. Thus, they can be used as a dopant without losing their magnetic behaviour. They can be grown on III–V semiconductors, making these materials interesting for the development of electronic devices [110]. The first experiments concerned the single crystal ErAs films deposited on GaAs [111]. Epitaxial growth of ErAs on GaAs and AlAs has been developed. ErAs is a semimetal with electron and hole concentrations of about 3×10^{20} cm^{-3} and a large exchange splitting induced by the open 4f shell. GaAs/ErAs/GaAs hetero-structures have been obtained from ultra thin layers of ErAs. The electrons can tunnel through hole states of the semimetal ErAs quantum well and these structures form resonant tunnelling diodes whose response depends on the magnetic field orientation [112]. Hetero-structures consisting of layers of ErAs islands separated by GaAs were also found to be ultra-fast photoconductors [113]. Carrier trapping occurs on a sub-picosecond time scale. As the structure period controls the carrier trapping time, it is possible to obtain a desired carrier trapping time and thus a photoconductor with a response time compatible with time-resolved differential reflectance measurement.

Spintronics, or spin transport electronics, has opened up a new class of applications, where the information is not carried by the charge of the electron but by its spin. New devices combining standard microelectronics with spin-dependent effects are being developed. Initially, this technique was limited by the lack of polarized current sources for spin injection into semiconductors. The use of half-metallic ferromagnets, i.e. fully spin-polarized ferromagnets, can circumvent the problem. But such materials are difficult to obtain. However, polarization near 100 % can be created by using the phenomenon of *spin filtering* [114]. For a magnetic semiconductor, ferromagnetic below the Curie temperature due to the spin splitting of the band, the height of the tunnel barrier is spin-dependent. As the tunnel current depends exponentially on the barrier height, one of the spin channels has a larger tunnelling probability than the other, resulting in a nearly 100 % spin-polarized current [115]. Non-magnetic metal/ferromagnetic semiconductor/ferromagnetic metal devices have been obtained. The ferromagnetic semiconductor layer acts as spin filter. From this type of hetero-structures, resulting from the combination of a spin filter tunnel barrier and a ferromagnetic electrode, large magneto-resistance effects are created. Numerous hybrid devices utilizing the typical properties of rare-earth monopnictides are to be expected in future applications.

2.1.4 Intermetallics

During the last fifteen years, numerous studies of intermetallic compounds with cerium [116] and ytterbium [117] have been made and have revealed an unusual and interesting behaviour of these materials and a variety of their crystal structures.

Among these compounds, the best known are the binary R_mT_n and ternary $R_mT_nX_p$ ones with R = rare-earth, T = transition element and X = fourth or fifth group elements. Most of these materials are metallic. However, at low temperatures, they show remarkable deviations from the Landau-Fermi liquid theory of metals.

In rare-earth intermetallic compounds, the localized 4f orbitals generally form a magnetically ordered subsystems interacting with the valence electron distribution. The dominant interaction is the 4f-valence electron interaction RKKY. This long range magnetic interaction can lead to complex magnetic structures. Indeed, while the RKKY interaction is responsible for magnetic ordering, this ordering is nearly always incommensurate with the crystal lattice. Another interaction to be considered is the Kondo interaction (cf. Chap. 1). Let us recall briefly that the Kondo effect refers to the changes undergone, at very low temperatures, by the valence electrons of a metallic compound when they are in strong interaction with magnetic impurity ions. The Kondo effect is generally treated as the exchange interaction between a local spin and the valence orbitals present in every cell of the crystal; this is the *Kondo singlet interaction* [118]. In the case of the rare-earths, the Kondo exchange interaction results from the coupling between the spin associated with the localized 4f sub shell and the spin density associated with the 6s5d valence electrons. That is equivalent to treating the 4f and 6s5d electrons as strongly interacting. In the presence of Kondo interaction, i.e. at strong coupling, the valence electrons are considered as *heavy fermion*. Within the framework of Landau-Fermi liquid theory, the heavy fermion systems are described as formed by quasi-particles with an itinerant character. They have the charge and quantum numbers of the non-interacting electrons but their effective mass m* exceeds the free electron mass by a factor that can attain a thousand at low temperatures. As a consequence of the high effective mass of these particles, the Fermi energy is reduced to the order of the magnetic energy and the Fermi temperature becomes of the order of the Néel temperature.

The relative importance of the RKKY and Kondo interactions varies with parameters such as pressure, chemical composition or magnetic field. When the Kondo interaction prevails, the system can be understood in terms of a Fermi liquid of heavy quasi-particles, with narrow band-like states located in the region near the Fermi level. The ions carry magnetic moments but are not ordered magnetically. Let us recall that in the Landau's Fermi-liquid theory, the excitations are analogous to those of a non-interacting Fermi gas and the system is in the paramagnetic phase. The specific heat C, which is the sum of electron and phonon contributions, varies with the temperature according the relation $C = \gamma T + aT^3$, where γT is the term due to electrons and aT^3 that due to phonons. The Sommerfeld coefficient γ is independent of the temperature T and proportional to the effective electron mass m*. Since the effective mass becomes bigger than the real mass of the electrons at low temperatures, the first term becomes dominant. Then the measurement of the specific heat gives an estimate of m*. The Pauli susceptibility χ is also independent of T. The electrical resistivity contribution, due to particle–particle collisions, is $\Delta\rho = AT^2$ with A independent of T. The three terms, specific heat, Pauli susceptibility, electrical resistivity, are connected by the relation $\gamma \propto \chi \propto \sqrt{A}$. Moreover,

from the Wiedemann–Franz law, applicable to all systems characterized by particles of spin 1/2 and of charge e, the thermal conductivity/electrical conductivity ratio, or Lorentz ratio, is a universal constant, $\pi^2/3\ (k_B/e)^2$ (equal to 2.44×10^{-8} WΩ K^{-2}) in the $T \rightarrow 0$ limit. Violation of the Wiedemann-Franz law implies a massive breakdown of the Fermi liquid model.

Numerous rare-earth intermetallic compounds are considered as being heavy fermion materials, i.e. materials whose valence electrons are slowed down dramatically by scattering with the magnetic ions below the Kondo temperature, i.e. at temperatures much inferior to T_{Debye} and T_{Fermi}. An important question is to what extent these compounds can be described as Fermi-liquids. Indeed, at very low temperature, breakdown of the Fermi-liquid model can occur and non-Fermi-liquid behaviour, or *heavy fermion behaviour*, is found in a large variety of materials including metallic, superconducting, insulating and magnetic ones. This heavy fermion behaviour is manifested by a large deviation of the thermodynamic and transport properties from those predicted for a Fermi-liquid. The transport properties are very indicative in this type of studies because they can be measured under extreme conditions, very high pressure, high magnetic field and very low temperature. Observations were made initially for the cerium alloy $CeCu_{6-x}Au_x$ at temperature $T \rightarrow 0$ K [119]. In the calculations for this alloy, the electronic term of the specific heat can be up to 1000 times bigger than the value expected from the free electron theory. The Sommerfeld coefficient γ acquires an unusual temperature dependence with $C/T = \gamma(T) = -\ln(T/T_0)$. The mass of the electrons present at the Fermi surface tends to become infinite and their energies to vanish with the lowering of temperature. The susceptibility χ depends on the inverse of the temperature and the temperature dependent part of the electrical resistivity Δρ varies as T^b with b close to unity. The anomalous logarithmic temperature dependence of the specific heat and of the thermo-power, observed at temperature close to zero, is explained by a gradual loss of the magnetic moments. The associated drop of entropy is compensated by an unusual increase of the entropy carried by "hot" electrons at the Fermi surface of the heavy fermion compound [120]. In the alloy $CeCu_{6-x}Au_x$, at least two among the fundamental properties characteristic of the normal metals, specific heat and electrical resistance, undergo dramatic changes with the temperature, showing a very different characteristics of this metallic compound with respect to the normal metals. This is found in materials typically containing cerium and ytterbium and also uranium and neptunium.

At very low temperature, cerium and ytterbium intermetallic compounds exhibit properties unaccounted for by the present physical models. The change of fundamental properties suggests that the characteristics of the electrons are strongly modified in these compounds. Physical properties, like conductivity, magnetism, arise from the collective motion of electrons and ions in the solid. In order to eliminate discrepancies between theory and experiment, a quantum model had been developed to explain the intricate complexities of electron and ion motions at very low temperature [121]. This model led to suggest the existence of a new kind of phase transition, called *quantum phase transition*. It takes place between an ordered and a disordered phase around zero temperature. There are continuous second-order

transitions driven not by the thermal motions, i.e. the phonons, but by quantum fluctuations associated with Heisenberg's uncertainty principle. Indeed, electrons and ions cannot be at rest at the absolute zero temperature because their position and their velocity would, then, be simultaneously determined. Each quantum phase transition is dependent on an *order parameter*. This parameter characterizes the symmetry breaking of the ordered phase and it vanishes in the disordered phase. Near-zero-point fluctuations are present and susceptible to modify the system. These fluctuations depend on the non-thermal parameters. When such quantum fluctuations are sufficiently strong, quantum phase transition is expected to occur in the vicinity of a *quantum critical point* located between the two stable phases [122]. The *quantum critical phase* at this point, distinct from the two previous phases, is characteristic of a strongly correlated electron system, i.e. heavy fermion system. A quantum critical point is thus present whenever a material undergoes a second-order quantum phase transition, i.e. phase transition where the system changes in a continuous fashion at zero temperature. New interest in this field has come because of accurate studies of the quantum critical points and the unusual effects observed in their vicinity. The quantum phase transitions have been considered as responsible for particular properties such as the zero resistivity in the superconducting metals and the zero viscosity in the superfluids.

According to this model, the abnormal characteristics of the rare-earth intermetallic compounds, observed at very low temperature, were interpreted as due to a continuous phase transition in the limit of absolute zero, taking place between a long range magnetically ordered phase, often antiferromagnetic, and a paramagnetic phase [122, 123]. A few examples of ferromagnetic cerium compounds or alloys are also known to exist, for example $CeSi_{1.81}$ under pressure [124]. Here, the order parameter characterizes the magnetic phase and is zero for the paramagnetic phase. The ordered magnetic phase is described via magnetic RKKY interactions. The disordered phase is a paramagnetic Fermi liquid. The quantum critical point separates the magnetically ordered phase, antiferromagnetic, from the paramagnetic Fermi-liquid regime (Fig. 2.10).

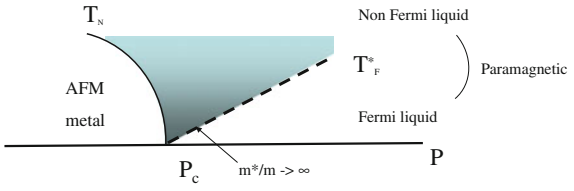

Fig. 2.10 A schematic representation of quantum critical point in heavy fermion metals: the pressure drives the system from the antiferromagnetic into the paramagnetic phase. But the reversed situation is possible. P_c is the critical point. If the Fermi temperature goes to zero at the quantum critical point, a new class of excitation processes is predicted above the Fermi temperature

These two regimes occur at very low temperatures, below the Néel and Fermi temperatures, respectively, and both are expected to disappear at the quantum critical point. A second-order quantum phase transition takes place in the vicinity of most quantum critical points. A new phase with non-Fermi-liquid characteristics is then present. In this quantum critical phase, also named *Kondo phase*, the 4f and valence electrons are considered as forming composite quasi-particles of very large masses. A phase diagram was calculated in a mean-field model as a function of the J_K/W ratio where J_K is the Kondo coupling between the localized and valence electrons and W the band width of the valence electrons (Fig. 2.11) [125]. On the other hand, phase diagrams have been obtained experimentally as a function of non-thermal parameters, like pressure, chemical composition or magnetic field. Indeed, it is possible to obtain a quantum critical state by reducing the transition temperature to zero using one of these non-thermal parameters.

As already underlines, the existence of a Kondo phase implies the presence of a critical point at $T \approx 0$ and is obtained whenever $T \rightarrow 0$ regardless of how this is achieved [119]. Secondly, a quantum critical transition depends on the presence of quantum critical fluctuations of the order parameter, i.e. in this case, fluctuations of the antiferromagnetic moment. Consequently, the quantum transition, i.e. the emergence of the Kondo phase, is associated with magnetic fluctuations, i.e. with a large number of low-energy magnetic excitations. A description of this type of phase transition was given based on the physics of electron fluids. In this non-local model, an itinerant antiferromagnet is developed and described in terms of a spontaneous spatial modulation of the spins associated with heavy quasi-particles of the paramagnetic phase, i.e. in terms of a *spin density wave* [126, 127]. The conditions for an ordered antiferromagnet to transit to such a heavy fermion system are given by the coordinates of the quantum critical points in the phase diagram. The

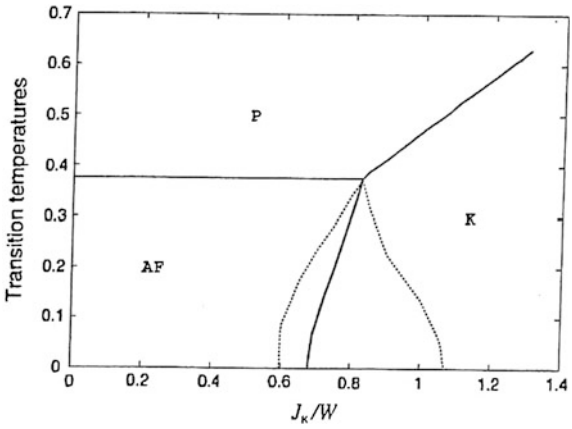

Fig. 2.11 Phase diagram showing the antiferromagnetic (AF), Kondo (K) and paramagnetic (P) regions. The first-order transition line between the AF and K phases is within a region limited by the two dashed lines, where metastable Kondo and magnetic solutions can coexist [125]

energy scale of these processes is much lower than the energy associated with the Kondo temperature.

In the spin density wave theory of the quantum phase transitions [128–131], the non-Fermi liquid properties observed in the vicinity of the magnetic–non-magnetic transition is therefore controlled by the fluctuations of the antiferromagnetic moment. The intensity of these fluctuations diverges at the quantum critical point and the Kondo temperature goes to zero. The quantum critical point between the localized antiferromagnetic and Kondo phases was observed in some cases along with a small *domain* in which the system is superconductor. The phase transition, induced by a parameter as pressure or composition, may, in principle, occur at $T = 0$. It is driven by quantum fluctuations instead of thermal fluctuations, present in classical phase transitions. Spin fluctuations in various Ce, Yb and U intermetallic compounds have been observed in many experiments, among them inelastic neutron scattering.

However, the standard spin density wave theory did not explain the entire experimental data and other models have been proposed. In the standard model, the Kondo phase partially overlaps the antiferromagnetic ordered phase. When the Kondo breakdown happens just at the onset of the antiferromagnetic phase, separation between the two phases occurs abruptly at the quantum critical point. The Kondo state exists only in the paramagnetic phase and, consequently, the presence of a new class of quantum critical point is expected. The order parameter is characteristic of the antiferromagnetic phase. The fluctuations of this antiferromagnetic order parameter can be considered as slow, in contrast with the dynamical nature present in the Kondo model. Various mechanisms, named Kondo breakdown models, have then been introduced in order to account for the presence of such critical quantum phase transitions. One of them, the spin-liquid formation among local moments, was proposed but not substantiated. Local magnetic fluctuations were then considered as explaining the entire experimental data [132–136].

Independently, the observation of a superconducting phase, clearly separated from the antiferromagnetic phase, in a cerium compound under high pressure [137], has lead to a search for an alternative model using another type of non-magnetic quantum fluctuations (Fig. 2.12).

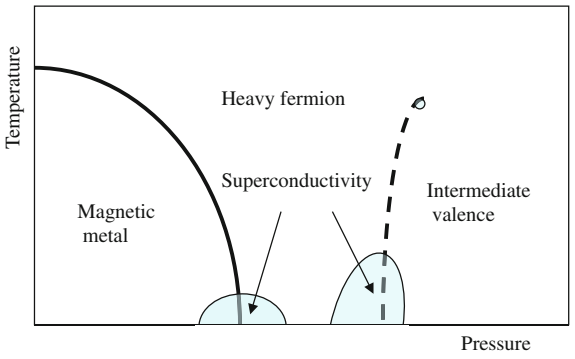

Fig. 2.12 A schematic representation of temperature versus lattice density phase diagram for cerium intermetallics of the $CeCu_2Si_2$-type

While in the Kondo model the heavy particles are composite objects arising from the 4f-valence electron strong interaction, in the presence of a Kondo breakdown these heavy particles disintegrate and this can be accompanied by charge density fluctuations [138]. Quantum transition to a superconducting state can then be driven by continuous localization–delocalization of electrons. Critical local fluctuations of valence have consequently been proposed to explain the presence of superconductivity at high pressure [139]. The interdependence of magnetic and electronic fluctuations will be discussed in the next paragraph.

Let us mention that a sudden variation of the magnetization in the absence of externally applied magnetic field is designated as *metamagnetic transition* [140]. Metamagnetism has been associated with various processes, first-order phase transitions, continuous phase transitions at a critical classical or quantum point, itinerant magnetism as well as antiferromagnetism. Here, it is generally associated with the change in the 4f electron character from localized to heavy fermion or itinerant, which accompanies a variation of temperature or pressure.

2.1.4.1 Cerium Intermetallic Compounds

In the cerium compounds, at low temperature, effective mass m* about two orders of magnitude heavier than the free electron mass was found experimentally. The first studied compound was $CeAl_3$ [141]. Later on $CeCu_2Si_2$ [142] and $CeCu_6$ [119] retained the attention, along with various uranium compounds. The Ce–Ni and Ce–Pt systems were also widely studied because the low symmetry of these noncubic compounds made possible the observation of anisotropic effects associated to the presence of the cerium 4f orbitals [143].

At standard and high temperatures, the cerium 4f electron is localized on each atomic site and does not contribute to the conductivity. At very low temperatures, the 4f electron can lose its localized character. This change induces an uncommon behaviour of heavy fermion type since a small variation of the number of 4f holes can have huge effects on the properties. More generally, compounds of the form CeT_2X_2 with T = Ni, Cu, Rh, Pd, Au, X = Si or Ge, were found to be of the heavy fermion type with a large variation of magnetic orderings and superconductivity. Among these compounds, $CeCu_2Si_2$ appeared as the prototype of heavy fermion superconductor. It was the first unconventional superconductor to be discovered [144, 145]. The superconducting state was induced by decreasing of the temperature down to 0.5 K or by the presence of an external magnetic field at a very low temperature. The transition temperature, T_c, is the temperature at which the electrical resistance of a superconducting material drops to zero. It should be remarked that the energy associated with a temperature of 1 K is less than 1 meV. With the increase of the external magnetic field, the superconducting state disappears and an antiferromagnetic state takes place (Fig. 2.13) [146]. From the value of the specific heat (1.1 J/mol K^2) at low temperature, $CeCu_{2.02}Si_2$ forms a heavy fermion system whose effective mass is approximately $100m_0$. Similar results have been obtained for stoichiometric samples with a high degree of lattice perfection [147]. In contrast

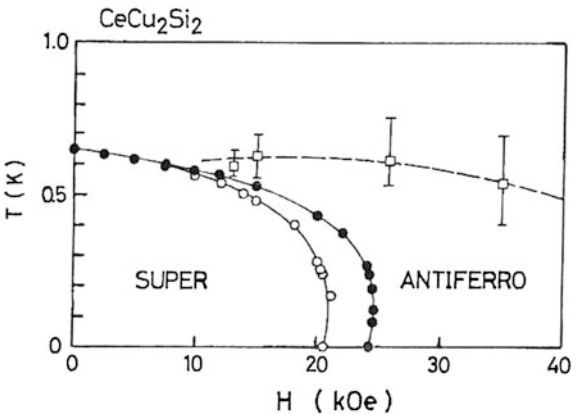

Fig. 2.13 Temperature versus magnetic field phase diagram for $CeCu_{2.02}Si_2$ [146]

with the conventional Bardeen–Cooper–Schrieffer (BCS) theory according to which the superconductivity is due to electron-phonon interactions, the superconductivity of this metallic system is due to electron–electron interactions [144].

Pressure is the parameter used for moving the antiferromagnetic ordered lattice Kondo compounds throughout their magnetic instability. Indeed, external pressure is a suitable parameter for investigating the physics of strongly correlated electron systems. As for pure cerium metal, the long distance magnetic interactions are modified by the application of pressure and one expects the localization of the cerium 4f electron to decrease with increasing pressure. The 4f energy level goes down and the compounds follow the sequence: magnetically ordered trivalent, non-magnetic trivalent or Kondo system, mixed valence system and eventually tetravalent. In the Kondo system, the 4f electron remains strongly correlated at very low temperature and has heavy fermion character, thus offering the possibility to induce a zero-temperature magnetic–non-magnetic quantum transition. The presence of such a transition is substantiated by the increase of the Sommerfeld coefficient when the temperature tends to zero. In the temperature-pressure phase diagrams, a narrow superconducting domain can be observed near the quantum critical point where magnetic order is suppressed and Kondo interaction is present.

In high-purity samples of $CeNi_2Ge_2$ with well-ordered atoms, superconductivity was observed at standard pressure and $T \approx 0.9$ K and this made this compound specially attractive. The observations were well described in the spin density wave model [148]. In contrast, at standard pressure, $CePd_2Si_2$ is antiferromagnetic below a Néel temperature of about 10 K [149, 150]. With increasing pressure, the Néel temperature decreases. The antiferromagnetic order is suppressed progressively and the system turns into a paramagnetic metal. The quantum critical point has not explicitly been observed. However, a small domain in which the system is a superconductor exists for a critical high pressure around 2.8 GPa and a very low temperature (Fig. 2.14) [136, 151].

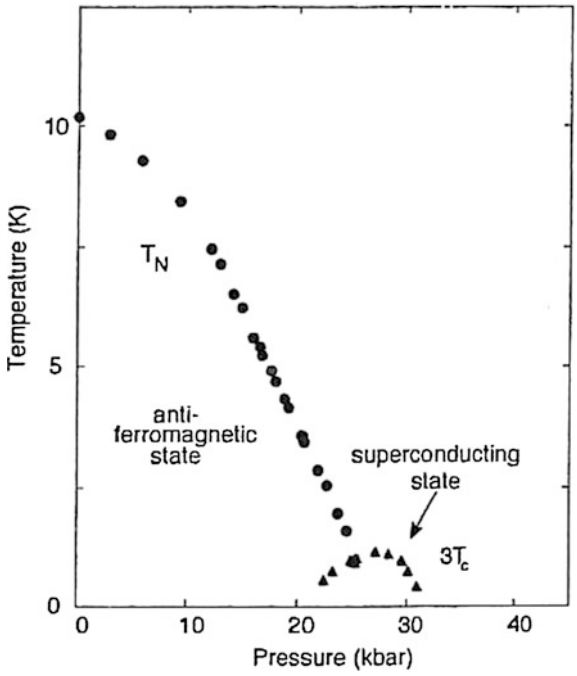

Fig. 2.14 Temperature versus pressure phase diagram of high-purity single crystal $CePd_2Si_2$ [151]

Contrary to previous examples, for some cerium compounds, either a relatively extended supraconducting domain or two clearly separate superconducting domains were observed, one near the magnetic phase and centred around the quantum critical point, the other widely separated from this point and observable at higher pressure [137]. Such two domains were observed for $CeCu_2Si_2$. The first domain was interpreted using the three-dimensional spin density wave model [152]. This model was supported by measurements made at 0.06 K [153]. The second superconducting domain appeared at high-pressure and was located far from the threshold of the magnetic phase. Complementary study was therefore necessary to explain it.

From measurements of specific heat and resistivity at low temperature and high pressure, the characteristic temperature of the appearance of superconductivity, named superconducting critical temperature, T_c, was determined for $CeCu_2Si_2$ [139]. This critical temperature varies with the pressure. At standard pressure, T_c is around 0.7 K. When pressure is applied, T_c increases suddenly at about 3 GPa, reaches a maximum value of 2 K at about 4.5 GPa then goes down to zero. This variation corresponds to the presence of the second domain of supraconductivity at high pressure. Moreover, resistivity measurements have shown a drastic decrease of the ratio m*/m, i.e. of the effective mass. This drop is characteristic of a decreasing of the localized character of the 4f electron and is associated with a change of the cerium valence. Considered as trivalent with the $4f^1$ configuration in the antiferromagnetic phase, then characterized as heavy fermion in the Kondo phase, cerium

becomes a mixed valence element at very high pressures. Both the heavy fermion and mixed valence states are nearly degenerate in the middle pressure region. At very high pressure, the cerium valence is considered as fluctuating between three and four. The 4f electron is then either localized on the ion of the $4f^1$ configuration or in orbitals near the Fermi level. The increasing of T_c can be related to the dual character of the 4f electron. This dual character induces the presence of critical valence fluctuations responsible of the quantum transition, leading to the superconductor domain observed at high pressure [139]. Consequently, two different processes are considered as responsible for the quantum phase transitions in $CeCu_2Si_2$: magnetic fluctuations, present in the low-pressure domain near the antiferromagnetic quantum critical point and charge fluctuations, responsible for the well separated high-pressure domain. However, not all the properties of $CeCu_2Si_2$ are fully understood and studies are going on. Very high-purity samples must be used because the results depend strongly on the stoichiometry.

For similar high-purity compounds such as $CeAu_2Si_2$ [154] or $CeCu_2Ge_2$ (Fig. 2.15) [138, 155], the pressure dependence of the various properties is almost quantitatively identical to that of $CeCu_2Si_2$ when pressure shifts are taken into account. The comparison is less straightforward with compounds in which Cu is replaced by a transition metal. In contrast, important variations of T_c take place according to the perfection of the sample. Indeed, large variations in the electronic properties result from extremely small differences in composition. This shows the important role of the chemical and structural conditions. Thus, the presence of germanium in $CeCu_2Si_2$ creates disorder and consequently decreases the superconductivity. However, for $CeCu_2Si_{2-x}Ge_x$, partial substitution of silicon by germanium is equivalent to a slight negative pressure effect and the same change is observed but at higher pressure. Thus, as for $CeCu_2Si_2$, two separate superconductivity domains are present (Fig. 2.16) [139]. The first is near the magnetic phase

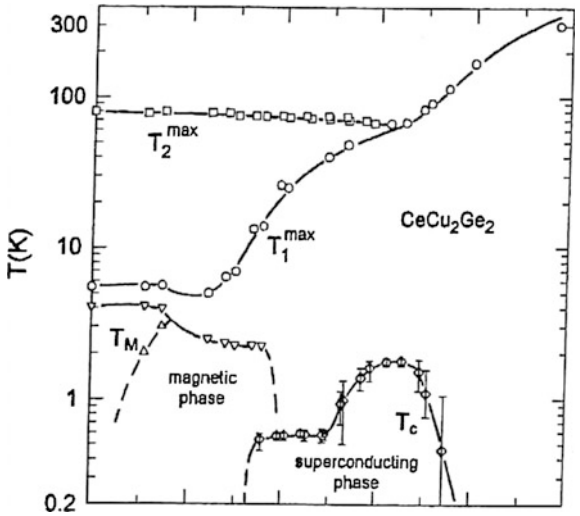

Fig. 2.15 Temperature versus pressure phase diagram for $CeCu_2Ge_2$ [138]

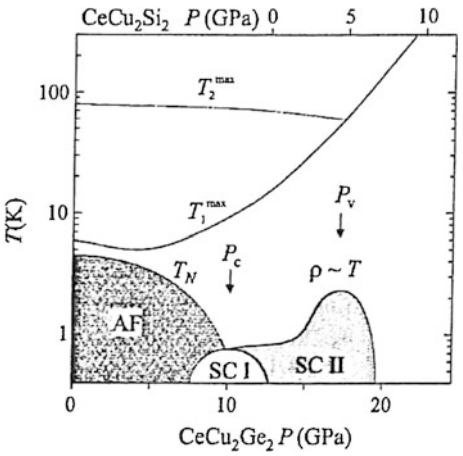

Fig. 2.16 Temperature versus pressure phase diagram for $CeCu_2(Si/Ge)_2$ showing two critical pressures P_c and P_v [139]

and is interpreted by spin fluctuations, the second is explained by an electronic configuration change of the same type as that described above, taking place at higher pressure.

Among the materials described by spin dynamics, it is possible to cite the heavy fermion system $Ce_{1-x}La_xRu_2Si_2$. Pure $CeRu_2Si_2$ is paramagnetic in the ground state. Lanthanum doping can be considered as equivalent to applying a negative pressure, thus as increasing the localization of the 4f cerium electron. The initially non-magnetic heavy fermion compound becomes antiferromagnetic. Investigation around the quantum critical point was performed using inelastic neutron scattering [156]. This was the first analysis made on a single crystal where pressure is the control parameter of the magnetic–non-magnetic phase diagram. The compound $Ce_{0.925}La_{0.075}Ru_2Si_2$ is characterized by a strong increase of the Sommerfeld coefficient, indicating the presence of a quantum critical regime. Indeed, the x-T phase diagram presents a paramagnetic regime for $x < x_c = 0.075$, accompanied by a Fermi liquid at low temperatures, and an RKKY antiferromagnetic phase for $x > x_c$. The quantum phase transition at x_c and $T \rightarrow 0$ K is characterized by an enhancement of the antiferromagnetic fluctuations [157]. All parts of the phase diagram were analyzed. From the observation of an enhancement at the critical point (x_c, $T \rightarrow 0$) it was shown that the antiferromagnetic fluctuations are responsible for the quantum transition between the paramagnetic and antiferromagnetic phases at x_c. It was, moreover, suggested that this could be a first-order quantum transition. The validity of the conventional spin fluctuation model appears to be confirmed by this compound.

Study of the quantum critical point by single-crystalline neutron scattering has been extended to the Kondo system $CeRu_2Si_2$ doped with rhodium, $CeRu_{2-x}Rh_xSi_2$ [158]. The lattice mismatch between $CeRu_2Si_2$ and $CeRh_2Si_2$ induces an important change of the magnetic field-temperature phase diagram at low temperatures. The system changes from an antiferromagnetic phase at field zero to a polarized paramagnetic phase at very high magnetic fields. Transitions among antiferromagnetic, paramagnetic and polarized paramagnetic phases depend on temperature, magnetic

field and pressure. It was shown, as in the previous study, that the quantum critical behaviour of $CeRu_{2-x}Rh_xSi_2$ is controlled by the spin density wave model [159].

Some compounds such as $CeCu_{6-x}Au_x$, seem to have more complex properties than the previously described ones. For $x = 0$, Fermi-liquid phase is observed. $CeCu_6$ is not magnetically ordered [160] and shows a strong Pauli paramagnetism. No localized 4f electrons are present. The large radius of the gold atom causes a lattice dilatation and the exchange interaction between 4f and s–d valence electrons varies with the composition. Au doping induces a non-Fermi-liquid phase, responsible for the anomalous logarithmic temperature dependence of specific heat observed in $CeCu_{6-x}Au_x$ [119]. The 4f localization increases and this leads to a stabilization of localized magnetic moments, which interact via the RKKY interaction. For a critical concentration $x \approx 0.1$, a long range antiferromagnetism, incommensurate with the crystalline arrangement, is induced. This can be understood as due to the partial 4f re-localization, having as consequence the change of the balance between dominant Kondo and RKKY interactions. The Fermi-liquid phase reappears in a sufficiently large magnetic field. At the critical concentration and zero temperature, a quantum phase transition from the long range magnetic order to a non-magnetic phase takes place due to the competition between RKKY and Kondo effects. Anomalies of the thermodynamic and transport properties are present at low temperatures and *unusual magnetic fluctuations* have been probed by inelastic neutron scattering [161, 162]. This complex spatial dependence of the magnetic fluctuations was already present in pure $CeCu_6$ and is therefore not due to disorder. The observed numerous low-energy magnetic excitations do not show the variations expected for spin fluctuations. The fluctuations are quasi-2D. This low dimensionality can be related to a strong anisotropy of the RKKY interaction in the presence of doping and underlines the importance of the atom arrangement around the rare-earth for the electronic properties. It has been suggested that the disorder in phase transitions may mask a first-order transition between magnetic and non-magnetic ground states thus mimicking a quantum critical point. Direct identification of critical fluctuations is therefore essential for a good understanding of the phenomena.

Generally, in the intermetallic compounds of the type CeX_3, the rare-earth magnetic moments are rather weakly coupled to each other or to the X element moments. Thus, compounds with X = Pd, Sn, In, have been generally found to be mixed valence compounds [163]. 4f levels would distribute in a narrow band for each of the three compounds. Upon increase of the thermoelectric power at high pressure, the 4f distributions have been found to widen with pressure as for metallic cerium (cf. Chap. 1) and the effect grows along the sequence $CeSn_3 \rightarrow CeIn_3 \rightarrow CePd_3$. $CePd_3$ shows Pauli paramagnetism. In some compounds, the 4f level lies very close to the valence band. No long range magnetic ordering is present in $CeAl_3$ but heavy fermions are present. The above suggests that cerium has an analogous behaviour to that of α-cerium in these compounds.

In contrast, $CeAl_2$ is an antiferromagnet with the magnetic moments localized on the cerium ions. The RKKY interaction is responsible for magnetic ordering, which is only slightly perturbed by the Kondo effect. A localized 4f electron is expected to

be present on each cerium ion, which is trivalent in this compound. Among the other compounds of the type CeX_2, $CeIr_2$ and $CeRu_2$ are supraconductors at very low temperature, 0.21 and 6 K, respectively [164]. Except for this particularity, they are analogous to α-cerium metal. No localized 4f electron is present and these materials are both non magnetic. The valence electron distribution has a 4f character mixed with a 5d one. These materials are mixed valence compounds in which the relative proportion of trivalent cerium ions is much less than unity. Below 3.5 K, $CeCu_2$ has a Kondo lattice with antiferromagnetic order and a Kondo temperature of about 6 K. CeNiSn and CeRbSb are Kondo semiconductors at 2–4 K with gaps of 8–10 and 20–27 meV, respectively, which are comparable to the Kondo temperatures. They move to a Kondo-metallic state upon increase of the temperature [165].

Intermetallic compounds of the type $CeTIn_5$ with T = Co, Rh, Ir, often designated as Ce-115, are actually actively studied because they exhibit all the typical properties. They are antiferromagnetic at standard pressure with Néel temperature of a few Kelvins. The Néel temperature decreases with increasing pressure and the antiferromagnetic ordering disappears progressively. The antiferromagnetic state vanishes when the Néel temperature equals the superconducting transition temperature and the material becomes superconductor. Antiferromagnetism and superconductivity coexist in a narrow pressure range and fluctuations of the magnetic order parameter, i.e. spin fluctuations, are expected to prompt the quantum transition. As an example, the heavy fermion compound $CeRhIn_5$ shifts under pressure from the antiferromagnetic phase to the superconducting phase at the temperature T_c = 2.1 K [166]. The two phases coexist in the pressure range between 1.6 and 1.9 GPa [167]. Above 2GPa the antiferromagnetic order vanishes suddenly leading to a pure superconducting ground state (Fig. 2.17) [168]. When a magnetic field is applied to $CeRhIn_5$ in the superconducting phase, a critical line is induced between the purely superconducting phase and the phase in which superconductivity and antiferromagnetism coexist. This line terminates at a point where the high magnetic field completely suppresses the superconductivity [169]. The effects of doping and of pressure were compared and it was shown that superconductivity is suppressed at

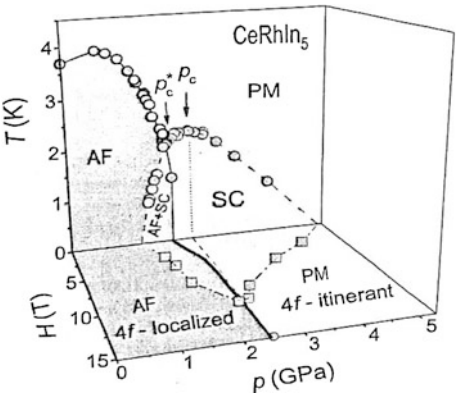

Fig. 2.17 Combined temperature, pressure and field phase diagram of $CeRhIn_5$ [168]

standard pressure by the substitution of In by Sn [168]. The crystalline structure of $CeRhIn_5$ was described as a quasi-2D structure formed by a stack of alternating layers of $CeIn_3$ and $RhIn_2$ The same structure was found in $CeCoIn_5$, which is a superconductor at standard pressure and at T_c = 2.3 K, i.e. at a relatively high temperature for a heavy fermion material [170]. In contrast, T_c is only 0.2 K for cubic $CeIn_3$. This temperature difference was attributed to the layered crystal structure of $CeCoIn_5$. Indeed, the presence of planes of magnetic Ce^{3+} ions renders $CeCoIn_5$, and more generally $CeTIn_5$, a quasi two-dimensional character, analogous to the layered structure of the superconductor cuprates. Consequently, it was suggested that their superconducting state could have a d-wave symmetry [171, 172]. A superconducting order parameter of d_{x2-y2} symmetry was proposed as the most probable [173]. Suppression of the superconductivity has been observed in single crystals of $Ce_{1-x}R_xCoIn_5$ with R = Ca^{2+}, Y^{3+}, Eu^{2+}, Yb^{2+}, La^{3+}, Gd^{3+}, Er^{3+}, Lu^{3+}, Th^{4+}. Substitution of cerium with another lanthanide or alkaline-earth element gives the same results, independently of the valence and the magnetic nature of the substituent [174]. Further calculations are necessary to explain these observations. The properties of $CeIrIn_5$ at very low temperature have also been investigated. T_c was found equal to 0.4 K [175] and magnetotransport measurements under pressure were explained by spin fluctuations [176]. Owing to the quasi-2D character of the crystalline structure, it was suggested that other members of this compound family with higher T_c could, perhaps, be found as long as dimensionality effects were considered.

More recently, first-order valence transitions, analogous to the cerium metal $\gamma \rightarrow \alpha$ transition, have been considered in Ce-115 compounds and their possible influence on the observed critical phenomena was investigated. Let us recall that the Ce $\gamma \rightarrow \alpha$ transition terminates at the *critical end point* characterized in the temperature-pressure plane by $T_V \approx 600$ K, P ≈ 2GPa where T_V is the temperature of the valence transition. But, in this case, no quantum criticality is present because at zero pressure T_V is relatively high, ≈120 K. The critical end point of a valence transition can be controlled by a magnetic field. In the presence of such a field, the critical end points form in the temperature-pressure-magnetic field space a continuous first-order transition line that can reach zero temperature. This critical line then emerges in the temperature–magnetic field phase diagram, where the effects due to magnetism and to valence coexist. It has been suggested theoretically that valence fluctuations could initiate the superconductivity when the first-order transition line is sufficiently close to the quantum critical line associated with the magnetic–non-magnetic transition [177]. Resistivity measurements under pressure and magnetic field showed that m*/m increased considerably in $CeIrIn_5$. This suggests the presence of local correlation effects, distinct from long range magnetic fluctuations. Under pressure, as already seen for $CeCu_2Si_2$ and $CeCu_2Ge_2$, the superconducting transition temperature increases in the region where the cerium valence is changing, i.e. in the region where the antiferromagnetic spin fluctuations are suppressed. Proximity exists between the critical points associated with the field-induced first-order valence transition and the quantum magnetic–non-magnetic transition. Consequently, the cerium valence transition can explain

the temperature–magnetic field phase diagram and the non-Fermi liquid phase observed in $CeIrIn_5$, and also the origin of the superconductivity.

Similar observations were made for $CeRhIn_5$, which at zero pressure is a heavy-fermion antiferromagnet with the Néel temperature ≈3.5 K. At zero magnetic field no evidence of first-order transition is found and a superconducting phase is detected at a pressure >2 GPa. Under magnetic field, antiferromagnetism is present up to ≈2.4 GPa where superconductivity and antiferromagnetism are mixed. From resistivity measurements, the temperature-pressure-magnetic field phase diagram was explained by the presence of valence fluctuations [177]. For this compound, the effective mass enhancement is due to local correlation and not to antiferromagnetic fluctuations. First-order valence transitions induced by the magnetic field appear necessary for understanding the entire experimental results. Actually, a difference seems to exist between $CeCoIn_3$ and the two previous compounds, thus their interpretation could be different.

Similar phase diagrams accompanied by remarkable physical properties have been observed also in the series $CeMSi_3$ with M = Rh or Ir [178]. Suppression of the antiferromagnetic ordering and appearance of the superconductivity have equally been observed under pressure. However, this is not a general phenomena and a variety of cerium intermetallic compounds do not exhibit a second-order phase transition, among them $CeRhIn_3$, $CeIn_3$.

2.1.4.2 Ytterbium Intermetallics

Ytterbium intermetallic compounds were studied at low temperature in order to establish a parallel between the 4f electron of trivalent cerium and the hole of trivalent $4f^{13}$ ytterbium. In the two cases, the pressure effect induces an increase of the valence. Thus, under pressure, ytterbium changes from divalent to trivalent according the transition $Yb^{2+}4f^{14} \rightarrow Yb^{3+}4f^{13}$. As well for ytterbium as for cerium, one 4f electron, initially localized in the vicinity of the ion core, is partially delocalized under pressure. However, for ytterbium, the ground configuration is non magnetic with an ionic radius larger than in the configuration under pressure while the inverse holds for cerium. Indeed, in ytterbium at the ground state, the 4f sub shell is full with all the fourteen 4f electrons localized on each Yb^{2+} ion while under pressure, the configuration is magnetic with only thirteen 4f electrons localized on each Yb^{3+} ion and the other non-localized 4f electron strongly correlated with the valence electrons. This shows that strong interconnection exists between valence and magnetic properties. The localization of the non-filled 4f shell and its quasi-atomic character induces an increase of the RKKY interaction. Consequently, unlike the cerium case, the magnetic order can be stabilized by means of volume compression. The competition between the Kondo effect and magnetic ordering is expressed by the ratio T_{RKKY}/T_K, which shows a very broad maximum for ytterbium compounds while it is monotonously decreasing for cerium compounds. Relatively few ytterbium compounds have been studied up to now because it is difficult to obtain their pure single crystals. Moreover, the experiments are more

difficult for ytterbium because the localized 4f electrons are closer to the nucleus when the sub shell is full, and therefore higher pressures have to be applied to obtain the valence change. On the other hand, an ytterbium valence change has also been predicted under magnetic field at low temperatures and a first-order valence transition was observed. The critical end point is controlled by the magnetic field. Heavy fermion states are present in a wider range of valence values in ytterbium than in cerium compounds.

The first observation of non Fermi liquid in an ytterbium compound was made at standard pressure in the absence of magnetic field for $YbRh_2Si_2$ [179]. Initially, $YbRh_2Si_2$ was considered as a 4f shell mixed valence compound like the others silicides or germanides. At 300 K and standard pressure, the valence of ytterbium in this compound is $\approx 2.9 \pm 0.05$. A fully localized Yb^{3+} state is reached at high pressures of about 8.5 GPa. In contrast, when the temperature decreases at standard pressure, the valence becomes of the order of 2.8 near $T = 0$ K. Slow valence fluctuations may be expected due to the number of the trivalent ions being different from unity. Dramatic changes of the Fermi surface as a function of temperature and magnetic field were observed using Hall effect measurements [180, 181]. These changes can be associated with the transition from the configuration where all 4f electrons are localized to the configuration with one itinerant-like 4f electron included in the Fermi volume. At low temperature, the electrical resistivity and the Sommerfeld coefficient show temperature dependence characteristic of a compound of heavy fermion type. Below the Néel temperature of 70 mK, $YbRh_2Si_2$ is antiferromagnetic with a magnetic moment of only $0.02\mu_B$ (Fig. 2.18) [182]. When a magnetic field is applied at standard pressure, this compound can pass through an experimentally accessible quantum critical point [181]. A weak critical field is sufficient to suppress the weak magnetic ordering and above this field Fermi-liquid (FL) is recovered. That seems to exclude the presence of spin density waves and, inversely, to favorize a local description in which the magnetic order is due to localized 4f moments. From the electrical resistivity and the Sommerfeld coefficient

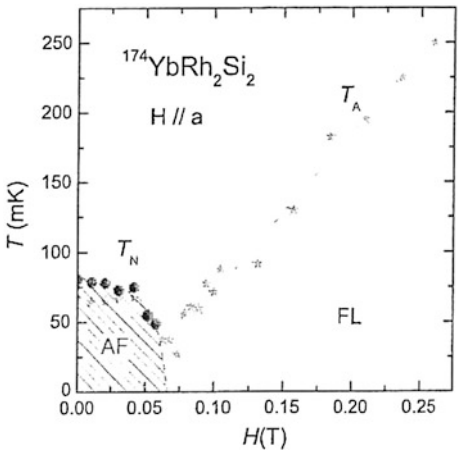

Fig. 2.18 Temperature versus field phase diagram of $YbRh_2Si_2$ [182]

measured at sufficiently low temperatures, the Wiedemann-Franz law was found valid for values of the magnetic field far from the critical field, i.e. near-zero, while it is not satisfied for a magnetic field of about $0.3T$ [183]. This reveals the presence of a non-Fermi liquid phase in the temperature—magnetic field phase diagram, coexisting with the antiferromagnetic and Fermi-liquid phases. Electronic quantum critical fluctuations, more often designated as valence fluctuations, could be responsible for all these observations.

Comparison was made between $YbRh_2Si_2$ and $CeRh_2Si_2$ [182]. The two compounds have the same crystalline structure. Pressure effect increases the valence in both but in ytterbium it stabilizes the magnetic order instead of destabilizing it in cerium. Indeed, the magnetic Yb^{3+} $4f^{13}$ state is stable with an ionic radius smaller than in the non-magnetic $4f^{14}$ state. The radial extension of the 4f orbital is much larger for cerium (0.37 Å) than for ytterbium (0.25 Å). In ytterbium long range magnetism is still conserved in the presence of a small amount of $4f^{14}$ ion while in cerium long range magnetism disappears even for a slight departure from Ce^{3+} configuration. The local atomic character of ytterbium is also reinforced by the size of the spin orbit interaction which splits the $j = l - s$ and $j = l + s$ individual 4f level (5/2 and 7/2) and is almost five times stronger for ytterbium than for cerium. Consequently, some of the usual rare-earth properties are found in $YbRh_2Si_2$. The degree of hybridization of the delocalized 4f electron with the valence electrons is smaller for ytterbium than for cerium and the pressure effect is less marked. Thus, even at 20 K, the number of the delocalized 4f electrons differs notably from unity and the valence fluctuations are slower in ytterbium. The Kondo temperatures of the two compounds have rather similar values while the ordering temperatures are quite different, 36 K for $CeRh_2Si_2$ and 70 mK for $YbRh_2Si_2$. This confirms how close $YbRh_2Si_2$ is to a quantum critical point at pressure equal to zero.

$YbCu_2Si_2$ is a heavy fermion system without magnetic order under standard pressure; it acquires a long range magnetic order for pressures higher than 8 GPa, whose magnetic moments values tend toward that of the free ion Yb^{3+}. The temperature dependence of the magnetic susceptibility of a single crystal was measured for a magnetic field parallel to the (100) direction and a maximum was observed around 50 K [184]. This maximum reveals the presence of a metamagnetic transition at this temperature. The observation of this transition reveals a change of the 4f orbital character from heavy fermion to an almost localized 4f electron. At pressure about 8 GPa and temperature equal to 1.2–1.3 K, high-quality single crystals of $YbCu_2Si_2$ could order ferromagnetically by first-order transition [185]. The transition temperature increases with the pressure, the applied magnetic field and also the quality of the crystal. Ytterbium valence under pressure was measured by RIXS (cf. Chap. 4) at room temperature and at 15 K (Fig. 2.19) [186]. The trivalent state appears only at very high pressure. Consequently the study of this fluctuating valence compound is difficult.

In several ytterbium compounds, ferromagnetic correlation dominates. This is the case, for example, in $YbInCu_4$ where magnetic order is induced at rather low pressure, about 3GPa [187]. Among the $YbXCu_4$ compounds [177], an isostructural first-order valence transition, analogous to that of cerium metal, is observed for

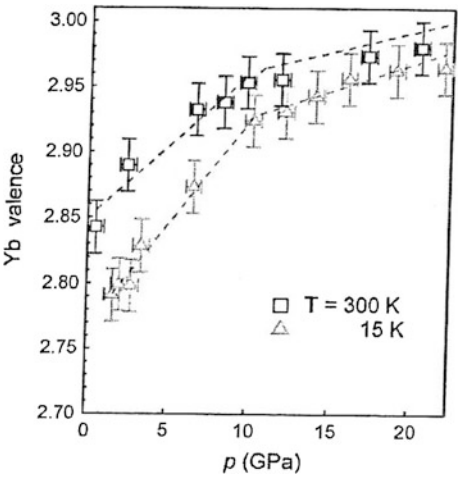

Fig. 2.19 Variation of Yb valence in $YbCu_2Si_2$ as function of the pressure at 300 and 15 K [186]

X = In. The transition temperature is 42 K. The ytterbium valence changes from 2.97 at high temperatures to 2.84 at low temperatures, with a volume expansion of about 0.5 %, i.e. much smaller than in cerium metal. The electron density is smaller in the high-temperature phase because of the higher entropy. On the other hand, the volume is expected to be higher when the 4f electron number increases. First-order valence transition is present with volume expansion when the temperature decreases (Fig. 2.20) [188]. These results have been confirmed by X-ray microscope experiments. $YbInCu_4$ is a clear example where a strong interplay exists between valence and magnetic fluctuations. In compounds such as $YbAgCu_4$ and $YbCdCu_4$, neither first-order valence transition nor magnetic transition has been observed. These two compounds have the paramagnetic metal ground state. Their magnetization curves are different in spite of the fact that both have nearly the same Kondo temperature, ≈200 K. A valence change of ytterbium occurs in the absence of magnetic field at $T = 40$ K in $YbAgCu_4$ but not in $YbCdCu_4$. Each compound has thus a specific character and its theoretical predictions appear difficult.

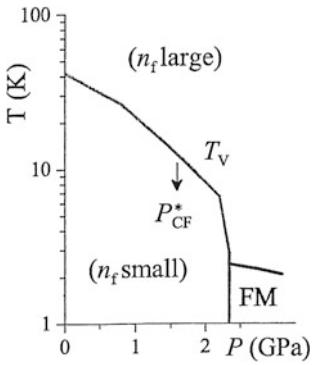

Fig. 2.20 Schematic temperature versus pressure phase diagram of $YbInCu_4$ [188]

Among the other studied ytterbium intermetallics, we can cite compounds of the type YbX_2Ge_2 with X = Cu, Ni and YbT_2Zn_{20} with T = Co, Rh, Ir and also $YbAl_3$ and $YbNi_3Al_9$ but actually their properties have not yet been completely established. Fundamental physicochemical data, such as valence and electronic distribution, depend on the atomic surroundings in the crystal and, consequently, these surroundings are responsible for the new physical properties observed in these artificial compounds. As already underlined, the 4f electrons are more localized in ytterbium than in cerium. Furthermore, it seems that strong ferromagnetism is favoured in ytterbium compounds, rather than antiferromagnetism, in contrast with the cerium compounds. This is related to the almost filled 4f sub shell that imposes the electron spin orientation, in contrast with the almost empty 4f shell in cerium. The presence of ferromagnetism is responsible for the order of the transition at low temperature and first-order transitions should be less favourable for magnetically induced superconductivity. However, it has been suggested that superconductivity could be present at extremely low temperature, in $YbCu_2Si_2$ for example. It should be noted that the ordering temperature and many other important properties depend strongly on the perfection of the crystal.

2.1.4.3 Comparison Between Cerium and Ytterbium Compounds

Over the past two decades, the cerium and ytterbium intermetallics have attracted much attention but these artificial materials are very difficult to obtain in pure crystalline phase. Consequently, only in the last few years, experimental studies have been performed on high-quality single crystals, resulting in a considerable recent progress of this research field. Known as non-Fermi liquids at low temperatures, these heavy fermion metallic compounds have physical properties that do not follow the laws applicable to metals. Violation of the Wiedemann-Franz law was observed and this implied that, in the low temperature range, the low-energy excitations could no longer be described as characteristic of particles with electron charge, obeying Fermi statistics. It appeared that low-temperature physics of many of these systems was controlled by second-order quantum phase transitions taking place between an ordered phase and a non-Fermi liquid.

These phase transitions at temperatures near absolute zero depend, among others, on the lattice density or the presence of a magnetic field. They result from the existence of critical fluctuations. Two models based on two different types of fluctuations have been developed. The more widely used one is the spin density wave model, based on long distance magnetic fluctuations. This model discusses the transitions between the antiferrromagnetic phase and the Kondo or supraconducting phases in several cerium and ytterbium compounds, among them $CePd_2Si_2$. The model is valid only in the vicinity of the magnetic phase. Consequently, the magnetic excitations were initially considered as playing a fundamental role in the unconventional supraconductivity of the heavy fermion alloys, contrary to the incompatibility existing between magnetism and conventional BCS supraconductivity. Another model, based on valence fluctuations, has been introduced to explain

the presence of superconducting phase in a more extended domain than the previous one, i.e. in a domain where the spin fluctuations are absent. It appears that these two apparently different models, based on critical magnetic or valence fluctuations, are necessary in order to interpret the experimental data of cerium compounds such as $CeCu_2Si_2$. In contrast, it has been suggested that in the absence of magnetic field, critical valence fluctuations are widely predominant in the heavy fermion metals having strong local electron correlations, such as, for example, $YbRh_2Si_2$ and $CeIrIn_5$ [189]. From a general point of view, if T_V is comparable to any characteristic temperature, T_N, T_{Curie} or T_C, or if the valence transition line intercepts the antiferromagnetic-paramagnetic boundary, the valence fluctuations must be considered in addition to the spin fluctuations.

The antiferromagnetic-Kondo phase transition, present in the vicinity of the critical quantum point in numerous intermetallics, is accompanied by a change of the 4f electron behaviour. Let us recall that the 4f electron of cerium metal is localized with properties equivalent to that of a core electron in the antiferromagnetic phase, and delocalized but keeping a strongly correlated character in the α-cerium Kondo phase. In the antiferromagnetic phase of an intermetallic compound, the 4f electron is localized on the Ce^{3+} ion with a quasi-atomic character. In the Kondo phase, on the contrary, the 4f electron is not localized but couples very strongly with the valence electrons to produce heavy fermions. A 4f narrow band is present. At the antiferromagnetic-Kondo phase transition, near the critical quantum point, electron localization–delocalization accompanies then the spin fluctuations. Therefore, magnetic and electronic parameters are strongly related and the two above models are not independent because both involve the character of the 4f electrons.

Consequently, the experimental results can be explained by a change in the characteristics of the 4f electrons, which are included in the total Fermi volume, i.e. have always their energy levels present below the Fermi level [177]. Experimentally, the most studied transitions were the second-order quantum phase transitions, taking place in the vicinity of the absolute zero, because this quantum criticality can generate unconventional superconductivity. Other studies concerned the first-order valence transitions, observed under high pressure. These transitions are associated with a strong reduction of the effective mass of the heavy fermions [139] and, therefore, a strong decrease of the electron correlations. The cerium 4f electron becomes similar to a valence electron and the cerium valence increases. Superconductor-paramagnetic transitions have been observed at high pressure in various cerium and ytterbium compounds and a relation has been established between these phase transitions and the presence of valence fluctuations.

In cerium and ytterbium, the same peculiarity related to their electronic configuration exists. In cerium, Ce^{3+} is more stable than Ce^{4+}. The number of 4f electrons remains always close to unity even in the absence of magnetic ordering and with the formation of heavy fermions. In ytterbium, the number of holes in the 4f sub shell is also close to unity. The valence change is larger and the ytterbium configuration is close to Yb^{3+} $4f^{13}$. Variation of the pressure and the atomic surroundings induces changes in the character of the 4f electrons of these two

elements. For example, in cerium, a volume reduction tends to squeeze the 4f electron out of the 4f sub shell. The character of the cerium 4f electron changes from almost localized in the antiferromagnetic phase to the heavy fermion state in the Kondo phase and to quasi-itinerant electron in the paramagnetic phase. Then, charge fluctuations have a role equivalent to that of the magnetic fluctuations present near the critical point because in the two cases there is a change of the 4f electron character. The fundamental problem is, therefore, the particularities of the 4f electrons, which can be localized and responsible of magnetic ordering or have Kondo or Fermi-liquid character according the considered system. In a magnetic field, first-order valence transition of the previously described type can also influence the electronic properties. The presence of the superconducting phase seems to be independent of the type of transition by which it is obtained: magnetic quantum critical transition near a quantum critical point or first-order valence transition. However, the superconductivity temperature is higher when the phase is obtained from valence fluctuations. The temperature parameter is an important factor and the research of a higher transition temperature is at the base of the actual activity in the domain.

In summary, cerium and ytterbium intermetallic compounds are subject to extensive fundamental research because they present particular physical effects, such as spin fluctuations, heavy fermions, coexistence of magnetism and superconductivity. This variety of properties is associated with the common feature of these two rare-earths whose number of localized 4f electrons is in accordance with the surrounding of the rare-earth in the material. Actually, superconductivity is observed for an increasing number of cerium and ytterbium compounds and efforts are being made in order to search compounds with higher critical temperatures. This research range is a very active field both experimentally and theoretically. There is a vast variety of these modern rare-earth materials. However, there is no complete theory that can treat the complexity of their properties. Further experimental results at very low temperatures using judicially selected spectroscopies are actually necessary.

2.1.4.4 Other rare-earth Compounds

Initially limited to cerium and ytterbium compounds, the study of the intermetallic compounds was extended to all the rare-earths. In the ternary compounds, the lattice is sufficiently complex for that two types of microscopic interaction such as magnetism and superconductivity could coexist. These compounds form large families of isostructural or nearly isostructural materials [190]. One of the most extensively investigated is the series of RA_4 or $RA_2A'_2$ compounds that crystallize in the $BaAl_4$-type or $ThCr_2Si_2$-type structures. Strong interest in this family of compounds was related to the intriguing properties of the cerium compounds such as $CeCu_2Si_2$. The layered arrangement of atoms in the lattice was considered as a critical factor contributing to the existence of remarkable properties. Studies of the RT_2X_2 intermetallics where R = rare-earth, T = transition element, X = Si or Ge, involved

mainly their magnetic properties [191]. One can cite $PrNi_2Si_2$, non magnetic at the ground state, which becomes ferromagnetic under an external magnetic field [192]. In the RMn_2Ge_2 compounds, the magnetic moments associated with the transition ions of the same atomic layer have a parallel arrangement at low temperature. The magnetic moments of the different layers are either subject to an antiferromagnetic coupling or adopt a parallel arrangement. Phase transitions between these two different magnetic states take place at a critical temperature and are first order. This is the case, for example, for $SmMn_2Ge_2$, which varies several times from ferromagnetic to antiferromagnetic as a function of the temperature [193, 194]. Calculations for this compound show that the interlayer coupling constant depends strongly on the unit cell volume, in particular on the interlayer distance, and varies linearly with the thermal expansion. Application of this model to other layered R-Mn intermetallics has been planned. Magnetic phase transitions can also take place under external pressure. These magnetovolume effects could be responsible for resistance anomalies and eventually the existence of giant magneto-resistance [195, 196]. Europium intermetallics are of a special interest because europium is divalent in the ground state $4f^7$ half-filled 4f shell, and can transit to trivalent europium with the $4f^6$ configuration, giving rise to mixed valence behaviour. The compounds EuT_2X_2 are generally antiferromagnetic. In germanides, europium is trivalent. In contrast, in the silicides, it shows mixed valence. The fluctuation time between the two valence states is short, of the order of 10^{-13} s.

A class of materials RT_4X_{12} with R = rare-earth, T = Fe, Ru, Os, X = P, As, Sb, named filled skutterudite compounds, have been widely studied because they reveal the properties characteristic of heavy fermion compounds and have the same crystal structure. Among them, $PrFe_4P_{12}$, $PrRu_4P_{12}$ and $PrOs_4P_{12}$ are especially interesting because they exhibit unusual features, not observed in the other praseodymium compounds. Thus, $PrFe_4P_{12}$ undergoes at 6.5 K a transition attributed to "the coupling between spin and quadrupole degrees of freedom" [197]. This quadrupole ordering phase is suppressed by a magnetic field. $PrFe_4P_{12}$ transits then to a heavy fermion state as indicated by specific heat and resistivity measurements under magnetic field at low temperature. In the ordered quadrupolar, or *antiferro-quadrupolar*, phase, the 4f electrons are localized. In the heavy fermion phase, the effective mass of the electrons is of the order of $80m_0$, indicating the presence of strongly correlated electrons. In the paramagnetic phase at the standard temperature, hybridization of 4f electrons with valence electrons has been considered. The presence of a non-magnetic order parameter with a multipolar component has been confirmed more recently [198]. In the $PrOs_4Sb_{12}$ compound, unconventional superconductivity is present below 1.8 K. An antiferroquadrupolar order was considered to be induced under magnetic field [199] and reveals the importance of the crystal field. From measurements of the Sommerfeld coefficient and the specific heat, heavy quasi-particles participate in the superconductivity. Compared to other heavy fermion supraconductors, this material is characterized by rather well localized 4f electrons.

Among the compound series having remarkable physical properties, one can cite the series R_mTIn_{3m+2} with T = Co, Rh or Ir and $m = 1, 2$. These materials grow in a

tetragonal variant of the Cu_3Au-type structure and can be described as layers of cubic cells RIn_3 stacked sequentially along the c axis with layers of TIn_2. Unconventional superconductivity was discovered in several of these compounds and was believed to be dependent on magnetic fluctuations and also on relationship with dimensionality and crystal structures. The interplay between crystalline electric field effects and exchange magnetic interaction was investigated. Linear dependence was found between T_C and the ratio c/a of the tetragonal lattice parameters at standard pressure: an increase of the quasi two-dimensional character of the crystal would favorize superconductivity. Among the $RRhIn_5$, $TbRhIn_5$ is antiferromagnetically ordered at the highest temperature T_N = 45.5 K while T_N is about 32 K for $TbIn_3$ [200]. It was shown that T_N depends on the crystalline electric field along the series. When the magnetic ordered moments are not aligned along the axis c, T_N is smaller than the value for the cubic TIn_3 parent compound. This is the case for $CeRhIn_5$. In contrast, when the moments point along the c axis, T_N is bigger than the value for TIn_3. This is verified for $NdRhIn_5$. Lastly, when the crystal effects are small, the magnetic properties remain nearly the same as those of TIn_3.

Another family of compounds of the R_5X_4-type or $R_5X_2X'_2$-type was developed [190, 201]. These compounds are built from weakly interacting slabs, each slab being formed by several strongly interacting monolayers of atoms. The study of gadolinium compounds was particularly developed following a giant magnetocaloric effect observed in $Gd_5Si_2Ge_2$ [202]. This alloy shows striking properties. The application of magnetic field induces a very large magnetic entropy change, concentrated over a narrow temperature interval in the vicinity of 276 K. This change is accompanied by a first-order ferromagnetic-ferromagnetic transition, which is reversible. Simultaneous contributions of the structural and magnetic entropy change can bring out a temperature change of the alloy. The two binary compounds Gd_5Si_4 and Gd_5Ge_4 crystallize in the same Sm_5Ge_4-type orthorhombic structure. However, there exist significant differences between the atomic arrangement of these two compounds. These differences were deduced from large displacements of atoms and the breaking of some Si_2 pairs during the transition from Gd_5Si_4 to Gd_5Ge_4 [203]. Difference exists also between the magnetism of the silicide and germanide of gadolinium: Gd_5Si_4 is ordered ferromagnetically at 335 K, i.e. at a temperature higher than that for Gd metal while Gd_5Ge_4 is ordered antiferromagnetically at much lower temperature [204]. Consequently, the solubility of silicon in solid Gd_5Ge_4 depends strongly on the temperature. The orthorhombic structure of the binary compounds undergoes a monoclinic distortion in the ternary compounds of $Gd_5(Si_xGe_{1-x})_4$-type. All these changes are due to significant differences in the inter-atomic interactions. Indeed, the hybridization between Ge 4p orbitals and spin-polarized Gd 5d orbitals leads to a magnetization of Ge and a ferromagnetic coupling between 4f Gd moments belonging to adjacent Gd slabs [205]. This coupling is very weakened by the break of the Ge-Ge or Si–Si bonds and the ferromagnetic order is then destroyed. The large differences in the bonding characters of Si and Ge in the Gd_5Si_4-Gd_5Ge_4 pseudobinary system are responsible for the variation of properties depending on the Si/Ge ratio.

Up to now, the studies of the R_5X_4 or $R_5X_2X'_2$ compounds concerned essentially gadolinium alloys [206]. They have been extended to $Gd_5(Si_xGe_{4-x})_{1-y}T_{2y}$ with T = Fe, Co, Ni, Cu, C, Al, Ga. Other R_5X_4 compounds with R = rare-earth and X = Si, Ge, Sn, Ga, In, Sb, are widely studied at present. Atomic and crystal structures are analyzed because they play a major role in the magnetic properties and much work remains in order to obtain a general description of these compounds. However the studies are mainly oriented towards compounds presenting a large magnetocaloric effect. Besides this family of compounds, this effect is very strong for other rare-earth intermetallics such as $La_{0.8}Ce_{0.2}Fe_{11.4}Si_{1.6}$, $La(Fe_{1-x}Si_x)_{13}$, $PrNi_5$, $TbCo_2Al$ [207]. Applications had initially concerned the low-temperature refrigeration. The extension to room temperature is actually an important challenge because of its potential impact on energy and environmental problems.

Among the intermetallics of interest for the study of the unconventional superconductivity, one can cite the compounds of the ROMPn-type with R = La-Nd, Sm or Gd, O = oxygen, M = transition metal and Pn = element of the group V (P, As, …). These compounds have a layered structure and are superconductors with transition temperatures T_c of 3–5 K. However, a transition temperature of the order of 26 K was obtained for LaOFeAs by dopage of F ions at the oxygen sites [208]. This material is composed of alternating LaO and FeAs layers, positively and negatively charged. The doping of the La-O layer with F ions increases the charge transfer and, consequently, increases T_c. Application of an external pressure was suggested to increase T_c because the pressure enhances charge transfer between the insulating and conducting layers. Indeed, a maximum of 43 K was obtained for F-doped LaOFeAs under 4 GPa [209]. The effect is expected to increase with the electronic polarisability of the ions. By replacing lanthanum by samarium, transition temperatures as high as 55 K were observed for $SmO_{1-x}F_xFeAs$ or $SmO_{1-x}FeAs$ at standard pressure [210, 211]. These temperatures are higher than the maximum predicted from Bardeen–Cooper–Schrieffer theory hence the interest of this type of materials for the development of unconventional superconductors.

Several remarkable physical properties of the rare-earth intermetallic compounds have lead to interesting technical applications. Thus, the fabrication of permanent magnets is possible from numerous hard rare-earth-transition metal intermetallics. Compounds with Curie temperatures between 260 and 650 K, of the type $RT_{12-x}T'_x$ with T = 3d transition metal, T′ = Ti, V, Cr, Mn, Mo, W, Al, Si, have been produced [212]. $SmCo_5$ and $SmCo_7$ have also a good thermal stability because their Curie temperatures are superior to 1000 K. However, compounds of the type Nd–Fe-B have preferentially been developed because they are cheaper. Nanocomposites formed from two magnetic phases, one hard $Nd_2Fe_{14}B$ and another soft Fe_3B, have been produced [213]. Certain transition metals, such as cobalt, were added to these

composites to improve the coercivity.[2] More recently, nanocrystalline alloys Sm $(Fe,Ga)_9C$ have been studied because of their high coercivity owing to their crystalline arrangement [214].

At low temperatures, the rare-earths are magnetostrictive materials, i.e. undergo a relatively large deformation in a magnetic field. In the RFe_2 Laves phase[3] compounds, the effect exists at high temperature and becomes useful for numerous applications. These compounds are used to obtain captors that change electrical energy to mechanical energy or vice versa.

Among the other potential applications of the rare-earth intermetallic compounds one can mentioned hydrogen storage, for example in $LaNi_5$ [215], a property of the spin glass type, for example in $Dy_xY_{1-x}Ru_2Si_2$ [216]. The presence of disorder in alloys such as $CeNi_{1-x}Cu_x$ [217] or $CePd_{1-x}Rh_x$ [218] can create cluster spin glass states at low temperatures [219]. Effects related to crystalline electric field can also be present. Magnetic frustration mechanism driven by this field can create, in a plane, magnetic fluctuations that can induce quasi-2D unconventional superconductivity. This list is not exhaustive. Numerous other alloys, in which interplay between heavy fermion, magnetism and superconductivity can exist, are being studied in order to understand how magnetic fluctuations stimulate the superconductivity. The aim is to discover new superconductor materials, to obtain a better understanding of their physics and to find new applications.

2.2 Actinide Compounds

The properties of the actinide compounds depend on the spatial extent of the 5f orbitals. By normalizing this extent taking into account the metal lattice spacing, one obtains for the 5f orbitals of the lighter actinides values intermediate between those of the 4f orbitals in the rare-earths and of the 3d orbitals in the transition elements. In the light actinides, the 5f orbitals are then less localized than the 4f orbitals and they overlap slightly, like in uranium metal. This overlap is reduced when the separation between the metal ions is increased by the introduction of various anions. However, some 5f electrons can participate in the bondings. In contrast, in the heavy actinides, where the 5f orbitals contract significantly, the 5f electrons are localized as shown by the rapid increase of the atomic volume in americium. Moreover, for a given actinide in various compounds, a small change in the chemical surrounding can cause a change of the 5f electrons from localized to itinerant. This has a large effect on the 5f electron contribution to the bonding.

[2]The coercivity of a material is the value of the magnetic field required to reduce to zero the magnetization.

[3]Laves phases are structures characteristic of AB_2 type intermetallic compounds. The unit cell is cubic or hexagonal. Tetrahedrally close packet structure is obtained if the ratio of the spheres characteristic of the A and B atoms is equal to $\sqrt{(3/2)}$.

Interchange between localization and delocalization makes then the electronic structure of these compounds difficult to anticipate.

Correlations effects of the 5f electrons play an important role in determining the properties of most of the compounds of the actinides. These properties cannot be predicted by a conventional band-structure approach. Strong electron-electron correlations enhance the effective electron mass and favorize the presence of Mott insulator in the 5f electron systems. Electronic structure is then strongly dependent on the on-site Coulomb repulsion U of the 5f electrons. Although an order of magnitude larger than for the rare-earths, the crystal field interactions still remain weak. They are clearly smaller than the 5f spin orbit interaction and are often neglected. Valence fluctuations are largely present; they are strongly dependent on the pressure because of the overlapping of the 5f wave functions. Consequently the hybridization increases when the volume decreases. Quasi-band model was considered as convenient for the calculation of several compounds of the lighter anions and actinides, among them the nitrure of uranium [220].

The IV valence is the most stable in the actinides up to californium. The stability of the III valence increases with Z. The VI valence is observed for the four first elements of the series. In contrast, most lanthanide compounds are trivalent and the IV valence occurs only in the beginning of the series, for cerium and praseodymium, and then for terbium. Model systems that have received a large attention are the simple cubic uranium compounds, such as the dioxide, monochalcogenides and mononitrides.

2.2.1 Oxides

The actinide dioxides are representatives of the tetravalent actinide compounds. They exist for all the elements thorium through californium and crystallize in fcc structures. Beyond that, the sesquioxides appear as the stable oxides. As already underlined (cf. Chap. 2, p. 87), it is important not to confuse oxidation state and ionicity. Indeed, the bonds are known to have a partially covalent character in the oxides. The number of 5f electrons on each actinide ion is not an integer and the presence of a fraction number of 5f electrons is not to be confused with the notion of intermediate valence. For the light actinides, most of the 5f electrons are expected to concentrate in narrow bands with narrow overlap, located just below the Fermi level E_F while a wide band of O 2p electrons having the same energy as the valence electrons of the actinide is located several eV under E_F. These dioxides are considered as Mott insulators. However, it has been suggested from recent spectroscopic measurements that the lowest energy transition is of the 5f–6d type and is associated with a band gap of about 4.4 eV [221]. Photoexcitation then involves charge carrier hopping between localized levels. When Z increases, the binding energy of the 5f electrons increases, the 5f-O 2p band distance decreases and a small overlap can be present, except if the radial contraction of the 5f wave functions becomes the dominating factor. When passing from one element to the

next the increase of the number of 5f electrons is accompanied by the contraction of the 5f sub shell. This contraction increases the stability of the 5f sub shell (cf. Chap. 1). Similarly, a monotonic decrease of the experimental lattice constant with increasing Z was observed from thorium to californium with a small deviation at curium, which corresponds to the half-filled shell [222]. As discussed in Chap. 1, this is due to a change in the characteristics of 5f wave functions around the middle of the series.

Thorium is tetravalent in all its compounds and no 5f electron is present in the ground state. In the stable oxide ThO_2, the O 2p valence band is large and extends between about −9 to −4 eV below the Fermi level, in agreement with the theoretical predictions.

Uranium has several oxides. The most stable is U_3O_8. It is obtained from UO_2 in contact with oxygen according to the reaction $3UO_2 + O_2 \rightarrow U_3O_8$ at 970 K. The dioxide UO_2 has the fluorite structure (CaF_2) like the dioxide of cerium and those of neptunium and plutonium. The experimental lattice constant is 5.47 Å. Each uranium ion is at the centre of a cube and coordinated to eight oxygen atoms located at the corners of the cube. The crystal field splits the f orbitals into three sub-orbits. Under normal conditions only the more stable would be occupied with two electrons, leading to an unsplit triplet ground term according to Hund's rules. However, this simple description is altered by the spin–orbit interaction and the triply degenerate ground state is split into three adjacent levels. Indeed, the $5f_{7/2}$–$5f_{5/2}$ spin–orbit splitting is expected to be of the order of 1–1.5 eV for UO_2 while the magnitude of the cubic crystal field splitting is 0.5–0.1 eV for $5f_{7/2}$ and $5f_{5/2}$, respectively. However, the inclusion of the spin–orbit interaction has only a small effect on the properties of this compound. UO_2 is a simple paramagnet above the Néel temperature T_N = 30.8 K and shows a first-order antiferromagnetic transition at T_N with a moment of $1.74\mu_B$. Pressure-induced weak ferromagnetism is also present [223]. UO_2 is an insulator with an optical gap of about 2 eV. Conventional LSDA and LSDA + U calculations had incorrectly predicted a non-magnetic metallic ground state. By including in LSDA + U a term describing the Hubbard on-site repulsion between 5f electrons, improvement was obtained, in particular for the equilibrium lattice constant [224]. More recently, an energy gap in reasonable agreement with the experimental value has been predicted from a hybrid DFT-type calculation [225].

From this theoretical approach, the 5f distribution has an energy width of about 1 eV and located very close to E_F. Experimentally this distribution was observed at about 1 eV below E_F. In the oxides, the bonds are often described as due to "charge transfers" from the metal to the ligand. Indeed, in the metal, 6d, 7s electrons are mixed with the ligand 2p valence electrons and charge density is present on and also between uranium and oxygen ions. The valence band associated with these electron distributions is located between −3 and −8 eV below E_F. A slight U 5f character is present in this band. The number of U 5f electrons engaged in the bonding is of the order of 0.2 while two 5f electrons are localized on each uranium site. There are more than two 5f electrons associated with each uranium ion and the effective charge of the uranium ions is less than 4 owing to the partially covalent

character of the bond. A charge close to 3.5 was observed. The levels at the onset of the conduction band are predicted to be unoccupied 5f levels and 5f–5f non radiative jump is expected from about 2.5 eV above E_F in a range of several eV. In the other uranium oxides, U_30_8 and UO_3, the uranium oxidation state progressively increases while the number of the localized 5f electrons decreases (cf. Chap. 5).

PuO_2 and Pu_2O_3 were studied theoretically by using the same approach used for UO_2 [226, 227]. This approach does not take into account the spin–orbit interaction. The two compounds were found antiferromagnetic at the ground state with magnetic coupling relatively weak. They were predicted to be insulators with energy gaps a slightly superior to 2 eV. The lattice constant of PuO_2 was calculated to be 5.39 Å, in agreement with the experimental value of 5.40 Å. For the two oxides, energy distributions characteristic of 5f electrons are located in the −1 to –3 eV energy range while distributions characteristic of the valence electrons are situated approximately in the 4–8 eV range. More recently, very detailed study of PuO_2 and particularly Pu_2O_3 was made using LDA/GGA + U formalism [228]. PuO_2 has the fluorite structure in standard conditions and the $PbCl_2$ structure beyond 39 GPa. It is insulator with a conductivity band gap of only 1.8 eV. Pu_2O_3 has several phases, two non-stoichiometric cubic α and α′-phases and a stoichiometric hexagonal β-phase. β-Pu_2O_3 is insulating and antiferromagnetic below 4 K. The atomic volumes of the two oxides increase with the Coulomb interaction U, which appears as a parameter. Indeed, increase of the correlations, due to the localization of the 5f electrons, has as consequence the decrease of the cohesion of the crystal and the increase of the lattice parameter. In PuO_2, the Pu 5f and O 2p distributions are very close in energy. In contrast, the Pu 5f levels are energetically separated from the valence band in Pu_2O_3. As expected, the Pu 5f electrons are more localized in the trivalent oxide than in the tetravalent one. In Pu_2O_3, only three plutonium valence electrons are necessary for the plutonium-oxygen bonds and, in principle, the 5f electrons do not participate. That is different for the tetravalent oxide because in this case one 5f electron contributes to the chemical bonds with the oxygens. The differences between these two oxides are somewhat analogous to the differences seen between Ce_2O_3 and CeO_2.

In going from UO_2 to PuO_2, one expects a reduction of the 5f orbital radius and a stabilization of the 5f orbitals. Stabilization is, indeed, obtained in PuO_2 and consequently the 5f-O 2p mixing is expected to be greater in PuO_2 than in UO_2. Thus, the Pu 5f peak is observed at −2.5 eV, while the calculated peak is at −0.5 eV. Theoretically, the 5f orbitals in PuO_2 show an intermediate character between being hybridized or not. Experimentally, they manifest partially hybridized electronic structure. PuO_2 is in the crossover between the Mott insulator family and the dioxides characterized by a normal band gap. The same behaviour is seen for AmO_2. The two compounds, PuO_2 and AmO_2, are characterized by a weak energy mixing of the 5f and oxygen 2p orbitals.

The stoichiometric oxide CmO_2 has a magnetic moment equal to $3.36\mu_B$. The magnetic moments of the ions Cm^{4+} $5f^6$ and Cm^{3+} $5f^7$ are, respectively, 0 and $7.94\mu_B$. The value of the observed magnetic moment in the oxide confirms the partially covalent character of the bond. Covalent picture has been predicted

theoretically [229]. It must be noted that if the spin–orbit interaction were dominant, the expected ground configuration of curium in CmO_2 would be mainly $5f^6$ because this configuration corresponds to the complete filling of the lower $f_{5/2}$ subband. Such a ground configuration is predicted to have a zero magnetic moment, contrary to the large moment found experimentally. In fact, curium has a number of 5f electrons between 6 and 7, but only a small part of them contributes to the bonds with oxygen, as in the preceding elements.

The actinide oxides are of great interest. The most important is PuO_2. It is a component of nuclear reactor fuels and an important compound for the very long-term storage of plutonium. Elemental plutonium rapidly oxidizes to PuO_2 when exposed to air. The products of the chemical reactivity of plutonium metal, oxides and hydrides, are very complex. Non-stoichiometric oxide, PuO_{2+x} with $x \leq 0.27$, was believed to take part in the fast corrosion of the metal [230]. More recently, the existence of such a compound has been questioned and the stability of any higher binary plutonium oxide has been excluded [231]. The presence of one extra oxygen would probably distort the lattice too much. It would seem that plutonium oxidation chemistry still needs further research.

With its various technical applications possible, UO_2 is sometimes compared to Si and GaAs. Its intrinsic conductivity at standard temperature is about the same as that of single crystal silicon. Its dielectric constant is about 22, i.e. twice as high as that of Si (11.2) and GaAs (14.1). This is an advantage in the construction of integrated circuits. Stoichiometry dramatically influences its electrical properties. This is a ceramic material resistant at high temperatures. It has a very small thermal conductivity and its applications for photovoltaic device can be considered.

2.2.2 *Monochalcogenides*

The actinide monochalcogenides have the NaCl-type cubic structure. In spite of their highly symmetrical crystal structure, the uranium monochalcogenides have very large anisotropy. Thus, the anisotropy constant of the cubic uranium compound, US, near 0 K, was found to be an order of magnitude greater than that of $TbFe_2$, which was the largest known anisotropy constant of a cubic material [232].

The uranium monochalcogenides US, USe and UTe, exhibit a ferromagnetic ground state with the uranium magnetic orbital moment more than twice larger than the magnetic spin moment and a very large magnetic anisotropy. Their Curie temperatures are 177, 160 and 104 K, respectively. They are higher than those of other ferromagnetic uranium compounds. The monochalcogenides are metallic. Their density of valence states is characterized by a broad feature located between −2 eV and E_F and centred around −1 eV and a rather small peak at the Fermi level, attributed to the 5f electrons. These data, deduced from spectroscopic experiments (cf. Chap. 5), were in disagreement with the densities of states calculated from LDA + U method but were reproduced approximately from DMFT associated with LDA + U calculations using U equal 2 eV [233]. The calculated chalcogen p band

is located between −6 and −3 eV in USe and UTe. The 5f distribution is split into a narrow occupied part crossing the Fermi level and a broader unoccupied band.

The plutonium monochalcogenides PuSe and PuTe are paramagnetic semiconductors with narrow energy gaps of the order of 10 meV and temperature independent magnetic susceptibility. For temperatures higher than the energy gap, the gap is irrelevant and these compounds can be considered as highly correlated metals. From spectroscopic experiments, energy distribution of 5f electrons was observed in a range between −1.5 eV and the Fermi level, the large part of the 5f electron spectral weight being concentrated in a narrow peak near E_F. Similar features were observed in δ-Pu and PuN and this 5f distribution appears to be independent of the chemical environment. As has already been often seen, the usual LDA-GGA-based and LDA + U calculations fail to provide the correct description of the electronic properties of the actinide compounds. However, the magnetic properties are correctly described by LDA + U calculations. In contrast, DMFT-LDA + U calculations with U equal 3 eV give a picture rather similar to the experimental 5f electron distribution [233]. The chalcogen p band is calculated to be in the range between −6 and −2.5 eV in PuSe and PuTe.

In summary, on the basis of the DMFT-LDA + U calculations including the spin–orbit interaction, the ground state magnetic properties of the ferromagnetic USe and UTe and non-magnetic PuSe and PuTe compounds have been correctly reproduced and an acceptable description of the electronic distributions has been obtained. In contrast, the electronic structure is not described successfully in the LDA + U approach except for the magnetic moments. These computational results underline the decisive role played by dynamic correlations in improving the agreement between theoretical 5f densities of states and experimental results.

2.2.3 Mononitrides and Monocarbides

Both nitrides and carbides have values of thermophysical constants higher than the corresponding ones in the oxides. They have higher melting point, higher heavy atom density, higher thermal conductivity [234]. This makes then possible alternatives to the oxide based fuels. Studies on their physics and chemistry are beginning to be developed.

Mononitrides and monocarbides, like a great number of actinide compounds, crystallize in the NaCl structure. Experimentally, the 5f orbital overlap was observed to decrease with increasing anion size. Consequently, the 5f electron localization increases. Thus, the 5f electron character and the details of the electronic structure are strongly interrelated. Generally, the 5f–5f overlap controls the characteristics of the compound. However, f–d and f–p hybridizations can also be present and influence those characteristics.

In UN and UC, owing to the small radii of the nitrogen and carbon atoms and the large extent of the uranium 5f orbitals, the uranium 5f electrons were considered initially as itinerant. The lattice parameters calculated by using a band model for the

two compounds were found in agreement with the experimental values. However, from SIC-LSD calculations, the electronic structure is dominated by a narrow uranium 5f density peak located at the Fermi level [235]. The 2p band is centred at about −4 eV in UN but only at −2.7 eV in UC. Overlap exists between the U 5f orbitals and the N, or C, 2p orbitals and it is bigger for UC. Finally, the ground configurations are predicted to be f^0 in UC and f^1 in UN. The electrons 5f are then considered as delocalized only in UC and it appears clearly that the influence of electron–electron correlations increases from UC to UN. However, it is not sure whether a localized picture is suitable to describe the UN properties.

In PuN, both $5f^3$ and $5f^4$ configurations contribute almost equally to the ground state electronic structure whereas in PuC, the f^3 configuration slightly dominates. This is due to the larger electronegativity of nitrogen. The f–p hybridization is then less pronounced. The p states are further separated from the 5f states in PuN than in PuC. In PuC, the $5f^3$ and $5f^4$ configurations have been found energetically close. The fact that $5f^3$ corresponds to the energy minimum and the localization of an additional electron is slightly less favourable has lead to suggest that three 5f electrons were localized and one 5f electron was itinerant in this compound.

From UN to CmN, the number of localized 5f electrons present in the ground state gradually increases. The same is true from NpC to CmC. With Z increasing, the 5f orbitals contract and their overlap with neighbouring sites decreases. The energy necessary for the localization becomes higher than the band formation energy. The valence decreases with the increase of the number of localized 5f electrons. The effect is stronger for the nitride than for the carbide compounds. Moreover, different valence configurations, closely separated in energy, are expected in these compounds and their presence characterizes the coexistence of localized and delocalized 5f electrons. Contribution from the more localized electrons gradually increases as one moves along the series. Abrupt increase of the lattice parameter was observed between PuN and AmN and reproduced by the calculation (cf. Fig. 5 in [235]). This variation was associated with the localization of the 5f electrons in Am. The ground state configuration in the nitride becomes the trivalent configuration Am^{3+} $5f^6$. In the carbides, the presence of fully localized 5f electrons is expected from CmC with Cm^{3+} f^7. The decrease of the number of itinerant electrons with increasing actinide atomic number was confirmed by the observed decrease of the thermal conductivity from UN to PuN [236].

2.2.4 Intermetallics

Spectacular properties, similar to those existing in rare-earth intermetallic compounds, were observed in the actinide intermetallics. Let us recall that at elevated temperatures, in the rare-earth intermetallics with a high 3d metal, the 4f–3d exchange interactions are strong and have led to the discovery of excellent materials used as permanent magnets and magnetostrictors. This is not the case for uranium intermetallics containing high 3d metals because 5f–3d hybridization reduces the

magnetic moment of the 3d ions. As an example, UFeAl is paramagnetic down to low temperatures. However, both uranium and 3d metal sublattices are known to be magnetic in some potentially interesting U-3d intermetallics.

As has already been shown in the case of the rare-earths, the actinide intermetallics at low temperature show various ground states revealing interplay between magnetism and heavy fermion states. These are non-Fermi liquid states characterized by a very large Sommerfeld coefficient, magnetically ordered phases, unconventional superconductor states and eventually some systems with both magnetic order and unconventional superconductivity. $Np_{1-x}Mo_6Se_8$, of critical temperature 5.6 K, was the first superconductor actinide compound, to be discovered [237]. Later on, heavy fermion phenomena and superconductivity were observed at low temperatures as a function of pressure or applied magnetic field, in a large number of intermetallic compounds of actinides, U, Np and Pu.

Heavy fermion phenomena and superconductivity were observed at low temperatures as a function of pressure or applied magnetic field, in a large number of intermetallic compounds of actinides, U, Np and Pu. The above characteristics result from the presence of the 5f electrons. Among the theoretical models used to describe the 5f electrons in these compounds, we cite a calculation which takes into account a weak 5f delocalization by considering simultaneously a finite 5f bandwidth within the Anderson Lattice Hamiltonian and localized f-spins S = 1 without f-band width to describe the U^{4+} $5f^2$ [238]. However, this model does not explain all the very particular properties of these compounds. Initially, heavy fermion phenomena were considered to occur only with very narrow 5f bands that did not order magnetically at all or else showed very small ordered moments. However, magnetic ordering was found to coexist at low temperature with heavy fermion state in numerous compounds. Whereas in the cerium intermetallics the ordering temperatures are typically of the order of 5–10 K, in some uranium compounds, such as UTe, $UCuSb_2$, a ferromagnetic order is present at Curie temperatures T_{Curie} as high as 102 K or 113 K. The same is observed in neptunium compounds, $NpNiSi_2$ and Np_2PdGa_3 with T_{Curie} equal, respectively, to 51.5 and 62.5 K and in plutonium compounds. Among the more studied compounds, it is important to mention UBe_{13}, UPt_3, URu_2Si_2, UFe_2Si_2, which were among the first ones whose unconventional superconductivity was observed and studied and also UGe_2, URhGe, UCoGe, which are the first discovered ferromagnetic superconductors.

Unconventional superconductivity of actinide intermetallic compounds was discovered for the first time in UBe_{13} [239]. The U–U distance is large, about 5.13 Å, in this compound. The uranium ions are tetravalent with two localized 5f electrons. Measurements of the electronic specific heat, the magnetic susceptibility and the electrical resistivity as a function of the temperature for a single crystal were made. Those three parameters increase with decreasing temperature in zero magnetic field and their values at about 1 K are characteristic of a heavy fermion system. At lower temperature, the electrical resistivity decreases rapidly and this variation reveals a superconducting transition at 0.86 K in agreement with the strong variations of specific heat and magnetic susceptibility in this same temperature range. This is heavy fermion superconductivity, in which no magnetic

ordering or magnetic correlation was found. At lower temperature transition in the superconductor phase of $U_{1-x}Th_xBe_{13}$ was observed [240, 241]. At about 0.25 K another transition was observed in UBe_{13}, initially attributed to the presence of an antiferromagnetic phase. Studies are being pursued to understand the mechanisms leading to these observations [242].

Superconductivity was also seen in UPt_3. Resistivity measurements showed that the resistance drops to zero at about 0.54 K [243]. The transition width is of about 0.030 K and is decreased by annealing the sample, namely reducing existing defects. However, the variation of the resistivity with the temperature was clearly different for UPt_3 and UBe_{13} (Fig. 2.21) [243].

Measurements of specific heat and magnetic susceptibility give the same transition temperature. The variation of the specific heat with the temperature in a zero magnetic field was interpreted as following the law predicted for a spin fluctuation system by Doniach and Engelsberg [244] and confirmed the presence of unconventional superconductivity in UPt_3. Improvements in the quality of the samples increased the resolution and two transitions were observed at temperatures between 0.3 and 0.4 K [245]. This splitting of the superconducting transition was compared with the second structure seen in UBe_{13} [240, 242] and attributed to an ordered phase.

In contrast with UPt_3, which is described as being of the heavy fermion type, UPd_3 has the localized $5f^2$ configuration [246, 247]. This material has a double hexagonal close-packed structure with two different sites for the uranium ions. Two transitions take place at low temperature; the one at 6.7 K involves the quadrupolar ordering of the uranium ions, the second at 4.5 K involves magnetic ordering with a very small magnetic moment. The quadrupolar moments are large in f compounds and a quadrupolar ordering has already been found at higher temperatures than those of magnetism for lanthanide compounds. This is not observed in systems where the interactions involving the f-valence electron states are stronger than the quadrupolar moments.

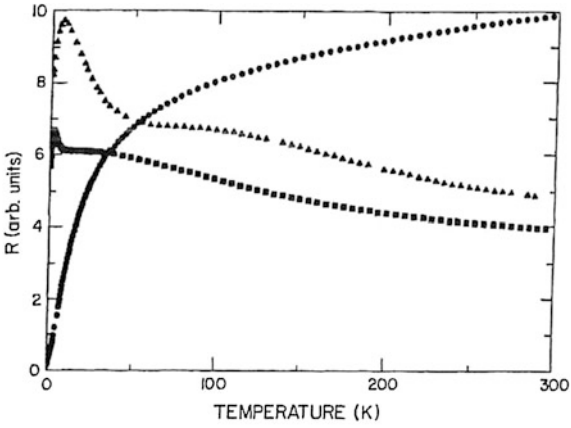

Fig. 2.21 Resistance versus temperature for $CeCu_2Si_2$ (*triangle*), UBe_{13} (*squares*) and UPt_3 (*dots*) [243]

Among the UT_2Si_2 compounds with T = transition metal, URu_2Si_2 was studied intensively [248–252]. In this heavy fermion compound, ordered phase and unconventional superconductivity at very low temperatures were obtained from thermal, electric and magnetic measurements. In fact, rapid decrease of the electrical resistivity was observed at standard pressure below 50 K but a sharp peak was observed at T_0 = 17.5 K. This peak was associated with a freezing of both the charge and the spin scattering and with a considerable decrease of the charge carrier number. Initially, an extremely weak antiferromagnetic moment was detected at a temperature near 0 K and associated with the presence of an ordered phase. But this moment was much too weak to account for the large anomaly observed in the vicinity of T_0. Another abrupt drop of resistivity was also observed below T_c = 1.7 K and associated with the onset of unconventional superconductivity, coexisting with the ordered state present in this range. These two temperatures changed differently with pressure, T_0 increased linearly while T_c decreased. From the measured Sommerfeld coefficient, the electron effective mass was found equal to about $25m_0$, where m_0 is the free electron mass. The nature of the order governing the phase observed below 17.5 K is actually a controversial subject and, for this reason, it was named a *hidden order*. Attributed at first to the development of a spin or charge density wave, this phase was associated with other order parameters, multipolar ordering, orbital antiferromagnetism, helicity. Actually, unexpected order parameters are still researched and this compound is the subject of a large variety of experiments. An anisotropic inelastic term of resistivity was observed in the hidden-order phase [253]. This suggests that an anisotropic scattering mechanism is present in this phase. Temperature versus pressure phase diagram is presented in Fig. 2.22 [252].

The unconventional superconductivity, present up to 1.2 K at P = 0 disappears at about 0.5 GPa for $T \rightarrow 0$ K. Simultaneously, the pressure induces a first-order phase transition from the hidden-order (HO) phase to a large moment antiferromagnetic (LMAF) phase. The border between the hidden-order phase and this antiferromagnetic phase follows a transition line up to a tricritical point located at

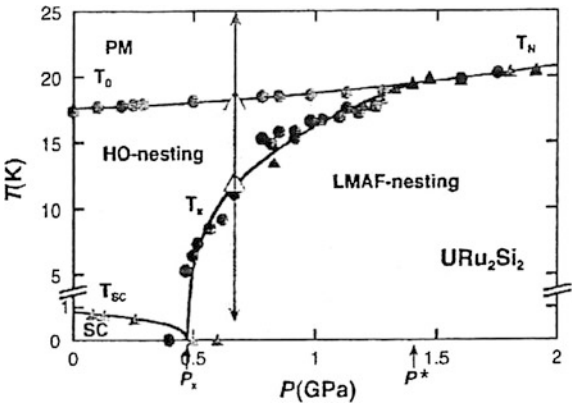

Fig. 2.22 Temperature versus pressure phase diagram for URu_2Si_2 from resistivity (*circles*) and ac calorimetry (*triangles*) measurements [252]

T = 19.3 K and P = 1.36 GPa corresponding to the transition to the normal paramagnetic (PM) phase. Above 1.36 GPa, a single transition occurs on cooling from the paramagnetic state to the large moment antiferromagnetic phase. The presence of a tricritical point suggests that the various phases have different symmetries and, consequently, no superconductivity could be present in the normal antiferromagnetic phase. Numerous experimental studies are pursued on high-quality single crystals in order to explain the unusual characteristics of the superconductor state as well as the hidden-order phase in which this state is embedded [188, 251].

The unusual phase diagram of URu_2Si_2 was attributed to the localization and delocalization of the uranium 5f electrons. In a metallic environment model, fluctuations occur between the $U^{3+}(5f^3)$ configuration and the $U^{4+}(5f^2)$ configuration with an extra 5f electron hybridized with the other valence electrons. In this model, the number of localized 5f electrons varies and one expects the presence of valence fluctuations. The phase diagram is influenced by a competition between these two different configurations. The decrease of the carrier number at the transition to the hidden-order phase suggests that this transition could be due to a partial localization of 5f electrons. In another possibility no valence fluctuations exist but only atoms situated in a particular space direction would have an increasing number of localized 5f electrons, thus explaining the anisotropy in the observed properties and the eventual presence of a multipolar order. In contrast, the pressure would favour the $5f^2$ configuration. Analogy had been researched with intermetallics of a rare-earth that has the same external electronic configuration as uranium and a parallel had been established with $PrFe_4P_{12}$ in which a hidden-order phase had been observed [254]. Initially identified with a antiferroquadripolar phase [197], it is expected to be a non-magnetic order phase with a multipolar component [251].

The coexistence of superconductivity and a ferromagnetic phase was observed for the first time in UGe_2 under pressure. This compound crystallizes in the orthorhombic structure. The uranium ions form chains with the distance between nearest neighbours d_{U-U} = 3.85 Å. UGe_2 is an itinerant ferromagnetic at standard pressure with a Curie temperature T_{Curie} equal to 52 K and a magnetic moment of $1.5\mu_B$. It is superconductor under pressure at about 1.2 GPa with a critical temperature T_C of 0.7 K [255]. Since T_C is lower than T_{Curie}, one deduces that the superconductor phase is present in the ferromagnetic phase. Two ferromagnetic phases have been identified, one at low pressure with the moment of $1.5\mu_B$, another at higher pressure with a moment of $1\mu_B$ (Fig. 2.23) [256].

It was shown that the pressure at the superconductivity maximum corresponds to the pressure for which the magnetic moment drops from $1.5\mu_B$ to $1\mu_B$. When the pressure increases, T_C decreases and ferromagnetism and superconductivity disappear simultaneously at the critical pressure of about 1.5 GPa through a first-order transition. This first-order transition was attributed to critical magnetic fluctuations [257].

Similar observations were made in compounds of the family UTGe with T = transition metal. Similar to UGe_2, the crystal structure of these compounds is orthorhombic with uranium chains ordered along the same axis. Their magnetic ordered temperatures vary as a function of the distance d_{U-U} between nearest

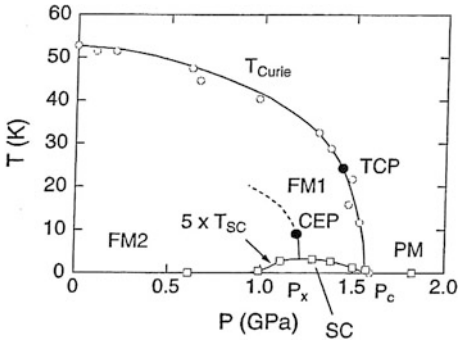

Fig. 2.23 Temperature versus pressure phase diagram for UGe_2. Two ferromagnetic phases, FM_1 and FM_2, have been identified, one at low pressure with the moment of $1.5\mu_B$, another at higher pressure with a moment of $1\mu_B$ [256]

neighbour uranium ions. For d_{U-U} equal to 3.5 Å, the compounds are ferromagnetic; below this value, they are paramagnetic and above it antiferromagnetic. In URhGe, d_{U-U} is equal to 3.50 Å. This value is very close to the distance for which there is a direct overlap of the 5f wave functions associated with two neighbouring atoms. Ferromagnetism and superconductivity are observed at standard pressure. URhGe has a magnetic moment of $0.4\mu_B$ and T_{Curie} is equal to 9.5 K. From temperature vs magnetic field phase diagram at standard pressure, superconductivity with T_C of about 0.25 K is observed at low field. As the field increases one observes a re-appearance of the superconductivity directly associated with an increase of the effective mass (Fig. 2.24) [188, 258, 259].

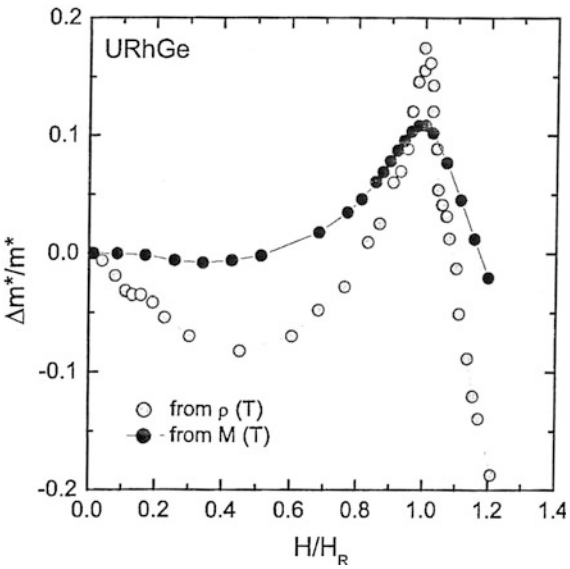

Fig. 2.24 Superconductivity directly associated with an increase of the effective mass for URhGe [188]

For the first time a link between the effective mass enhancement and the appearance of supraconductivity is directly observed. As in UGe_2, supraconductivity should be due to critical magnetic fluctuations.

The compound UCoGe is a weak itinerant ferromagnet with T_{Curie} equal to 2.8 K and an unusually small magnetic moment of about $0.05\mu_B$. From electronic specific heat measurements, the electron interactions are found relatively weak and it was shown that at standard pressure supraconductivity coexists with metallic ferromagnetism below the superconducting transition temperature T_C = 0.7 K. T_C increases with the pressure. Because T_{Curie} and T_C are close, interplay between ferromagnetism and superconductivity is strong. In contrast with the two precedent compounds, superconductivity persists in the paramagnetic regime above a critical pressure of 1.40 GPa. Pressure-temperature phase diagram was determined for high-quality single crystals (Fig. 2.25) [260].

In fact, the temperatures T_{Curie} and T_C depend on the quality of the sample and decrease when the quality decreases. Ferromagnetism vanishes above 1.3 GPa. Near this ferromagnetic critical point, superconductivity is enhanced and this diagram is different from that of other superconducting ferromagnets. Consequently, this compound presents an unusual behaviour and is considered as particularly interesting for studying the relation between unconventional superconductivity and magnetic interactions. But it is essential that high-quality single crystals be available. This has not yet been achieved for UCoGe nor for URhGe. It is important to underline that up to now the known ferromagnetic superconductors are all uranium compounds.

Many other uranium intermetallics have been studied. Thus, in UPd_2Al_3 and UNi_2Al_3, antiferromagnetism and superconductivity coexist at low temperature [261–263] like in Chevrel phase compounds (of the type RMo_6Se_8 with R = rare-earth). These systems are antiferromagnetic and have two separate classes of localized and delocalized electrons responsible either for magnetic properties or superconductivity. For UPd_2Al_3, it was deduced from the quasi-atomic magnetic moment measured below $T_N(0.85\mu_B)$ and from the large Sommerfeld coefficient, that two 5f electrons are localized in the U^{4+} ion, while the other 5f electrons are

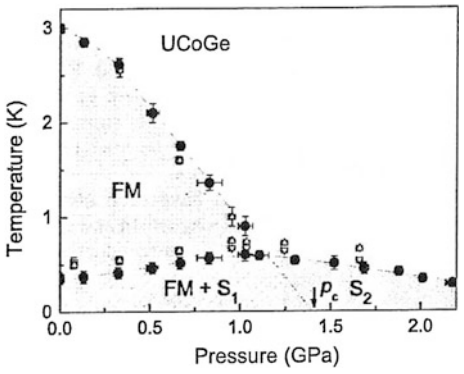

Fig. 2.25 Temperature versus pressure phase diagram of UCoGe [260]. FM: ferromagnetism; S_1, S_2: superconductivity; critical pressure $P_c = 1.40 \pm 0.05$ GPa

hybridized with the valence electrons. In the alloy system $Y_{1-x}U_xPd_3$, no Fermi liquid phase was found from measurements of specific heat, magnetic susceptibility and electric resistance [264]. Later on, this phase was observed in a number of other f-electron alloy systems, including $Sc_{1-x}U_xPd_3$, $UCu_{3.5}Pd_{1.5}$, $Th_{0.1}U_{0.9}Be_{13}$, $Th_{1-x}U_xRu_2Si_2$, $Th_{1-x}U_xPd_2Al_3$. Let us mention also that uranium and neptunium compounds of the $U_2(Np_2)T_2X$ type have been obtained with nearly all transition metals of the Fe, Co and Ni column. X represents Sn or In. From these materials, interaction of the 5f electrons with the d electrons of the transition metal was studied and found decreasing with the gradual filling of the d band.

The discovery of superconductivity in $PuCoGa_5$ [265] has lead to make this family of 115 compounds the best studied among the plutonium intermetallics. The transition temperature of $PuCoGa_5$, T_C, is 18.5 K, i.e. about an order of magnitude greater than that of the heavy fermion superconductors of cerium and uranium. $PuCoGa_5$ crystallizes in the tetragonal structure and is formed of alternating layers of $PuGa_3$ and $CoGa_2$ stacked along the c axis. This structure is similar to that of the 115 analogous rare-earths compounds that include several unconventional superconductors. Electrical resistivity, magnetic susceptibility and specific heat of $PuCoGa_5$ were measured as function of the temperature and the magnetic field. Zero resistivity transition was observed around 18.2 K and a sharp diamagnetic transition was observed slightly above 18 K. A local magnetic moment close to that expected for Pu^{3+} was found at higher temperature. Its Sommerfeld coefficient value of 95 mJ mol^{-1} K^{-2} [266], is about one order of magnitude lower than that of the isostructural $CeCoIn_5$ and its spin fluctuation temperature T_{cf}, which is inversely proportional to Sommerfeld coefficient, is therefore one order of magnitude higher. Analogous variation is predicted for T_C in case the model of magnetically mediated superconductivity proves applicable. This variation was proposed in order to explain the high value of T_C. The presence of antiferromagnetic spin fluctuations just above T_C as well as that of a d-wave pairing below T_C were deduced from nuclear magnetic resonance measurements [267]. Analogy appears, then, with the properties of the $CeMIn_5$ heavy fermion superconductors. However, for the latter, superconductivity is observed near the antiferromagnetic quantum critical point, making the use of the same model for $PuCoGa_5$ difficult. Increase of T_C with increase of the c/a ratio of the tetragonal lattice parameters was observed in the $PuTGa_5$ and $CeTIn_5$ (T = Co, Rh, Ir) superconductors and the existence of a common mechanism of superconductivity related to the structure was, then, suggested [266]. Independently, a value of the Coulomb interaction U equal to 3 eV was found necessary in order to provide a good description of the phonon spectrum [268]. On the other hand, since the spin fluctuation temperature is inversely proportional to the effective mass, it was suggested that the increase of the transition temperature implies that a hybridization of the f electrons with the valence electrons in the plutonium compounds is more complete than in the cerium ones. Charge fluctuations associated with a change in the 5f configuration as well as density fluctuations associated with different ionic radii of the $5f^n$ and $5f^{n-1}$ configurations have, then, been proposed to account for the unconventional superconductivity, and could also be responsible for spin fluctuations. For $PuRhGa_5$, the critical transition

temperature T_C is 8.7 K [269]. The two $PuRhGa_5$ and $PuCoGa_5$ compounds display very similar properties. The quasi two-dimensional structure of tetragonal compounds is advantageous for superconductivity [270]. Indeed, this structure was shown to be preferable to the formation of pairs by density fluctuations than a three-dimensional structure [271].

More recently, properties of $PuCoIn_5$ have been investigated [272]. Its unit cell is about 30 % larger than that of $PuCoGa_5$. This volume expansion is associated with a change in the electronic properties. The unit cell volume of $PuCoIn_5$ is nearly identical to that of $SmCoIn_5$, i.e. to the volume expected for Sm ions with localized 4f electrons. In contrast, the unit cell volume of $PuCoGa_5$ is smaller than that of $SmCoGa_5$, suggesting a mixed valence ground state of the 5f electrons. $PuCoIn_5$ is a superconductor with $T_C = 2.5$ K. Its Sommerfeld coefficient is 200 mJ mol^{-1} K^{-2}. $PuCoIn_5$ can then be classified as a heavy fermion compound with 5f electrons more localized than those of $PuCoGa_5$ for which a possibility of a mixed valence state exists. Consequently, it was suggested that the high superconducting transition temperature of $PuCoGa_5$ could be due to valence fluctuations while the superconductivity of $PuCoIn_5$ would be associated with antiferromagnetic spin fluctuations. Schematic phase diagram, based on such a scenario, was proposed (Fig. 2.26) [272].

This model presents similarities with that describing $CeCu_2Si_2$ under pressure, according to which a second domain of superconductivity is observed at higher T_C,

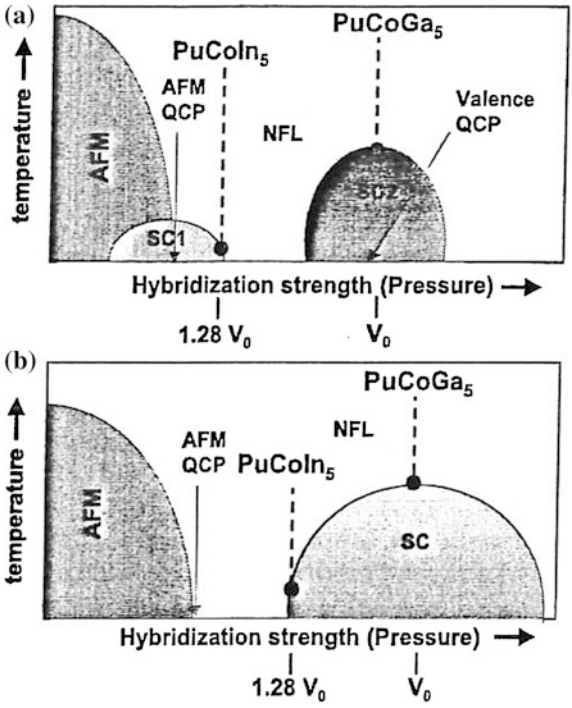

Fig. 2.26 Schematic Temperature versus pressure phase diagram of $PuCoX_5$ (X = In, Ga) [272]. AFM: antiferromagnetic; QCP: quantum critical point; SC: superconductor; NFL: non Fermi liquid; **a** SC1 corresponds to $PuCoIn_5$ and SC_2 to $PuCoGa_5$; **b** $PuCoIn_5$ and $PuCoGa_5$ have the same superconducting dome

along with valence instability, and is attributed to critical valence fluctuations. However, these interpretations have not been substantiated and other alternative models have been proposed. Further experiments would be necessary in order to reach a conclusion. Actually, the superconductivity in $PuCoGa_5$ is considered as directly dependent on the plutonium anomalous electronic properties. This material is considered as an intermediate addition, in terms of T_c, to the two other classes of "magnetic well known" superconductors: the heavy-fermion materials, which have T_cs of about 1 K and the copper oxides, which have T_cs of about 100 K.

In contrast with $PuCoGa_5$, temperature independent paramagnetism was seen in the isostructural $UCoGa_5$ compound. No local moment was detected and low Sommerfeld coefficient of about 10 mJ mol^{-1} K^{-2} was measured. A value of Coulomb interaction U close to zero provided a good theoretical description of the phonon spectrum. This compound is not a superconductor within the observed temperature limits. From these results, the localization of the 5f electrons is expected to be weaker in this compound than in $PuCoGa_5$.

In spite of numerous studies, the interpretation of the phase diagrams of 5f electrons systems and of their superconductivity remains an open problem. Application of pressure, doping or presence of a magnetic field can lead to quantum phase transitions between a magnetically ordered state and a paramagnetic state. These transitions are attributed to critical quantum fluctuations, often considered as having a magnetic origin. Nevertheless, no clear evidence has been given. Quantum critical phenomena, which are not explained by the conventional quantum critical model with spin fluctuations, are explained by a model with local critical valence fluctuations. This is extensively discussed [189]. In the case of heavy fermion materials, the effective electron mass can be sufficiently large for the electronic energies to be of the same order of magnitude or superior to the magnetic energies. The localization or delocalization of the 5f electrons is, then, an important parameter because it governs the electronic energies and can give a predominant role to the valence fluctuations. An intensive research into magnetic superconductors is conducted actually in order to understand the bases for stimulating the superconductivity, since that is crucial in the search for new superconducting materials.

References

1. P. Jonnard, F. Vergand, C. Bonnelle, E. Orgaz, M. Gupta, Phys. Rev. B **57**, 12111 (1998)
2. J.C. Slater, Symmetry and Energy bands in crystals, vol. 2 (McGraw-Hill, New York, 1965)
3. E. Holland-Moritz, Z. Phys. B:Condens. Matter **89**, 285 (1992)
4. L. Eyring, Handbook on the physics and chemistry of rare earths, vol. 3, ed. by K.A. Gschneider, L. Eyring (North-Holland, Amsterdam, 1979), p. 337
5. G. Scarel, A. Svane, M. Fanciulli, Topics Appl. Phys. **106**, 1 (2007)
6. A. Delin, L. Fast, B. Johansson, J.M. Wills, O. Eriksson, Phys. Rev. Lett. **79**, 4637 (1997)
7. J. Danan, C. deNovion, R. Lallement, Solid State Commun **7**,1103 (1969)
8. Y. Baer, C. Zürcher, Phys. Rev. Lett. **39**, 956 (1977)

9. C.M. Varma, Rev. Mod. Phys. **48**, 219 (1976)
10. J.M. Lawrence, P.S. Riseborough, R.D. Parks, Rep. Prog. Phys. **44**, 1 (1981)
11. P. Wachter, *Handbook on the physics and chemistry of rare earths*, vol. 19, Chap. 132, eds. by K.A. Gschneidner, L. Eyring, G.H. Lander, G.R. Choppin (Elsevier Science, Amsterdam, 1994)
12. M.B. Maple, D. Wohlleben, Phys. Rev. Lett. **27**, 511 (1971)
13. J.R. Iglesias Sicardi, A.K. Bhattacharjee, R. Jullien, B. Coqblin, Solid State Commun. **16**, 499 (1975)
14. P.W. Anderson, Phys. Rev. **79**, 350 (1950)
15. P.W. Anderson, Phys. Rev. **115**, 2 (1959)
16. R.A. de Groot, F.M. Mueller, P.G. van Engen, K.H.J. Buschow, Phys. Rev. Lett. **50**, 2024 (1983)
17. L. Petit, R. Tyer, Z. Szotek, W.M. Temmerman, A. Svane, New J. Phys. **12**, 113041 (2010)
18. L.V. Pourovskii, B. Amadon, S. Biermann, A. Georges, Phys. Rev. B **76**, 235101 (2007)
19. J.D. Thompson, J.M. Lawrence, *Handbook of the physics and chemistry of rare earths*, vol. 19 (1994), p. 383
20. T. Kasuya, Europhys. Lett. **26**, 283 (1994)
21. J. Derr, G. Knebel, G. Lapertot, B. Salce, M.-A. Méasson, J. Flouquet, J. Phys.: Condens. Matter **18**, 2089 (2006)
22. A. Menth, E. Buehler, T.H. Geballe, Phys. Rev. Lett. **22**, 295 (1969)
23. S. Wolgast, C. Kurdak, K. Sun, J.W. Allen, D.-J. Kim, Z. Fisk, Phys. Rev. B **88**, R180405 (2012)
24. L. Petit, A. Svane, Z. Szotek, W.M. Temmerman, Phys. Rev. B **72**, 205118 (2005)
25. P. Patsalas, S. Logothetidis, L. Sygellou, S. Kennou, Phys. Rev. B **68**, 035104 (2003)
26. N.V. Skorodumova, S.I. Simak, B.I. Lundqvist, I.A. Abrikosov, B. Johansson, Phys. Rev. Lett. **89**, 166601 (2002)
27. N.V. Skorodumova, R. Ahuja, S.I. Simak, I.A. Abrikosov, B. Johansson, B.I. Lundqvist, Phys. Rev. B **64**, 115108 (2001)
28. H. Pinto, M.N. Mintz, M. Melamud, H. Shaked, Phys. Lett. **88**, 81 (1982)
29. A. Fujimori, Phys. Rev. B **27**, 3992 (1983)
30. A. Fujimori, Phys. Rev. B **28**, 2281 (1983)
31. F.L. Normand, J.E. Fallah, L. Hiliaire, P. Légaré, A. Kotani, J.C. Parlebas, Solid State Commun. **71**, 885 (1989)
32. E. Wuilloud, B. Delley, W.-D. Schneider, Y. Baer, Phys. Rev. Lett. **53**, 202 (1984)
33. D.D. Koelling, A.M. Boring, J.H. Wood, Solid State Commun. **47**, 227 (1983)
34. R. Gillen, S.J. Clark, J. Robertson, Phys. Rev. B **87**, 125116 (2013)
35. T. Hanyu, H. Ishii, M. Yanagihara, T. Kamada, T. Miyahara, H. Kato, K. Naito, S. Suzuki, T. Ishii, Solid State Commun. **56**, 381 (1985)
36. A. Bianconi, A. Kotani, K. Okada, R. Giorgi, A. Gargano, A. Marcelli, T. Miyahara, Phys. Rev. B **38**, 3433 (1988)
37. H. Ogasawara, A. Kotani, K. Okada, B.T. Thole, Phys. Rev. B **43**, 854 (1991)
38. L. Petit, A. Svane, Z. Szotek, W.M. Temmerman, Top. Appl. Phys. **106**, 331 (2007)
39. R.C. Karnatak, J.-M. Esteva, H. Dexper, M. Gasgnier, P.E. Caro, L. Albert, Phys. Rev. B **36**, 1745 (1987)
40. J. Lettieri, V. Vaithyanathan, S.K. Eah, J. Stephens, V. Sih, D.D. Awschalom, J. Levy, D.G. Schlom, Appl. Phys. Lett. **83**, 975 (2003)
41. A. Werner, H.D. Hocheimer, A. Jayaraman, J.M. Leger, Solid State Commun. **38**, 325 (1981)
42. B. Johansson, Phys. Rev. B **19**, 6615 (1979)
43. J.M. Leger, N. Yacoubi, J. Loriers, J. Solid State Chem. **36**, 261 (1981)
44. M. Alessandri, A. Del Vitto, R. Piagge, A. Sebastiani, C. Scozzari, C. Wierner, L. Lamagna, M. Perego, G. Ghidini, M. Fanciulli, Microelectron. Eng. **87**, 290 (2010)
45. E. Bonera, G. Scarel, M. Fanciulli, P. Delugas, V. Fiorentini, Phys. Rev. Lett. **94**, 27602 (2005)
46. J.P. Liu, P. Zaumseil, E. Bugiel, H.J. Osten, Appl. Phys. Lett. **79**, 671 (2001)

47. M. Hong, J. Kwo, A.R. Kortan, J.P. Mannaerts, A.M. Sergent, Science **283**, 1897 (1999)
48. A. Jayaraman, A.K. Singh, A. Chatterjee, S. Usha Devi, Phys. Rev. B **9**, 2513 (1974)
49. A. Svane, G. Santi, Z. Szotek, W.M. Temmerman, P. Strange, M. Horne, G. Vaitheeswaran, V. Kanchana, L. Petit, H. Winter, Phys. Status Solidi B **241**, 3185 (2004)
50. K. Syassen, H. Winzen, H.G. Zimmer, H. Tups, J.M. Leger, Phys. Rev. B **32**, 8246 (1985)
51. M. Colarieti-Tosti, M.I. Katsnelson, M. Mattesini, S.I. Simak, R. Ahuja, B. Johansson, C. Dallera, O. Eriksson, Phys. Rev. Lett. **93**, 96403 (2004)
52. A. Jayaraman, V. Narayanamuri, E. Bucher, R.G. Maines, Phys. Rev. Lett. **25**, 368 (1970)
53. A. Jayaraman, V. Narayanamuri, E. Bucher, R.G. Maines, Phys. Rev. Lett. **25**, 1430 (1970)
54. B. Batlogg, E. Kaldis, A. Schlegel, B. Wachter, Phys. Rev. B **14**, 653 (1976)
55. K. Syassen, J. Phys. (Paris) Colloq. **45**, C8-123 (1984)
56. M. Campagna, E. Bucher, G.K. Wertheim, L.D. Longinotti, Phys. Rev. Lett. **33**, 165 (1974)
57. S.-J. Oh, J.W. Allen, Phys. Rev. B **29**, 589 (1984)
58. E. Kaldis, P. Wachter, Solid State Commun. **11**, 907 (1972)
59. V.P. Zhuze, A.V. Golubkov, E.V. Goncharova, T.I. Komarova, V.M. Sergeeva, Sov. Phys. Solid State **6**, 213 (1964)
60. A. Jayaraman, in *Handbook on the physics and chemistry of rare earths*, Chap. 9, vol. I, eds. by K.A. Gschneidner, Jr, I. Eyring (North-Holland, Amsterdam, 1979)
61. A. Chatterjee, A.K. Singh, A. Jayaraman, Phys. Rev. B **6**, 2285 (1972)
62. A. Svane, V. Kanchana, G. Vaitheeswaran, G. Santi, W.M. Temmerman, Z. Szotek, P. Strange, L. Petit, Phys. Rev. B **71**, 045119 (2005)
63. A. Rosengren, B. Johansson, Phys. Rev. B **13**, 1468 (1976)
64. E. Rogers, P.F. Smet, P. Dorenbos, D. Poelman, E. VanderKolk, J. Phys, Condens. Matter **22**, 015005 (2010)
65. E. Bucher, K. Andres, F.J. Disalvo, J.P. Maita, A.C. Gossard, A.S. Cooper, G.W. Hull, Phys. Rev. B **11**, 500 (1975)
66. A. Berger, E. Bucher, P. Haen, F. Holzberg, F. Lapierre, T. Penney, R. Tournier, in *Valence instabilities and related narrow band phenomena*, ed. by R.D. Parks (Plenum, New York, 1977), p. 491
67. R. Suryanarayanan, G. Guntherodt, J.L. Freeouf, F. Hultzberg, Phys. Rev. B **12**, 4215 (1975)
68. S. Lebègue, G. Santi, A. Svane, O. Bengone, M.I. Katsnelson, A.I. Lichtenstein, O. Eriksson, Phys. Rev. B **72**, 245102 (2005)
69. T. Matsumura, T. Kosaka, J. Tang, T. Matsumoto, H. Takahashi, N. Mori, T. Susuki, Phys. Rev. Lett. **78**, 1138 (1997)
70. P. Link, I.N. Goncharenko, J.M. Mignot, T. Matsumura, T. Suzuki, Phys. Rev. Lett. **80**, 173 (1998)
71. A.I. Lichtenstein, M.I. Katsnelson, Phys. Rev. B **57**, 6884 (1998)
72. P. Strange, A. Svane, W.M. Temmerman, Z. Szotek, H. Winter, Nature **399**, 756 (1999)
73. G.G. Gadzhiev, ShM Ismailov, KhKh Abdullaev, M.M. Khamidov, Z.M. Omarov, High Temp. **38**, 875 (2000)
74. G.G. Gadzhiev, ShM Ismailov, M.M. Khamidov, KhKh Abdullaev, Z.M. Omarov, High Temp. **39**, 407 (2001)
75. C.-G. Duan, R.F. Sabirianov, W.N. Mei, P.A. Dowben, S.S. Jaswal, J. Phys.: Condens. Matter **19**, 315220 (2007)
76. A. Hasegawa, A. Yanase, J. Phys. Soc. Jpn **42**, 492 (1977)
77. M.R. Norman, D.D. Koelling, A.J. Freeman, Phys. Rev. B **32**, 7748 (1985)
78. A.G. Petukhov, W.R.L. Lambrecht, B. Segall, Phys. Rev. B **50**, 7800 (1994)
79. A.G. Petukhov, W.R.L. Lambrecht, B. Segall, Phys. Rev. B **53**, 4324 (1996)
80. D.B. Ghosh, M. De, S.K. De, Phys. Rev. B **67**, 035118 (2003)
81. G. Vaitheeswaran, L. Petit, A. Svane, V. Kanchana, M. Rajaagopalan, J. Phys. Condens. Matter **16**, 4429 (2004)
82. T. Adachi, I. Shirotani, J. Hayashi, O. Shimomura, Phys. Lett. A **250**, 389 (1998)
83. L.V. Pourovskii, K.T. Delaney, C.G. Van de Walle, N.A. Spaldin, A. Georges, Phys. Rev. Lett. **102**, 096401 (2009)

84. M.S.S. Brook, J. Magn. Mater, **47–48**, 260 (1985)
85. F. Patthey, Europhys. Lett. **2**, 883 (1986)
86. F. Patthey, Phys. Rev. B **42**, 8864 (1990)
87. A. Delin, P.M. Oppeneer, M.S.S. Brooks, T. Kraft, J.M. Wills, B. Johansson, O. Eriksson, Phys. Rev. B **55**, R10173 (1997)
88. A. Jayaraman, W. Lowe, L.D. Longinotti, E. Bucher, Phys. Rev. Lett. **36**, 366 (1976)
89. G. Busch, O. Vogt, Phys. Lett. **20**, 152 (1968)
90. A. Svane, W. Temmerman, Z. Szotek, Phys. Rev. B **59**, 7888 (1999)
91. J. Laegsgaard, A. Svane, Phys. Rev. B **58**, 12817 (1998)
92. N. Kioussis, D. Swearinger, B.R. Cooper, J.M. Wills, J. Appl. Phys. **69**, 5475 (1991)
93. P. Wachter, E. Kaldis, R. Hauger, Phys. Rev. Lett. **40**, 1404 (1978)
94. D.X. Li, Y. Haga, H. Shida, T. Suzuki, T. Koide, G. Kido, Phys. Rev. B **53**, 8473 (1996)
95. T. Kasuya, D.X. Li, J. Magn. Mater. **167**, L1 (1997)
96. E. Kaldis, C. Zurcher, Helv. Phys. Acta **47**, 421 (1974)
97. J.Q. Xiao, C.L. Chien, Phys. Rev. Lett. **76**, 1727 (1996)
98. W.R.L. Lambrecht, Phys. Rev. B **62**, 13538 (2000)
99. C.M. Aerts, P. Strange, M. Home, W.M. Temmerman, Z. Szotek, A. Svane, Phys. Rev. B **69**, 045115 (2004)
100. M. Home, P. Strange, W.M. Temmerman, Z. Szotek, A. Svane, H. Winter, J. Phys.: Condens. Matter **16**, 5061 (2004)
101. Z. Szotek, W.M. Temmerman, A. Svane, L. Petit, P. Strange, G.M. Stocks, D. Kodderitzsch, W. Hergert, H. Winter, J. Phys.: Condens. Matter **16**, S5587 (2004)
102. C.-G. Duan, R.F. Sabirianov, J. Liu, W.N. Mei, P.A. Dowben, J.R. Hardy, Phys. Rev. Lett. **94**, 237201 (2005)
103. C.-G. Duan, R.F. Sabiryanov, W.N. Mei, P.A. Dowben, S.S. Jaswal, E.Y. Tsymbal, Appl. Phys. Lett. **88**, 182505 (2006)
104. A.N. Chantis, M. van Schilfgaarde, T. Kotani, Phys. Rev. B **76**, 165126 (2007)
105. P. Larson, W.R.L. Lambrecht, A. Chantis, M. van Schilfgaarde, Phys. Rev. B **75**, 045114 (2007)
106. S. Granville, B.J. Ruck, F. Budde, A. Koo, D.J. Pringle, F. Kuchler, A.R.H. Preston, D.H. Housden, N. Lund, A. Bittar, G.V.M. Williams, H.J. Trodahl, Phys. Rev. B **73**, 235335 (2006)
107. F. Natali, B.J. Ruck, H.J. Trodahl, Do Le Binh, S. Vezian, B. Damilano, Y. Cordier, F. Semond, C. Meyer, Phys. Rev. B **87**, 035202 (2013)
108. S.A. Wolf, D.D. Awschalom, R.A. Buhrman, J.M. Daughton, S. van Molnar, M.L. Roukes, A.Y. Chtchelkanova, D.M. Treger, Science **294**, 1488 (2001)
109. H. van Leuken, R.A. de Groot, Phys. Rev. Lett. **74**, 1171 (1995)
110. S.J. Allen, D. Brehmer, C.J. Palmstrom, *Rare earth doped semiconductors*, eds. by G.S. Pomrenke, P.B. Klein, D.W. Langer. Material Research Society symposia proceedings, vol. 301 (1993), p. 307
111. C.J. Pamstrom, N. Tabatabaie, S.J. Allen, Appl. Phys. Lett. **53**, 2608 (1988)
112. D.E. Brehmer, K. Zhang, ChJ Schwarz, S.P. Chau, S.J. Allen, J.P. Ibbetson, J.P. Zhang, C.J. Palmstrom, B. Wilkens, Appl. Phys. Lett. **67**, 1268 (1995)
113. C. Kadow, A.W. Jackson, A.C. Gossard, S. Matsuura, G.A. Blake, Appl. Phys. Lett. **76**, 3510 (2000)
114. L. Esaki, P. Siles, S. van Malnar, Phys. Rev. Lett. **19**, 852 (1967)
115. P. LeClair, J.K. Ha, H.J.M. Swagten, J.T. Kohlhepp, C.H. van de Vin, W.J.M. de Jonge, Appl. Phys. Lett. **80**, 625 (2002)
116. L. Degiorgi, Rev. Mod. Phys. **71**, 687 (1999)
117. K.A. Gschneidner, L.R. Eyring, G.H. Lander (eds.), *Handbook on the physics and chemistry of rare earths*, vol. 32 (2002)
118. S. Doniach, Phys. B **91**, 231 (1977)
119. H.V. Löhneysen, T. Pietrus, G. Portisch, H.G. Schlager, A. Schröder, M. Sieck, T. Trappmann, Phys. Rev. Lett. **72**, 3262 (1994)

120. I. Paul, G. Kotliar, Phys. Rev. B **64**, 184414 (2001)
121. J. Hertz, Phys. Rev. B **14**, 1165 (1976)
122. G.R. Stewart, Rev. Mod. Phys. **73**, 797 (2001)
123. H.V. Löhneysen, A. Rosch, M. Vojta, P. Wölfle, Rev. Mod. Phys. **79**, 1015 (2007)
124. H. Yashima, H. Mori, T. Satoh, Solid State Commun. **43**, 193 (1982)
125. B. Coqblin, M.A. Gusmao, J.R. Iglesias, A.R. Ruppenthal, C. Lacroix, J. Magn. Magn. Mat. **226–230**, 115 (2001)
126. G.R. Stewart, Rev. Mod. Phys. **56**, 755 (1984)
127. A.C. Hewson, *The Kondo problem to heavy fermions* (Cambridge University Press, Cambridge, 1993)
128. T. Moriya, *Spin fluctuations in itinerant electron magnetism* (Springer, Berlin, 1985)
129. A. Millis, Phys. Rev. B **48**, 7183 (1993)
130. T. Moriya, K. Ueda, Adv. Phys. **49**, 555 (2000)
131. T. Moriya, K. Ueda, Rep. Prog. Phys. **66**, 1299 (2003)
132. A. Schroder, G. Aeppli, R. Goldea, M. Adams, O. Stockert, H.v. Löhneysen, E. Bucher, R. Ramazashvill, P. Coleman, Nature **407**, 351 (2000)
133. Q. Si, S. Rabello, K. Ingersent, J.L. Smith, Nature **413**, 804 (2001)
134. P. Coleman, C. Pépin, Q. Si, R. Ramazashvili, J. Phys.: Condens. Matter **13**, R723 (2001)
135. P. Coleman, A.J. Schofield, Nature **433**, 226 (2005)
136. Q. Si, F. Steglich, Science **329**, 1161 (2010)
137. H.Q. Yuan, F.M. Grosche, M. Deppe, C. Geibel, G. Sparn, F. Steglich, Science **302**, 2104 (2003)
138. D. Jaccard, H. Wilhelm, K. Alami-Yadri, E. Vargoz, Phys. B **259–261**, 1 (1999)
139. A.T. Holmes, D. Jaccard, K. Miyake, Phys. Rev. B **69**, 024508 (2004)
140. E. Stryjewski, N. Giordano, Adv. Phys. **26**, 487 (1977)
141. K. Andres, J.E. Graebner, H.R. Ott, Phys. Rev. Lett **53**, 1779 (1975)
142. W. Franz, A. Griessel, F. Steglich, D. Wohlleben, Z. Phys. B **31**, 7 (1978)
143. D. Gignoux, J.C. Gomez-Sal, J. Appl. Phys. **57**, 3125 (1985)
144. F. Steglich, J. Aarts, C.D. Bredl, W. Lieke, D. Meschede, W. Franz, H. Schäfer, Phys. Rev. Lett. **43**, 1892 (1979)
145. W. Assmus, M. Herrmann, U. Rauchschwalbe, S. Riegel, W. Lieke, H. Spille, S. Hom, G. Weber, F. Steglich, Phys. Rev. Lett. **52**, 469 (1984)
146. H. Nakamura, Y. Kitaoka, H. Yamada, K. Asayama, J. Magn. Magn. Mater. **76–77**, 517 (1988)
147. P. Gegenward, C. Langhammer, C. Geibel, R. Helfrich, M. Lang, G. Spam, F. Steglich, R. Hom, L. Donnevert, A. Link, W. Assmus, Phys. Rev. Lett. **81**, 1501 (1998)
148. P. Gegenward, F. Kromer, M. Lang, G. Sparn, C. Geibel, F. Steglich, Phys. Rev. Lett. **82**, 1293 (1999)
149. R.A. Steeman, E. Frikkee, B. Helmholdtr, J. Menovsky, J. Vandenberg, G.J. Nieuwenhuys, J.A. Mydosh, Solid State Commun. **66**, 103 (1988)
150. S.R. Julian, C. Pfleiderer, F.M. Grosche, N.D. Mathur, G.J. McMullan, A.J. Diver, I.R. Walker, G.G. Lonzarich, J. Phys.:Condens. Matter **8**, 9675 (1996)
151. N.D. Mathur, F.M. Grosche, S.R. Julian, I.R. Walker, D.M. Freye, R.K.W. Haselwimmer, G.G. Lonzarich, Nature **394**, 39 (1998)
152. F. Steglich, J. Arndt, O. Stockert, S. Friedemann, M. Brando, C. Klingner, C. Krellner, C. Geibel, S. Wirth, S. Kirchner, Q. Si, J. Phys.: Condens. Matter **24**, 294201 (2012)
153. O. Stockert, J. Arndt, E. Faulhaber, C. Geibel, H.S. Jeevan, S. Kirchner, M. Loewenhaupt, K. Schmali, W. Schmidt, Q. Si, F. Steglich, Nat. Phys. **7**, 119 (2011)
154. P. Link, D. Jaccard, Phys. B **230–232**, 31 (1997)
155. K. Miyake, O. Narikiyo, Y. Onishi, Phys. B **259–261**, 676 (1999)
156. S. Raymond, L.P. Regnault, J. Flouquet, A. Wildes, P. Lejay, J. Phys.: Condens. Matter **13**, 8303 (2001)
157. W. Knafo, S. Raymond, P. Lejay, J. Flouquet, Nat. Phys. **5**, 753 (2009)

158. H. Kadowaki, Y. Tabata, M. Sato, N. Aso, S. Raymond, S. Kawarazaki, Phys. Rev. Lett. **96**, 016401 (2006)
159. D. Aoki, C. Paulsen, H. Kotegawa, F. Hardy, C. Meingast, P. Haen, M. Boukahil, W. Knafo, E. Ressouche, S. Raymond, J. Flouquet, J. Phys. Soc. Jpn. **81**, 034711 (2012)
160. Y. Onuki, et al., J. Magn. Magn. Mater. **54–57**, 389 (1986)
161. H.V. Löhneysen, J. Magn. Magn. Mater. **200**, 532 (1999)
162. H.V. Löhneysen, H. Bartolf, S. Drotziger, C. Pfleiderer, O. Stockert, D. Souptel, W. Löser, G. Behr, J. Alloys Compd. **408**, 9 (2006)
163. N.V. ChandraShekar, M. Rajagopalan, J.F. Meng, D.A. Polvani, J.V. Badding, J. Alloys Compd. **388**, 215 (2004)
164. M. Wilhelm, B. Hillenbrand, J. Phys. Chem. Solids **31**, 559 (1970)
165. T. Ekino, T. Takabatake, H. Tanaka, H. Fujii, Phys. Rev. Lett. **75**, 4262 (1995)
166. H. Hegger, C. Petrovic, E.G. Moshopoulou, M.F. Hundley, J.L. Sarrao, Z. Fisk, J.D. Thompson, Phys. Rev. Lett. **84**, 4986 (2000)
167. T. Mito, S. Kawasaki, Y. Kawasaki, G.-Q. Zheng, Y. Kitaoka, D. Aoki, Y. Haga, Y. Onuki, Phys. Rev. Lett. **90**, 077004 (2003)
168. G. Knebel, J. Buhot, D. Aoki, G. Lapertot, S. Raymond, E. Ressouche, J. Flouquet, J. Phys. Soc. Jpn. **80**, SA001 (2011)
169. T. Park, F. Ronning, H.Q. Yuan, M.B. Salamon, R. Movshovich, J.L. Sarrao, J.D. Thompson, Nature **440**, 65 (2006)
170. C. Petrovic, P.G. Pagliuso, M.F. Hundley, R. Movshovich, J.L. Sarrao, J.D. Thompson, Z. Fisk, P. Monthoux, J. Phys.: Condens. Matter **13**, L337 (2001)
171. C. Stock, C. Broholm, J. Hudis, H.J. Kang, C. Petrovic, Phys. Rev. Lett. **100**, 087001 (2008)
172. B.B. Zhou, S. Misra, E.H. da Silva Neto, P. Aynajian, R.E. Baumbach, J.D. Thompson, E.D. Bauer, A. Yazdani, Nat. Phys. **9**, 474 (2013)
173. F. Ronning, J.-X. Zhu, T. Das, M.J. Graf, R.C. Albers, H.B. Rhee, W.E. Pickett, J. Phys.: Condens. Matter **24**, 294602 (2012)
174. C. Capan, G. Seyfarth, D. Hurt, A.D. Bianchi, Z. Fisk, J. Phys.:Conf. Ser. **273**, 012027 (2011)
175. C. Petrovic, R. Movshovich, M. Jaime, P.G. Pagliuso, M.F. Hundley, J.L. Sarrao, Z. Fisk, J.D. Thompson, Europhys. Lett. **53**, 354 (2001)
176. Y. Nakajima et al., Phys. Rev. B **77**, 214504 (2008)
177. S. Watanabe, A. Tsuruta, K. Miyake, J. Flouquet, J. Phys. Soc. Jpn. **78**, 104706 (2009)
178. R. Settai, K. Katayama, D. Aoki, I. Sheikin, G. Knebel, J. Flouquet, Y. Onuki, J. Phys. Soc. Jpn. **80**, SA069 (2011)
179. O. Trovarelli, C. Geibel, S. Mederle, C. Langhammer, F.M. Grosche, P. Gegenwart, M. Lang, G. Spam, F. Steglich, Phys. Rev. Lett. **85**, 626 (2000)
180. P. Gegenwart et al., New J. Phys. **8**, 171 (2006)
181. P. Gegenwart, Q. Si, F. Steglich, Nat. Phys. **4**, 186 (2008)
182. G. Knebel, R. Boursier, E. Hassinger, G. Lapertot, P.G. Niklowitz, A. Pourret, B. Salce, J.P. Sanchez, I. Sheikin, P. Bonville, H. Harima, J. Flouquet, J. Phys. Soc. Jpn. **75**, 114709 (2006)
183. H. Pfau, S. Hartmann, U. Stockert, P. Sun, S. Lausberg, M. Brando, S. Friedemann, C. Krellner, C. Geibel, S. Wirth, S. Kirchner, E. Abrahams, Q. Si, F. Steglich, Nature **484**, 493 (2012)
184. K. Sugiyama et al., Phys. B **403**, 769 (2008)
185. A. Fernandez-Panella, D. Braithwaite, B. Salce, G. Lapertot, J. Flouquet, Phys. Rev. B **84**,134416 (2011)
186. D. Braithwaite, A. Fernandez-Panella, E. Colombier, B. Salce, G. Knebel, G. Lapertot, V. Baldent, J.-P. Rueff, L. Paolasini, R. Verben, J. Flouquet, Proceedings of international conference on superconductivity and magnetism, ICSM (2012)
187. T. Mito, M. Nakamura, M. Otani, T. Koyama, S. Wada, M. Ishizuka, M.K. Forthaus, R. Lengsdorf, M.M. Abd-Elmeguid, J.L. Sarrao, Phys. Rev. B **75**, 134401 (2007)

188. J. Flouquet, D. Aoki, F. Bourdarot, F. Hardy, E. Hassinger, G. Knebel, T.D. Matsuda, C. Meingast, C. Paulsen, V. Taufour, J. Phys. Conf. Ser. **273**, 012001 (2011)
189. S. Watanabe, K. Miyake, J. Phys.: Condens. Matter **24**, 294208 (2012)
190. V.K. Pecharsky, K.A. Gschneidner Jr, Pure Appl. Chem. **79**, 1383 (2007)
191. A. Szytula, in *Ferromagnetic materials*, vol. 5, ed. by K.H.J. Buschow (North-Holland, Amsterdam, 1991)
192. J.A. Bianco, B. Fak, E. Ressouche, B. Grenier, M. Rotter, D. Schmitt, J.A. Rodriguez-Velamazan, J. Campo, P. Lejay, Phys. Rev. B **82**, 054414 (2010)
193. E.M. Gyorgy, B. Batlogg, J.P. Remeika, R.B. vanDower, R.M. Fleming, H.E. Bair, G.P. Espinosa, A.S. Cooper, R.G. Maihes, J. Appl. Phys. **61**, 4237 (1987)
194. M. Duraj, R. Duraj, A. Skytula, Z. Tomkowicz, J. Magn. Magn. Mater. **73**, 240 (1988)
195. J.H.V.J. Brabers, A.J. Nolten, F. Kaysel, S.H.J. Lenczowski, K.H.J. Buschow, F.R. deBoer, Phys. Rev. B **50**, 16410 (1994)
196. H. Fujii, T. Okamoto, Solid State Commun. **53**, 715 (1985)
197. J.-G. Park, D.T. Adroja, K.A. McEwen, M. Kohgi, K. Iwasa, Y.S. Kwon, Phys. B **359–361**, 868 (2005)
198. E. Hassinger, J. Derr, J. Levallois, D. Aoki, K. Behnia, F. Bourdarot, G. Knebel, C. Proust, J. Flouquet, J. Phys. Soc. Jpn. **77**(supplement A), 172 (2008)
199. M. Kohgi, K. Iwasa, K. Kuwahara, Phys. B **385–386**, 23 (2006)
200. R. Lora-Serrano, C. Giles, E. Granado, D.J. Garcia, E. Miranda, O. Aguero, L. Mendoça Ferreira, J.G.S. Duque, P.G. Pagliuso, Phys. Rev. B **74**, 214404 (2006)
201. G.S. Smith, A.G. Tharp, Q. Johnston, Acta Crystallogr. **22**, 940 (1967)
202. V.K. Pecharsky, K.A. Gschneidner Jr, Phys. Rev. Lett. **78**, 4494 (1997)
203. V.K. Pecharsky, K.A. Gschneidner Jr, Alloys. Compd. **260**, 98 (1997)
204. F. Holtzberg, R.J. Gambino, T.R. McGuire, J. Phys. Chem. Solids **28**, 2283 (1967)
205. D. Haskel, Y.B. Lee, B.N. Harmon, Z. Islam, J.C. Lang, G. Srajer, Y. Mudryk, K.A. Gschneidner Jr., V.K. Pecharsky, Phys. Rev. Lett. **98**, 247205 (2007)
206. J.H. Belo, A.M. Pereira, C. Magen, L. Morellon, M.R. Ibarra, P.A. Algarabel, J.P. Araujo, J. Appl. Phys. **113**, 133909 (2013) and references cited
207. R. Tetean, E. Burzo, I.G. Deac, J. Opt. Adv. Mat. **8**, 501 (2006)
208. Y. Kamihara, T. Watanabe, M. Hirano, H. Hosono, J. Am. Chem. Soc. **130**, 3296 (2008)
209. H. Takahashi, K. Igawa, K. Arii, Y. Kamihara, M. Hirano, H. Hosono, Nature **453**, 376 (2008)
210. X.H. Chen, T. Wu, G. Wu, R.H. Liu, H. Chen, D.F. Fang, Nature **453**, 761 (2008)
211. Z.-A. Ren et al., Europhys. Lett. **83**, 17002 (2008)
212. W. Suski, in *Handbook on the physics and chemistry of rare earths*, vol. 22, eds. by K.A. Gschneidner Jr, L. Eyring (Elsevier, Amsterdam, 1996)
213. E. Burzo, Rep. Progr. Phys. **61**, 1099 (1998)
214. L. Bessais, E. Dorolti, C. Djega-Mariadassou, Appl. Phys. Lett. **87**, 192503 (2005)
215. L. Shlapbach, Top. Appl. Phys. **67** (1992)
216. Y. Tabata, K. Matsuda, S. Kanada, T. Waki, H. Nakamura, K. Sato, K. Kindo, J. Phys. Conf. Ser. **200**, 022063 (2010)
217. N. Marcano, J.C.G. Sal, J.I. Espeso, L.F. Barquin, Phys. Rev. B **76**, 224419 (2007)
218. T. Westerkamp, M. Deppe, R. Kuchler, M. Brando, C. Geibel, P. Gegenwart, A.P. Pikul, F. Steglich, Phys. Rev. Lett. **102**, 206404 (2009)
219. F.M. Zimmer, S.G. Magalhaes, B. Coqblin, J. Phys. Conf. Ser. **273**, 012069 (2011)
220. G.H. Lander et al., Phys. Rev. B **43**, 13672 (1991)
221. P. Roussel, P. Morrall, S.J. Tull, J. Nucl. Mat. **385**, 53 (2009)
222. L.R. Morss, J. Fuger, N.M. Edelstein, *The chemistry of the actinide and transactinide elements*, 3rd edn (Springer, Dordrecht, 2006)
223. H. Sakai, H. Kato, Y. Tokunaga, S. Kambe, R.Z. Walstedt, A. Nakamura, N. Tateiwa, T.C. Kobayashi, J. Phys. Cond. Matt. **15**, S2035 (2003)
224. S.L. Dudarev, D. Nguyen Manh, A.P. Sutton, Phil. Mag. **B75**, 613 (1997)
225. K.N. Kudin, G.E. Scuseria, R.L. Martin, Phys. Rev. Lett. **89**, 266402 (2002)

226. I. Prodan, G. Scuseria, J. Sordo, K. Kudin, R. Martin, J. Chem. Phys. **123**, 014703 (2005)
227. M.T. Butterfield et al., Surf. Sci. **600**, 1637 (2006)
228. G. Jomard, B. Amadon, F. Bottin, M. Torrent, Phys. Rev. B **78**, 075125 (2008)
229. I.D. Prodan, G.E. Scuseria, R.L. Martin, Phys. Rev. B **76**, 033101 (2007)
230. J.M. Haschke, T.H. Allen, L.A. Morales, Science **287**, 285 (2000)
231. T. Gouder, A. Seibert, L. Havela, J. Rebizant, Surf. Sci. **601**, L77 (2007)
232. G.H. Lander, M.S.S. Brooks, B. Lebech, P.J. Brown, O. Vogt, K. Mattenberger, Appl. Phys. Lett. **57**, 989 (1990)
233. L.V. Pourovskii, M.I. Katsnelson, A.I. Lichtenstein, Phys. Rev. B **72**, 115106 (2005)
234. D. Srivastava, S.P. Garg, G.L. Goswami, J. Nucl. Mater. **161**, 44 (1989)
235. L. Petit, A. Svane, Z. Szotek, W.M. Temmerman, G.M. Stocks, Phys. Rev. B **80**, 045124 (2009)
236. Y. Arai, K. Nakajima, Y. Suzuki, J. Alloys Compd. **271–273**, 602 (1998)
237. D. Damien, C.H. de Novion, J. Nucl. Mater. **100**, 167 (1981)
238. C. Thomas, A.S.R. Simies, J.R. Iglesias, C. Lacroix, N.B. Perkins, B. Coqblin, J. Phys.: Conf. Ser. **273**, 012028 (2011)
239. H.R. Ott, H. Rudigier, Z. Fisk, J.L. Smith, Phys. Rev. Lett. **50**, 1595 (1983)
240. H.R. Ott, H. Rudigier, Z. Fisk, J.L. Smith, Phys. Rev. B **31**, 1651 (1985)
241. B. Batlogg, D. Bishop, B. Golding, C.M. Varma, Z. Fisk, J.L. Smith, H.R. Ott, Phys. Rev. Lett. **55**, 1319 (1985)
242. Y. Shimizu, Y. Ikeda, T. Wakabayashi, K. Tenya, Y. Haga, H. Hidaka, T. Yanagisawa, H. Amitsuka, J. Phys.:Conf. Ser. **273**, 012084 (2011)
243. G.R. Stewart, Z. Fisk, J.O. Willis, J.L. Smith, Phys. Rev. Lett. **52**, 679 (1984)
244. S. Doniach, S. Engelsberg, Phys. Rev. Lett. **17**, 750 (1966)
245. R.A. Fisher, S. Kim, B.F. Woodfield, N.E. Phillips, L. Taillefer, K. Hasselback, J. Flouquet, A.L. Giorgi, J.L. Smith, Phys. Rev. Lett. **62**, 1411 (1989)
246. U. Steigenberger et al., J. Magn. Magn. Mater. **108**, 163 (1992)
247. K.A. McEwen et al., Phys. B **186**, 670 (1993)
248. T.T.M. Palstra, A.A. Menovsky, J. van den Berg, A.J. Dirkmaat, P.H. Kes, G.J. Nieuwenhuys, J.A. Mydosh, Phys. Rev. Lett. **55**, 2727 (1985)
249. M.B. Maple, J.W. Chen, Y. Dalichaouch, T. Kohara, C. Rossel, M.S. Torikachvili, M.W. McElfresh, J.D. Thompson, Phys. Rev. Lett. **56**, 185 (1986)
250. C. Broholm, J.K. Kjems, W.J.L. Buyers, P. Matthews, T.T.M. Palstra, A.A. Menovsky, J.A. Mydosh, Phys. Rev. Lett. **58**, 1467 (1987)
251. E. Hassinger, G. Knebel, K. Izawa, P. Lejay, B. Salce, J. Flouquet, Phys. Rev. B **77**,115117 (2008) and references cited
252. A. Villaume, F. Bourdarot, E. Hassinger, S. Raymond, V. Taufour, D. Aoki, J. Flouquet, Phys. Rev. B **78**, 012504 (2008)
253. Z.W. Zhu, E. Hassinger, Z.A. Xu, D. Aoki, J. Flouquet, K. Behnia, Phys. Rev. B **80**, 172501 (2009)
254. M.A.L. De La Torre, P.Visani, Y. Dalichaouch, B.W. Lee, M.B. Mapple, Phys. B **179**, 208 (1992)
255. S.S. Saxena, P. Agarval, K. Ahilan, F.M. Grosche, R.K.W. Haselwimmer, M.J. Steiner, E. Pugh, L.B. Walker, S.R. Julian, P. Monthoux, G.G. Lonzarich, A. Huxley, L. Shelkin, D. Braithwaite, J. Flouquet, Nature **106**, 587 (2000)
256. D. Aoki, J. Flouquet, J. Phys. Soc. Jpn. **81**, 011003 (2012) and references cited
257. K.G. Sandeman, G.G. Lonzarich, A.J. Schofield, Phys. Rev. Lett. **90**, 167005 (2003)
258. F. Levy, I. Sheikin, B. Grenier, A.D. Huxley, Science **309**, 1343 (2005)
259. A. Miyake, D. Aoki, J. Flouquet, Phys. Soc. Jpn. **77**, 094709 (2008)
260. E. Slooten, T. Naka, A. Gasparini, Y.K. Huang, A. de Visser, Phys. Rev. Lett. **103**, 097003 (2009) and references cited
261. C. Geibel et al., Z. Phys. B **81**, 1 (1991)
262. A. Krimmel et al., Z. Phys. B **86**, 161 (1992)

263. A. Hiess, N. Bernhoeft, N. Metoki, G.H. Lander, B. Roessli, N.K. Sato, N. Aso, Y. Haga, Y. Koike, T. Komatsubara, Y. Onuki, J. Phys. Cond. Matter **18**, R437 (2006)
264. C.L. Seaman et al., Phys. Rev. Lett. **67**, 2882 (1991)
265. J.L. Sarrao, L.A. Morales, J.D. Thompson, B.L. Scott, G.R. Stewart, F. Wastin, J. Rebizant, P. Boulet, E. Colineau, G.H. Lander, Nature **420**, 297 (2002)
266. E.D. Bauer, J.D. Thompson, J.L. Sarrao, L.A. Morales, F. Wastin, J. Rebizant, J.C. Griveau, P. Javorsky, P. Boulet, E. Colineau, G.H. Landre, G.R. Stewart, Phys. Rev. Lett. **93**, 147005 (2004)
267. N.J. Curro, T. Caldwell, E.D. Bauer, L.A. Morales, M.J. Graf, Y. Bang, A.V. Balatsky, J.D. Thompson, J.L. Sarrao, Nature **434**, 622 (2005)
268. S. Raymond, P. Piekarz, J.P. Sanchez, J. Serrano, M. Krisch, B. Janousova, J. Rebizant, N. Metoki, K. Kaneko, P.T. Jochym, A.M. Oles, K. Parlinski, Phys. Rev. Lett. **96**, 237003 (2006)
269. F. Wastin, P. Boulet, J. Rebizant, E. Colineau, G.H. Lander, J. Phys.: Condens. Matter **15**, S2279 (2003)
270. P. Monthoux, G.G. Lonzarich, Phys. Rev. B **59**, 14598 (1999)
271. P. Monthoux, G.G. Lonzarich, Phys. Rev. B **69**, 064517 (2004)
272. E.D. Bauer et al., J. Phys.: Condens. Matter **24**, 052206 (2012)
273. F. Hulliger, *Handbook on the physics and chemistry of rare earths,* vol. 4, eds. by K.A. Gshneidner, L. Eyring (North-Holland, Amsterdam, 1979), p. 153

http://www.springer.com/978-90-481-2878-5

Rare-Earths and Actinides in High Energy Spectroscopy

Bonnelle, C.; Spector, N.
2015, XVII, 380 p. 120 illus., 107 illus. in color.,
Hardcover
ISBN: 978-90-481-2878-5